



Multiaxial fatigue

The influence of principal stress directions on the fatigue assessment of a stinger structure

M.J.C. (Matthijs) van der Linden

Faculty 3mE

MULTIAXIAL FATIGUE

THE INFLUENCE OF PRINCIPAL STRESS DIRECTIONS ON THE FATIGUE ASSESSMENT OF A STINGER STRUCTURE

by

M.J.C. (Matthijs) van der Linden

in partial fulfillment of the requirements for the degree of

Master of Science
in Offshore Engineering

at the Delft University of Technology,
to be defended publicly on Friday April 29, 2016 at 14:00 PM.

Supervisor:	Dr. ir. A. Romeijn	Delft University of Technology
Thesis committee:	Ir. P.S. van Lieshout,	Delft University of Technology
	Dr. ir. S.A. Miedema	Delft University of Technology
	Dr. ir. J.H. den Besten	Delft University of Technology
	Dr. ir. N. Ermolaeva,	Allseas Engineering B.V.
	Dr. ir. Y. Yu,	Allseas Engineering B.V.

This thesis is confidential and cannot be made public



PREFACE AND ACKNOWLEDGMENTS

This report describes the research conducted as part of my thesis to obtain the Master of Science degree in Offshore and Dredging Engineering. This research is done in close collaboration with Allseas Engineering B.V. and the Delft University of Technology. The support by Allseas is gratefully acknowledged.

During this project I have been supported by many people, in different ways. First of all I would like to thank my daily supervisors, both at Allseas and university: Natalia Ermolaeva, Arie Romeijn, Paula van Lieshout and Yanrong Yu. The meetings we had during this graduation period were valuable experiences to me. A special thanks to Natalia for the thorough review of this report. Yunsong Yan and Jasper Slob most definitely deserve a 'thank you' for helping me understand the Femap software. Furthermore, at Allseas I would like to thank my colleagues from the Innovations Department for providing enough distractions throughout the project, in the most positive sense of the word.

Lastly I would like to express my gratitude to my parents for their infinite love and support since the day I was born. This report is dedicated to them.

I wish you an interesting read,

Matthijs

Delft, April 2016

ABSTRACT

The Allseas Group S.A. has made a name for itself in the field of offshore pipelaying and subsea construction by staying innovative. The company has six specialized vessels operating worldwide and the biggest vessel in the world is almost ready for operations. One of the company vessels is the Solitaire and lays pipe using the S-lay installation method. This method allows fast installation together with the applicability to lay pipe in a wide range of water depths. A stinger, a space frame structure consisting of welded circular hollow sections, is designed to prevent excessive bending of the pipeline while laying. This structure is attached to the vessel and after the pipe joints are welded on board they leave the vessel horizontally guided by the stinger.

A known failure mode of the stinger structure is fatigue. Fatigue can be characterized as a mechanism whereby cracks initiate and grow in a material due to fluctuating stresses. For the stinger these fluctuating stresses originate from environmental loads, mainly waves. Although Allseas has already developed an in-house fatigue assessment procedure for the stinger structures to calculate fatigue life, there is an interest in gaining a more fundamental understanding of multiaxial fatigue phenomena with respect to stinger joints. This leads to the following research goal:

“The goal of this research is to gain a more fundamental understanding of the multiaxial stress field for a stinger structure and in the end improve the fatigue assessment.”

Allseas has performed real time strain measurements on a tubular joint of the Solitaire stinger and already used the data for validating their fatigue assessment (Korakidou, 2013) and evaluating the Stress Concentration Factors (Zhao, 2010). In this study the nominal strain data of two braces were decomposed into three load components: axial forces, in-plane bending moments and out-of-plane bending moments. Their time histories are used as load input for a 4-noded shell finite element model of the stinger joint under investigation. The change of principal stress direction during loading around the braces-to-chord connections was researched, for this is an indication of the stress state multiaxiality variation which could lead to multiaxial fatigue. The saddle and in-between locations showed variations of 20 degrees or more, which is seen as a threshold, for two boundary condition sets analysed: all fixed ends and a combination of pin-rollers. Furthermore, the chord saddle location showed an 18 percent higher Hot Spot Stress for axial loading when principal stresses were used for extrapolation compared to primary stresses perpendicular to the weld toe. The hypothesis that this difference is due to a deviation in principal stress directions between extrapolation locations has been investigated. In order to achieve this, 13 simple T/Y-joint configurations with varying joint parameters were analysed in Femap through its application programming interface. The focus was only on the chord saddle location with axial loading and the chord ends were fixed. Although it was found that joint parameters β , τ and θ have an effect on the difference of principal stress directions between extrapolation locations A and B, no noticeable difference was found between the Stress Concentration Factors of the two extrapolation methods, leading to the conclusion that other factors cause the difference in Hot Spot Stress.

Lastly the ratio of Stress Concentration Factor(SCF) to Strain Concentration Factor(SNCF) has been investigated for the same 13 T/Y-joint configurations. This ratio showed to be dependent on the individual joint parameters with values varying from 1.17 to 1.30.

Based on the results it can be concluded that the in-between locations around the welded connection showed to be most prone to multiaxial fatigue based on the change in principal stress directions during loading. The difference in Hot Spot Stress between extrapolating principal stresses and primary stresses perpendicular to the weld toe cannot be explained by a difference in principal stress directions, so further research should be done in order to find the actual cause. Nevertheless, based on the results it can be considered conservative to use the principal stresses. Lastly, when converting strains to stresses by using a standard value of 1.20 for the SCF/SNCF-ratio this can lead to a too conservative fatigue life estimation in case the real ratio is lower and vice versa.

CONTENTS

List of Figures	ix
List of Tables	xi
1 Introduction	1
1.1 Allseas Engineering B.V.	1
1.2 S-Lay method	1
1.3 Stinger	1
1.4 Fatigue	1
1.4.1 In-house developed fatigue assessment procedure	2
1.5 Problem definition	3
1.6 Research objective	3
1.7 Thesis outline	4
2 Theory background	7
2.1 Tubular joints	7
2.1.1 T/Y-joint	7
2.1.2 K/N-joint	7
2.1.3 Multiplanar	8
2.1.4 Type of loading	8
2.2 Stress	9
2.2.1 State of stress	9
2.2.2 Principal stress	9
2.2.3 Nominal stress	10
2.2.4 Hot spot stress	10
2.2.5 Stress Concentration Factor	10
2.2.6 Extrapolation	11
2.3 Fatigue	12
2.3.1 Fatigue loading	12
2.4 Fatigue life assessment methods	14
2.5 Finite element method	14
2.5.1 Element types	15
2.5.2 Mesh refinement	15
2.6 Coordinate systems	15
2.6.1 Vessel	15
2.6.2 Member	15
2.6.3 Element	15
3 Strain gauge data analysis	17
3.1 Strain gauge locations	17
3.2 Strain gauge properties	19
3.3 Voltage to strain	19
3.4 Data selection	20
3.5 Strains to stresses	20
3.5.1 Strain measurements	20
3.5.2 Statics check	23
3.6 Stresses to Forces	27
3.6.1 Axial Force	27
3.6.2 Bending Moment	27
3.6.3 Load analysis	29

4	Finite element models	31
4.1	Stinger joint	31
4.1.1	Element type	31
4.1.2	Mesh refinement	31
4.1.3	Spider nodes	33
4.1.4	Boundary conditions	33
4.1.5	Loads	34
4.1.6	Analysis type	35
4.1.7	Desired output	35
4.2	T/Y-joints	36
4.2.1	Element type	36
4.2.2	Mesh refinement	36
4.2.3	API-script	36
4.2.4	Joint configurations	36
4.2.5	Boundary conditions	36
4.2.6	Load	36
4.2.7	Analysis type	37
4.2.8	Desired output	37
5	Results	41
5.1	Stinger joint	41
5.1.1	Principal stress directions	41
5.1.2	Hot Spot Stresses	49
5.2	T/Y-joints	50
5.2.1	SCF calculation using three methods	50
5.2.2	Parametric study SCF to SNCF ratio	56
6	Summary and Conclusions	59
6.1	Stinger joint	59
6.2	T/Y-joints	60
6.3	Recommendations	62
A	Stinger drawing	63
B	API-script for Femap configurations of T/Y-joint	65
C	T/Y-joint configurations	77
	Bibliography	81

LIST OF FIGURES

1.1 Solitaire with attached Stinger	1
1.2 S-lay pipeline configuration	2
1.3 Four-sectioned Stinger	2
1.4 Vessel coordinate system	3
1.5 Fatigue calculation scheme [1]	5
2.1 Tubular Y-joint configuration with specified joint dimensions and joint parameters, [4]	8
2.2 Tubular K-joint configuration with specified joint dimensions and joint parameters, [4]	8
2.3 Example of a multiplanar KK-joint [4]	8
2.4 Types of loading [4]	8
2.5 (l) General state of stress, (c) Plane stress, (r) Plane stress (two dimensional view) [5]	9
2.6 (l) Stresses in given coordinate system, (r) Principal stresses	10
2.7 Illustration of nominal stress and hot spot stress [7]	11
2.8 Extrapolation locations according to DNV	12
2.9 Fatigue strength divided into different fatigue loading situations [14]	13
2.10 Fatigue loading [15]	13
2.11 The influence of non-proportional loading [18]	14
2.12 non-proportional change of stress components: P force, M moment [19]	14
2.13 Element types [22]	15
2.14 Member coordinate system	16
2.15 Element coordinate system	16
3.1 Stinger joint for strain gauge measurements	17
3.2 Stinger joint for strain gauge measurements	18
3.3 Numbering of the strain gauges	18
3.4 Joint under investigation with the strain gauge locations.	21
3.5 Original Strains	21
3.6 Mean Zero Strains	21
3.7 Brace A within the StAAD.Pro model with the strain gauge locations depicted	22
3.8 Brace B within the StAAD.Pro model with the strain gauge locations depicted	22
3.9 Selfweight applied on complete model with the relevant joint under investigation indicated by the black circle.	23
3.10 Buoyancy applied on part of structure under the waterline with the relevant joint indicated by the black circle.	23
3.11 Brace A: Bending Moments due to SelfWeight	24
3.12 Brace A: Axial Force due to Selfweight	24
3.13 Brace A: Bending Moments due to Buoyancy	24
3.14 Brace A: Axial Force due to Buoyancy	24
3.15 Brace A: Bending Moments due to Rollerbox Loads	24
3.16 Brace A: Axial Force due to Rollerbox Loads	24
3.17 Rollerbox loads applied on the corresponding nodes in the model with the joint under investigation indicated by the black circle.	25
3.18 Resulting static stress in Brace A at strain gauge location 1	26
3.19 Total Stresses at the strain gauge locations of Brace A	26
3.20 Axial force in Braces A and B	27
3.21 The strain gauge locations 1-4 and the locations used for bending moment calculations A-D	28
3.22 In-plane and out-of-plane bending moments in Brace A	29
3.23 Load components acting on braces A and B	30

4.1	Shell model of the Stinger joint	32
4.2	Finer mesh at the brace-chord connections	32
4.3	Shell element: (l) 4 noded, (c) 8 noded, (r) four times 4 noded	32
4.4	Mesh refinement model for principal stress direction determination	32
4.5	Mesh refinement model for Hot spot stress determination	32
4.6	Spider nodes	33
4.7	Loads on Brace A; Axial force (1), IPB moment (5), OPB moment (3)	33
4.8	Boundary conditions tested on maximum Von Mises stress	33
4.9	Boundary conditions used, left: all fixed, right: pinned-rollers	34
4.10	Femap function of the axial force in Brace A	34
4.11	Mesh refinement at the brace-to chord connection	36
4.12	Configuration with fixed chord ends and axial force on brace	37
4.13	Extrapolation locations	38
4.14	Principal Stress directions	38
5.1	Investigated locations of braces A, B and C	42
5.2	Typical deformation for the model with pinned-rollers boundary conditions	42
5.3	Typical deformation for the model with fixed boundary conditions	42
5.4	Principal stress angle changes and MAPS of Brace A connection, fixed constraints	44
5.5	Principal stress angle changes and MAPS of Brace A connection, pinned-rollers constraints	44
5.6	Principal stress angle changes and MAPS of Brace B connection, fixed constraints	45
5.7	Principal stress angle changes and MAPS of Brace B connection, pinned-rollers constraints	46
5.8	Principal stress angle changes and MAPS of Brace C connection, fixed constraints	47
5.9	Principal stress angle changes and MAPS of Brace C connection, pinned-rollers constraints	48
5.10	Refined mesh along extrapolation region at weld toe of brace A	49
5.11	Load histories used for HSS calculation	50
5.12	Basic configuration with SCF equations of Efthymiou [2]	51
5.13	Principal Stresses directions for different θ	52
5.14	SCF for different θ	52
5.15	Principal Stresses directions for different τ	53
5.16	SCF for different τ	53
5.17	Principal Stresses directions for different β	54
5.18	SCF for different β	54
5.19	Principal Stresses directions for different γ	55
5.20	SCF for different γ	55
5.21	relationship between snf-ratio and individual joint parameters	57
6.1	Investigated locations of braces A, B and C	60
6.2	Investigated T/Y-joint configuration	60
C.1	Configuration 1	77
C.2	Configuration 2	77
C.3	Configuration 3	77
C.4	Configuration 4	77
C.5	Configuration 5	78
C.6	Configuration 6	78
C.7	Configuration 7	78
C.8	Configuration 8	78
C.9	Configuration 9	78
C.10	Configuration 10	78
C.11	Configuration 11	78
C.12	Configuration 12	78
C.13	Configuration 13	79

LIST OF TABLES

2.1	Joint parameter ranges	8
3.1	Joint specifications	17
3.2	Strain gauge parameters	20
3.3	Time slots of pipe-laying	20
3.4	Static Stresses at strain gauge locations	25
3.5	Average stresses during measurements at locations depicted in Figure 3.21	29
3.6	Comparison of Bending Moments	29
4.1	Dimensions and joint parameters of the FEM configurations	37
4.2	Extrapolation points	39
5.1	Change of principal stress angles for chord and brace locations of the brace A connection for different boundary conditions	43
5.2	Change of principal stress angles for chord and brace locations of the brace B connection for different boundary conditions	45
5.3	Change of principal stress angles for chord and brace locations of the brace C connection for different boundary conditions	47
5.4	Maximum difference in HSS between extrapolation methods	49
5.5	Change of θ	51
5.6	Change of τ	53
5.7	Change of β	54
5.8	Change of γ	55
5.9	snf-ratios at chord saddle for 13 T/Y-joint configurations with axial loading	57
6.1	multiaxial fatigue sensitive locations of investigated stinger joint	59
6.2	joint parameter influence on principal stress angle difference between extrapolation locations A and B	61
6.3	snf-ratios with respect to joint parameters	61

1

INTRODUCTION

1.1. ALLSEAS ENGINEERING B.V.

Founded in 1985, Allseas Group S.A. is a major innovation driven offshore pipelay and subsea construction company. The business of Allseas comprises project management, engineering, procurement, installation and commissioning. The in-house designed fleet of specialised vessels provide high-quality pipelaying for oil and gas companies. Currently the company is completing the construction of the biggest vessel in the world: the Pioneering Spirit. With this vessel Allseas will enter the oil rig decommissioning and removal business.



Figure 1.1: Solitaire with attached Stinger

1.2. S-LAY METHOD

The method of pipe-laying adopted by Allseas is the S-lay method, as depicted in Figure 1.2. Great advantages of this method include a high production rate and the suitability for laying pipe in water depths varying from shallow to very deep. Additionally, the possibility to install concrete coated pipe makes the S-lay method a good fit for Allseas. Using this installation method, pipe joints are welded onboard. The pipe is guided by a 'stinger' structure as it leaves the vessel horizontally. The stinger is described below.

1.3. STINGER

In order to be able to use the S-lay method a stinger structure is required. This is a space frame structure consisting of welded circular hollow sections. These sections are made up from chords and braces. The main loads on the chords are due to bending, where the primary loads in the braces are due to axial forces. The working principle of the stinger is to prevent excessive bending and buckling of the pipeline during laying. For this thesis the stinger consists of sections I and II in stead of all four shown in Figure 1.3.

1.4. FATIGUE

In the field of materials science the definition of fatigue is the weakening of a material caused by repeatedly applied loads. Load cycles lead to progressive and localised structural damages. Most offshore structures are

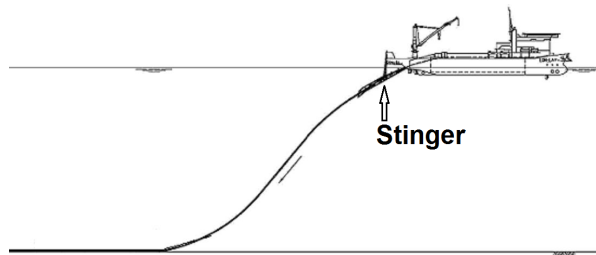


Figure 1.2: S-lay pipeline configuration

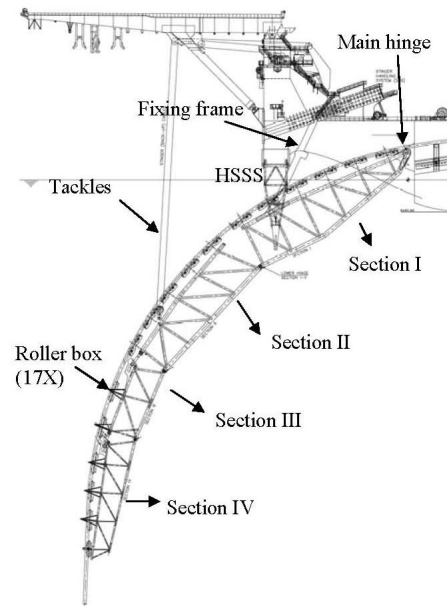


Figure 1.3: Four-sectioned Stinger

subject to cyclic loads due to waves for example, which leads to structural damage, classified as fatigue. How Allseas implements fatigue within their stinger structures is explained next.

1.4.1. IN-HOUSE DEVELOPED FATIGUE ASSESSMENT PROCEDURE

The stinger is a structure that is prone to fatigue. Hydrodynamic loads cause repeatedly loading and unloading conditions. Allseas Engineering B.V. has developed a fatigue assessment procedure that can be divided into the following stages, visualized in Figure 1.5 and further explained below,[1]:

1. Life matrix The construction of a life matrix of the Solitaire stinger is the first big step in the fatigue damage calculation. Although the stinger is designed for operational use, harbour and transit situations have to be taken into account as well. The estimated duration of all three aforementioned situations is used to create an expected profile. In combination with constructed scatter diagrams of the expected operations and transit routes the life matrix is created.

2. Hydrodynamic & Rollerbox loads With the use of the life matrix different load cases are determined, defined by the configuration of the Stinger, the wave height, wave frequency and wave approach angle. The vessel and Stinger are hydrodynamically analysed for all load cases with 3-hour runs using the dedicated software AQWA. The analyses are statistically processed resulting in six sets of hydrodynamic loads, one set for every direction as illustrated in Figure 1.4. The pipelaying software package Offpipe is used to define the operational loads acting on the rollerboxes. Again, the results from the analyses are statistically processed resulting in four sets of rollerbox loads.

3. Finite element analysis → hot spot stresses ranges The load sets from the hydrodynamic and rollerbox analyses are used as input for Finite element analysis (FEA) in order to calculate the member forces for each load case. The finite element software Femap is used for modelling the joints for which fatigue analysis is performed. The joints of interest are modelled with shell elements and the rest of the Stinger structure is modelled by simple beam elements. The hot spot stresses are derived from Femap by extrapolating the principal stresses to the weld toe according to DNV [2]. The hot spot stresses of tubular connections not analysed with Femap are derived by parametric stress concentration factor equations. For the fatigue assessment the hot spot stress ranges are of interest, so the hot spot stresses are combined to obtain the maximum hot spot stress ranges for each load case.

- Assess the difference between SCFs obtained from extrapolating principal stresses and extrapolating primary stresses perpendicular to the weld toe in relation with joint parameters for simple T/Y-joint configurations. Do this for axial loading and look only at the chord saddle position.
- Assess the influence of the individual joint parameters on the snf-ratio for simple T/Y-joint configurations. Again for axial loading and chord saddle position only.

In addition, the method of deriving hot spot stresses is subject to debate. Where some use the principal stresses for extrapolation, others use the primary stresses perpendicular to the weld toe. If there exists a significant difference between the two, this can lead to overestimation or underestimation and an inaccurate fatigue assessment.

1.7. THESIS OUTLINE

This report continues with Chapter 2 that elaborates on the concepts relevant for this study. Then Chapter 3 explains the strain measurements that were performed on a tubular joint of the stinger and how the strain data is converted to and decomposed into different load components. Chapter 4 gives a detailed description of the finite element models that were created for this study. The results are presented in Chapter 5 after which the conclusions and recommendations are given in Chapter 6.

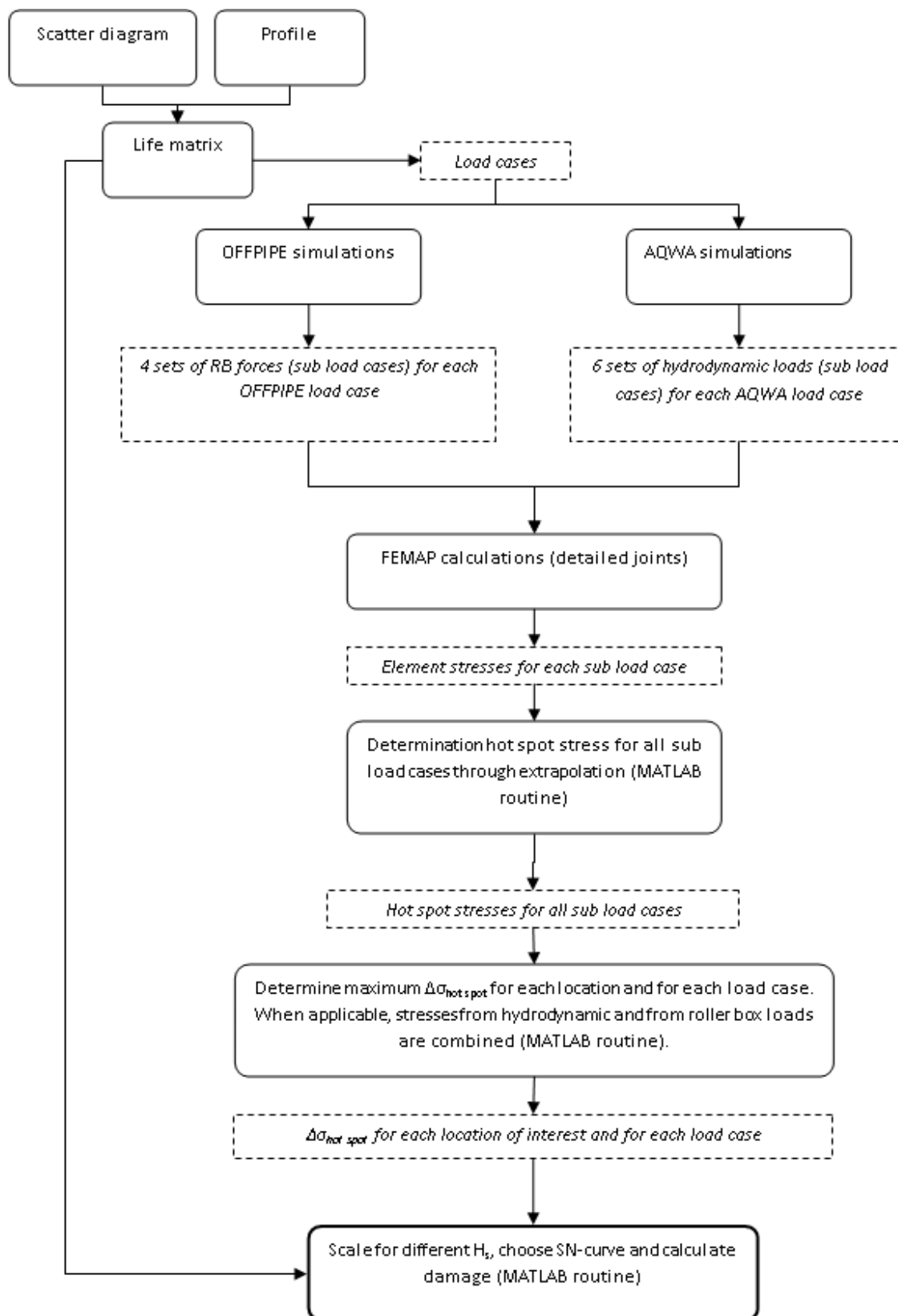


Figure 1.5: Fatigue calculation scheme [1]

2

THEORY BACKGROUND

This chapter elaborates on the different literature studies performed during this thesis project. The different subjects are divided over multiple sections. Firstly a general study on the subject of fatigue. However, before going in detail on the subject of fatigue, it is necessary to understand the concepts that are relevant for this phenomenon.

2.1. TUBULAR JOINTS

Although there exists a wide variety of tubular joint configurations, two configurations are of importance for this research: T/Y-joint and K/N-joint. Both with circular hollow sections (CHS).

2.1.1. T/Y-JOINT

A uniplanar CHS Y-joint is shown in Figure 2.1 with corresponding joint dimensions and joint parameters. The saddle and crown locations are depicted by the arrows in the same figure. This joint is classified as a T-joint when the normal component of a brace member force is equilibrated by beam shear (and bending) in the chord member, [3]. If this is not the case, it is a Y-joint. The joint dimensions are:

- Chord diameter d_0
- Brace diameter d_1
- Chord wall thickness t_0
- Brace wall thickness t_1

And the joint parameters are given below and their ranges in Table 2.1:

- Relative chord length α
- Diameter ratio β
- Half chord diameter to thickness ratio γ
- Acute angle between chord and brace axes θ
- Wall thickness ratio τ

2.1.2. K/N-JOINT

A uniplanar K-joint is shown in Figure 2.2 with corresponding joint dimensions and joint parameters. For a joint to be classified as a K-joint, the normal component of a brace member force should be equilibrated by the normal force component of another brace member on the same side with a maximum deviation of 20 percent, [3]. If one of the braces is perpendicular to the chord, it is considered a N-joint. If both braces are inclined, it is considered a K-joint.

Table 2.1: Joint parameter ranges

parameter	Typical range	Validity range	
		min	max
β	0.4-0.8	0.2	1
γ	12-20	8	32
τ	0.3-0.7	0.2	1
θ	$40^\circ - 90^\circ$	30°	90°

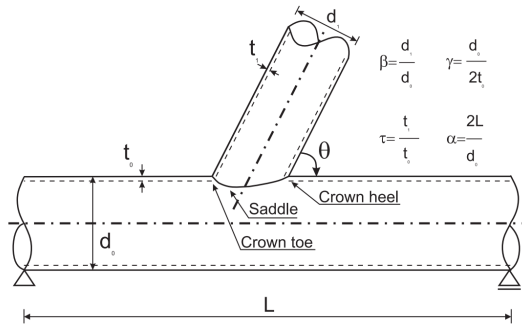


Figure 2.1: Tubular Y-joint configuration with specified joint dimensions and joint parameters, [4]

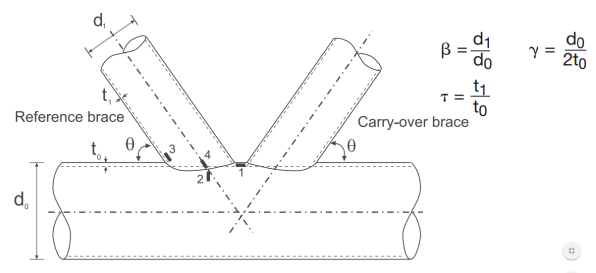


Figure 2.2: Tubular K-joint configuration with specified joint dimensions and joint parameters, [4]

2.1.3. MULTIPLANAR

For multiplanar joints the same definitions and range apply, except that these joints have members in multiple planes, see Figure 2.3 for example.

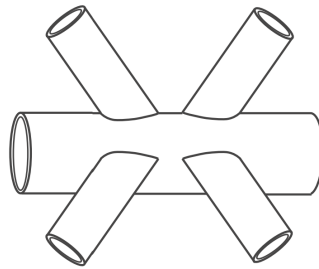


Figure 2.3: Example of a multiplanar KK-joint [4]

2.1.4. TYPE OF LOADING

The types of loading relevant for this study are axial loading, in-plane bending (IPB) and out-of-plane bending (OPB), as illustrated in Figure 2.4.

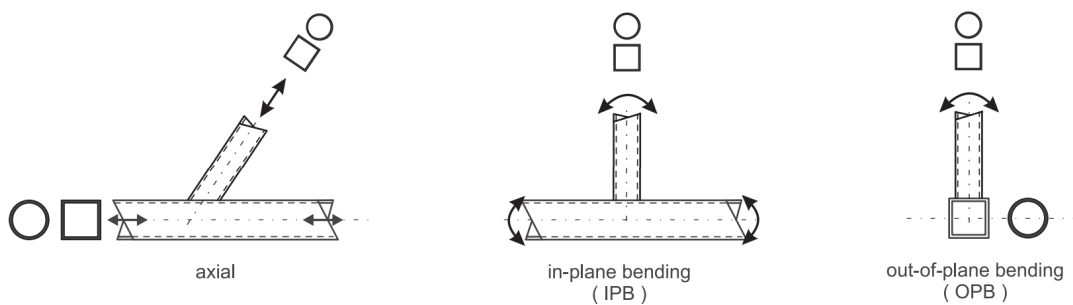


Figure 2.4: Types of loading [4]

2.2. STRESS

2.2.1. STATE OF STRESS

It starts with understanding the state of stress of a component. Stress at a point in a continuous and cohesive body can be decomposed into two components: a shearing stress τ acting tangent to the plane and a normal stress σ perpendicular to the plane. For a three dimensional state of stress six shear stress components (τ_{xy} , τ_{yx} , τ_{xz} , τ_{zx} , τ_{yz} and τ_{zy}) are needed to describe the stresses acting on the six sides and three normal stress components (σ_x , σ_y , σ_z), see left of Figure 2.5. However, the six shear stress components can be brought back to just three, for $\tau_{xy} = \tau_{yx}$, $\tau_{xz} = \tau_{zx}$ and $\tau_{yz} = \tau_{zy}$ due to equilibrium of the element. So just six independent normal and shear stress components characterize the general state of stress at a point.

As the above described general state of stress is not often encountered in engineering practice, a simplification is made in this study. Instead of a three dimensional state of stress, a plane stress state is assumed. This implies that the analyses can be performed in a single plane, resulting in only three stress components (σ_x , σ_y and τ_{xy}) describing the state of plane stress on an element, shown by the center and right figures in Figure 2.5.

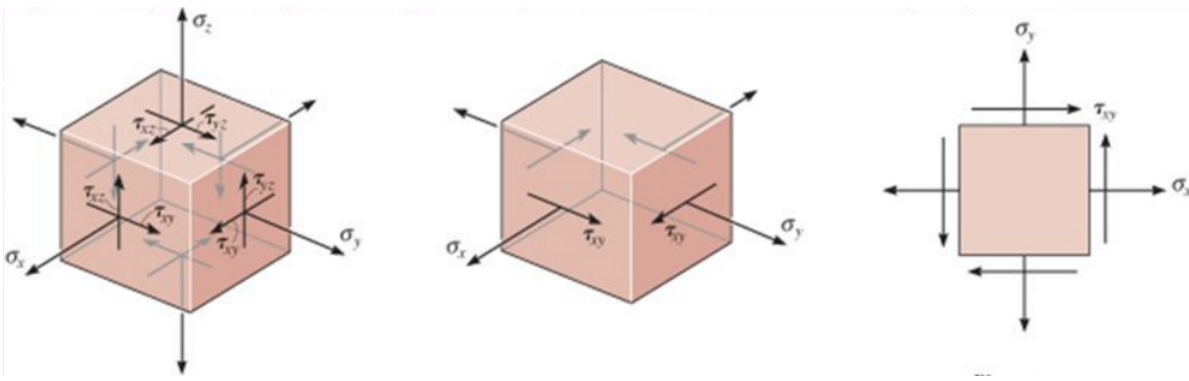


Figure 2.5: (l) General state of stress, (c) Plane stress, (r) Plane stress (two dimensional view) [5]

2.2.2. PRINCIPAL STRESS

In a three dimensional body that is stressed, there are at every point in that body also at least three planes where no shear stresses are acting. The planes where this is the case are called principal planes. The normal vectors at these principal planes are the principal directions, they are perpendicular to the planes. The stresses normal, thus parallel to the principal directions, are the principal stresses. These are in fact the maximum normal stresses at that point.

For this thesis it is assumed that stresses only occur in a single plane, simplifying the general state of stress to a plane stress, so two dimensional, see Figure 2.6. In that case there are only two principal directions with corresponding principal stresses.

The principal stresses can be calculated with equation 2.1:

$$\sigma_{1,2} = \frac{\sigma_x + \sigma_y}{2} \pm \sqrt{\left(\frac{\sigma_x - \sigma_y}{2}\right)^2 + \tau_{xy}^2} \quad (2.1)$$

The principal directions are defined by the angle θ_p and it is at this angle that the shear stresses become zero. The angles θ_p are calculated with equation 2.2. In this study the principal stress angle is defined as positive when principal stress σ_1 rotates counter-clockwise away from the x -axis as depicted in Figure 2.6. The x -axis within the finite element models is defined as perpendicular to the 'welded connection'.

$$\tan(2\theta_p) = \frac{2\tau_{xy}}{\sigma_x - \sigma_y} \quad (2.2)$$

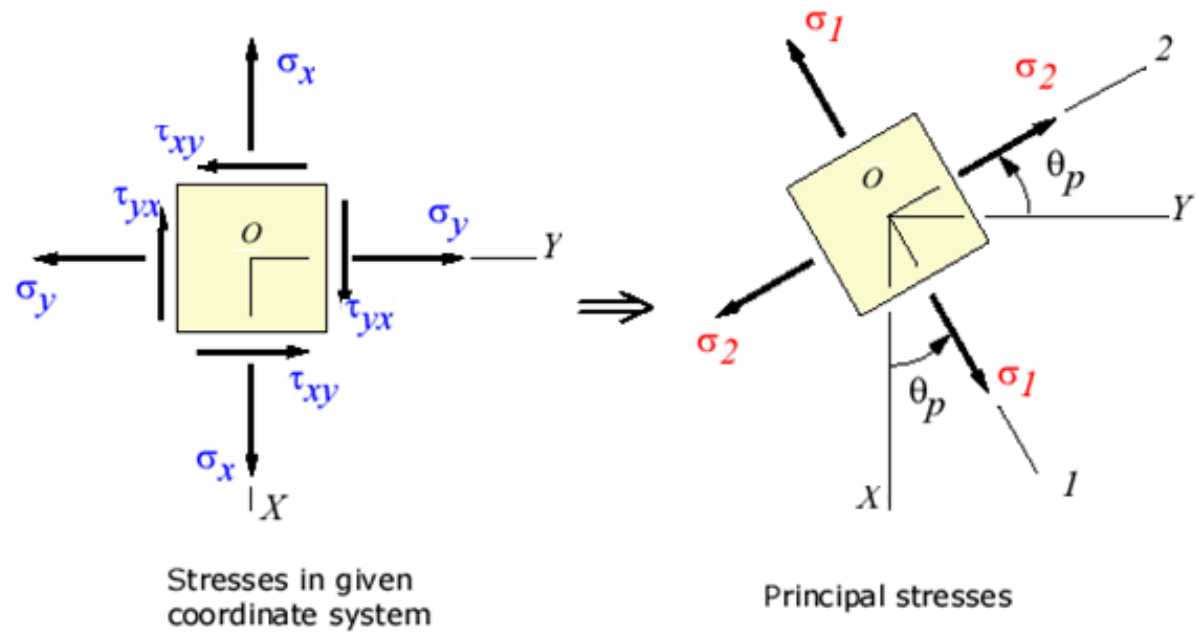


Figure 2.6: (l) Stresses in given coordinate system, (r) Principal stresses

2.2.3. NOMINAL STRESS

Assuming that the stress is constant over a net cross-sectional area A_0 of a specimen, the nominal stress can be calculated with equations 2.3 and 2.4. This stress does not take into account the effect of geometric discontinuities, e.g. holes and welds.

$$\sigma_{N_{ax}} = \frac{P}{A_0} \quad (2.3)$$

$$\sigma_{N_{mom}} = \frac{My}{I} \quad (2.4)$$

Where $\sigma_{N_{ax}}$ and $\sigma_{N_{mom}}$ are the nominal stress due to axial loading and bending moment. P is the axial force normal to the cross section. M is the bending moment, y is the distance from the centre of the brace to the point considered and I is the moment of inertia of the cross section.

2.2.4. HOT SPOT STRESS

The term hot spot is used to refer to the critical point in a structure. It is at a hot spot that fatigue cracking can be expected to initiate, [6]. Often this is caused by notches or discontinuities in the structure. For tubular joints, a hot spot is located at the weld toe.

Hot spot stress σ_{hs} is the structural stress at the hot spot, also called geometric stress. It includes all stress raising effects of a structural detail apart from the weld itself. So the effects of joint geometry are included as well as the type of load. The local effects, notch effects, are excluded. The hot spot stress is determined by extrapolation of the stresses at defined locations a and b in Figure 2.7. The extrapolation procedure is described in more detail in Section 2.2.6.

2.2.5. STRESS CONCENTRATION FACTOR

Stress Concentration Factor (SCF) is the ratio of hot spot stress to nominal stress and is used as a conversion factor to calculate the hot spot stress with a known nominal stress. The Stress Concentration Factor is an important parameter in fatigue calculations and will be used extensively in this study. In addition to a Stress Concentration Factor, there is a Strain Concentration Factor (SNCF):

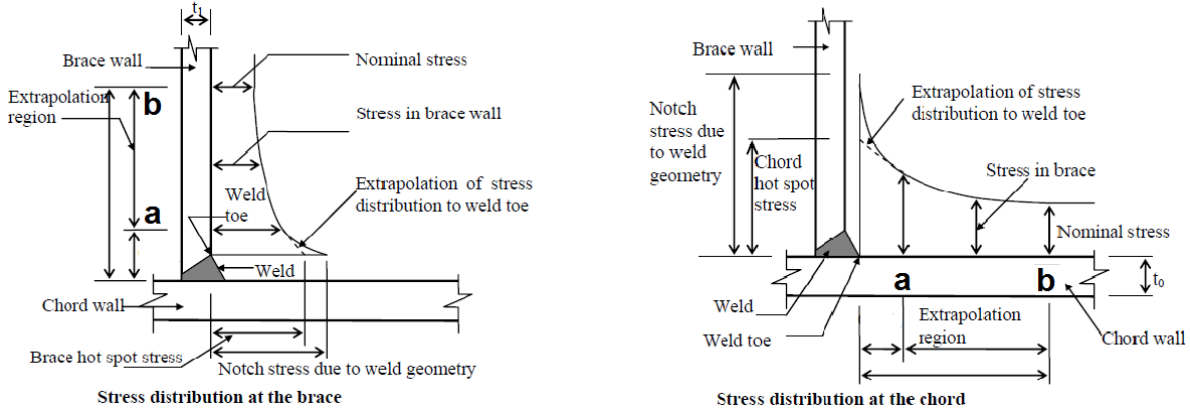


Figure 2.7: Illustration of nominal stress and hot spot stress [7]

$$SCF = \frac{\sigma_{hs}}{\sigma_N} \quad (2.5)$$

$$SNCF = \frac{\epsilon_{hs}}{\epsilon_N} \quad (2.6)$$

Where nominal stress(strain) is the stress(strain) calculated on the basis of the net cross section of the circular hollow section, without taking into account the effect of geometric discontinuities, e.g. holes or welds. The SCF at both chord and brace locations depends on the nominal stress in the brace. Substantial studies have investigated the SCF for different tubular joint configurations in order to come up with standardized formulas. Widely used are the Efthymiou equations [8]. Allseas implements these equations in their fatigue assessment.

2.2.6. EXTRAPOLATION

The method of obtaining the HSS is subject to debate. The discussions involve:

- The type of stresses and strains that needs to be extrapolated
- The extrapolation region
- The way the stresses are extrapolated, linearly or quadratic

On the type of stresses and strains that need to be extrapolated, the debate is mainly about principal stresses and primary stresses. Primary stresses are favored by [9] and [10] and the design codes of the American Welding Society [11] and the American Petroleum Institute [12] use the primary stresses perpendicular to the weld as well. Design codes of the IIW [13] and Det Norske Veritas [2] use the principal stresses. For Allseas uses the DNV code for their fatigue assessment, principal stresses are used. This thesis will, among other subjects, investigate the difference in HSS for the two extrapolated stresses.

The extrapolation region used in this thesis follows the code of DNV [2] and the extrapolation locations are visualized in Figure 2.8 and the corresponding equations below.

For extrapolation of stress along the brace surface normal to the weld toe:

$$a = 0.2\sqrt{rt} \quad (2.7)$$

$$b = 0.65\sqrt{rt} \quad (2.8)$$

For extrapolation of stress along the chord surface normal to the weld toe at the crown position:

$$a = 0.2\sqrt{rt} \quad (2.9)$$

$$b = 0.4\sqrt[4]{rtRT} \quad (2.10)$$

For extrapolation of stress along the chord surface normal to the weld toe at the saddle position:

$$a = 0.2\sqrt{rt} \quad (2.11)$$

$$b = 2\pi R \frac{5}{360} = \frac{\pi R}{36} \quad (2.12)$$

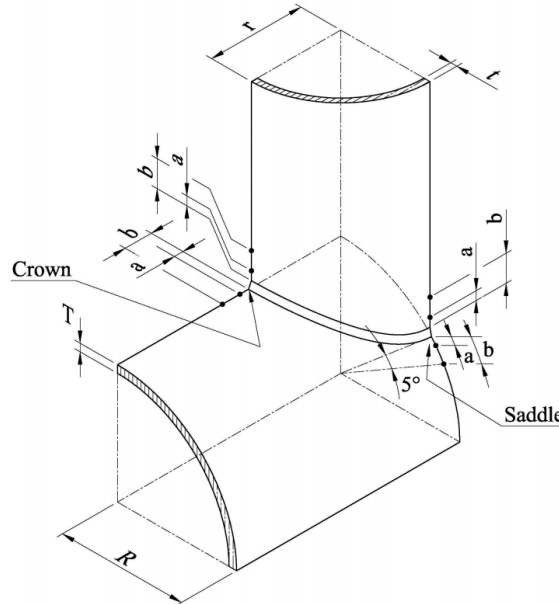


Figure 2.8: Extrapolation locations according to DNV

These locations deviate from for example the $0.4t$ and $1.4t$ proposed by Van Wingerde [10]. Especially the locations a and b on the chord surface normal to the weld toe at the saddle position will be used extensively during this study.

Extrapolation can be done linearly or quadratically. For this study the extrapolation has been done linearly.

2.3. FATIGUE

In the field of materials science the definition of fatigue is the weakening of a material caused by repeatedly applied loads. Load cycles lead to progressive and localised structural damages. Most offshore structures are subject to cyclic loads due to waves for example, which leads to structural damage, classified as fatigue.

Fatigue strength is a term that describes the range of cyclic stress that can be applied to a material without resulting in fatigue failure. Structures are designed to resist fatigue by engineering it in such a way that the stress it endures does not exceed its fatigue limit, which is a different name for fatigue strength. Usually this value will be determined from an S-N diagram as the maximum stress the structure can resist when subjected to a specified number of loading cycles, [5].

2.3.1. FATIGUE LOADING

The situation of fatigue loading can roughly be separated into Constant Amplitude (CA) loading and Variable Amplitude (VA) loading, see Figure 2.9. In this thesis the VA loading is most relevant, as the stinger structure is subject to waves with different wave heights, wave periods and wave approach angles, be it direct or indirect through stinger-vessel interaction.

MULTIAXIAL LOADING

The difference between uniaxial and multiaxial loading might seem obvious. A structure subjected to uniaxial loading has either an axial force, bending moment or torsion moment applied on it. A structure subjected

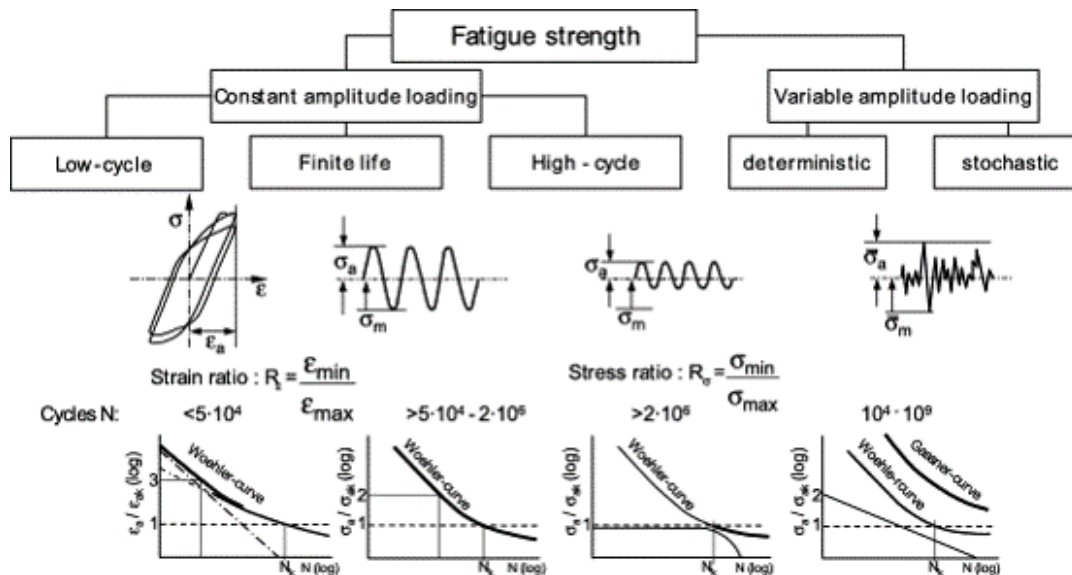


Figure 2.9: Fatigue strength divided into different fatigue loading situations [14]

to multiaxial loading is subjected to a combination of these load components. However, the effect on the structure in terms of stresses is less obvious. For example, uniaxial loading can locally (e.g. at the bottom of a notch) induce a complex state of stress. On the contrary, multiaxial loading could produce a complex state of stress, but due to the predominant properties of one component (e.g. the axial force) the strength analysis may be done uniaxially [14]. Figure 2.10 illustrates this difference, where uniaxial loading conditions can produce uniaxial states as well as multiaxial states of stress and strains, while multiaxial loading may be characterised by both a uniaxial and multiaxial state of stress and strain as well.

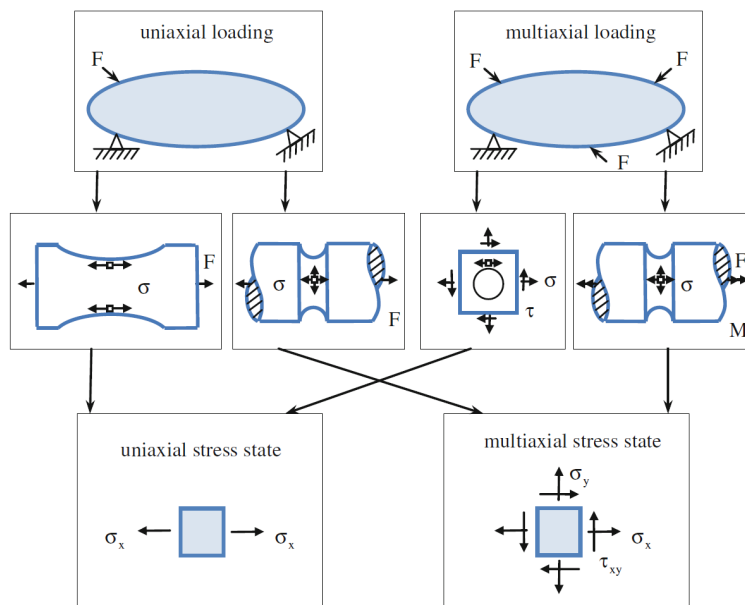


Figure 2.10: Fatigue loading [15]

NON-PROPORTIONAL LOADING

The most destructive form of loading from a fatigue point of view is *non-proportional* multiaxial fatigue loading. A loading with a high degree of non-proportionality can decrease fatigue strength by a factor 10 compared to proportional loading [16] [17]. This is illustrated in Figure 2.11. Non-proportional stress occurs when the principal axes of stress (or strain) rotates during the fatigue process, so during loading. Due to

the rotation of the principal axes more slip planes are active, which results in the interaction of multiple slip planes. Ultimately this results in additional strain hardening, which decreases fatigue life. Under proportional loading additional strain hardening is not observed.

A non-proportional loading case can be best explained by looking at Figure 2.12. It occurs when the components of multiaxial loading change in relation to one another non-proportionally. One objective of this study is to find the change in principal stress direction during loading along the intersection lines of the joint members in order to conclude on the level of non-proportional multiaxial loading.

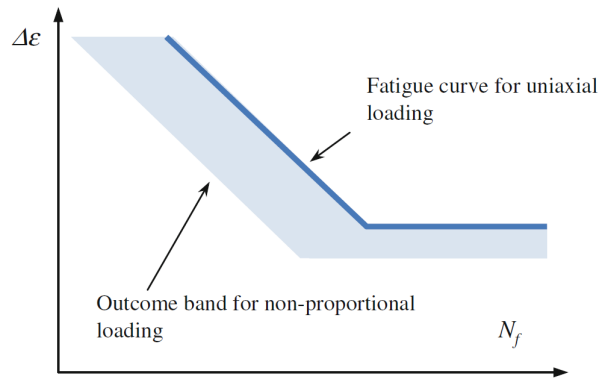


Figure 2.11: The influence of non-proportional loading [18]

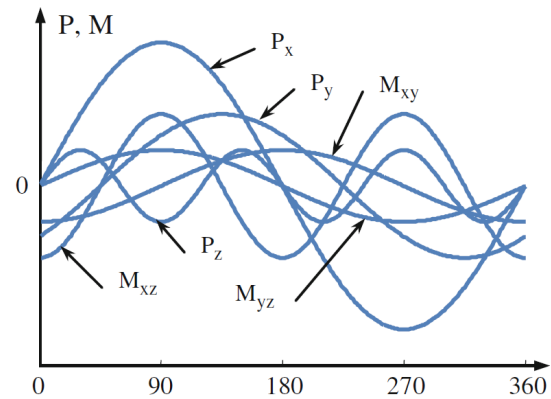


Figure 2.12: non-proportional change of stress components: P force, M moment [19]

2.4. FATIGUE LIFE ASSESSMENT METHODS

In order to calculate the fatigue life of a structure, an engineer has a wide variety of options concerning the approach to use. Especially the approaches to use for multiaxial fatigue are subject to debate. The study of Wang [20] divides the multiaxial fatigue criteria in three groups, according to the parameters used to describe the fatigue life, namely stress criteria, strain criteria and energy criteria.

This study does not propose a multiaxial approach that should be used. It only investigates whether or not the stinger is subjected to non-proportional multiaxial fatigue loading. With the outcome future research can be done into which method should be used.

The method that is used by Allseas is the hot spot stress approach. This method is widely used for welded tubular connections and a major advantage of this method is that the stress raising effect caused by the joint members are taken into account in the fatigue stress calculations. However, the effects from the weld itself are excluded. Although the HSS method is only applicable for fatigue failures starting from the weld toe [21], this is no disadvantage for the fatigue assessment of the stinger, for the fatigue failure of welded tubular connections tends to occur at the weld toe. The basic principle of the HSS approach is to combine a to be determined hot spot stress at the weld toe with the appropriate S-N curve in order to estimate the fatigue life.

2.5. FINITE ELEMENT METHOD

The finite element method (FEM) is a numerical tool for solving problems of engineering and mathematical physics. In the field of structural engineering it is especially useful for problems with complicated geometries, loadings and material properties for which analytical solution are difficult to obtain. The development of the FEM goes hand in hand with the increase of computational capabilities. The structure of interest is modelled by dividing it into an equivalent system of multiple smaller bodies, the 'finite elements', that are interconnected at nodes and constricted by boundary conditions. The accuracy of the analysis depends on the type of element, the mesh refinement, the weld shape modelled and boundary conditions applied on the model.

2.5.1. ELEMENT TYPES

Elements are the basic building blocks of finite element analysis. There exists a wide variety of element types, as can be seen in Figure 2.13. One-dimensional elements are straight lines or curved segments. In 2D, the shapes can be triangular or quadrilateral and in 3D the shapes are usually tetrahedral, pentahedral and hexahedral. In this study four-noded 2D plate elements are used with mainly quadrilateral shapes.

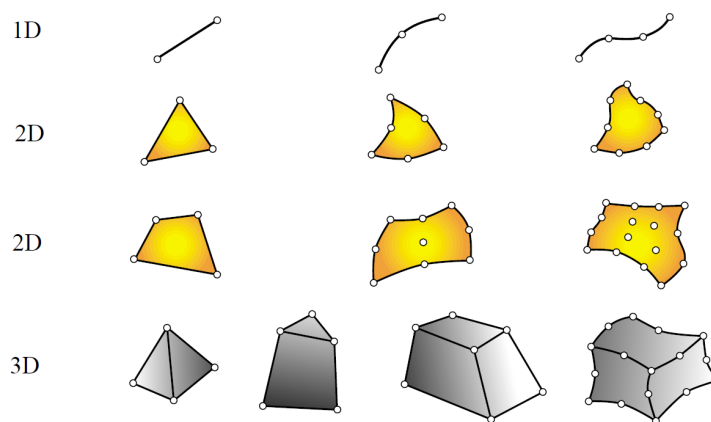


Figure 2.13: Element types [22]

2.5.2. MESH REFINEMENT

In order to increase the accuracy of the results of any finite element analysis, mesh refinement needs to be taken into account. In areas of high (low) stress or strain gradients a relatively fine (coarse) mesh should be used. In this study areas with high stress/strain gradients are around the welded connections. Hence those areas are finely meshed. The refinement itself can be achieved by two methods:

1. *h-refinement*: This method increases the number of elements used by reducing the individual element size and is the method used in this thesis.
2. *p-refinement*: The method that does not change the element size, but increases the order of the polynomials used as interpolation functions.

2.6. COORDINATE SYSTEMS

The coordinate systems used throughout this thesis can be divided into three main systems, a vessel system, member system and elemental system.

2.6.1. VESSEL

The vessel coordinate system has been shown in the previous chapter, see Figure 1.4.

2.6.2. MEMBER

For the strain gauge data analysis and the finite element analyses the member coordinate system is used. Each member has its own coordinate system, as showed in Figure 2.14. This means that for braces A and B axial forces are applied in the members y-direction, the in-plane bending moment is applied around the x-axis and the out-of-plane bending moment is applied around the z-axis.

2.6.3. ELEMENT

Within the finite element software the elements have their own coordinate system. Figure 2.15 shows an example of one of the T/Y-joints that are analysed during this study. The element coordinate system at the welded connection has its x-axis perpendicular to the weld toe and the z-axis normal to the plate surface.

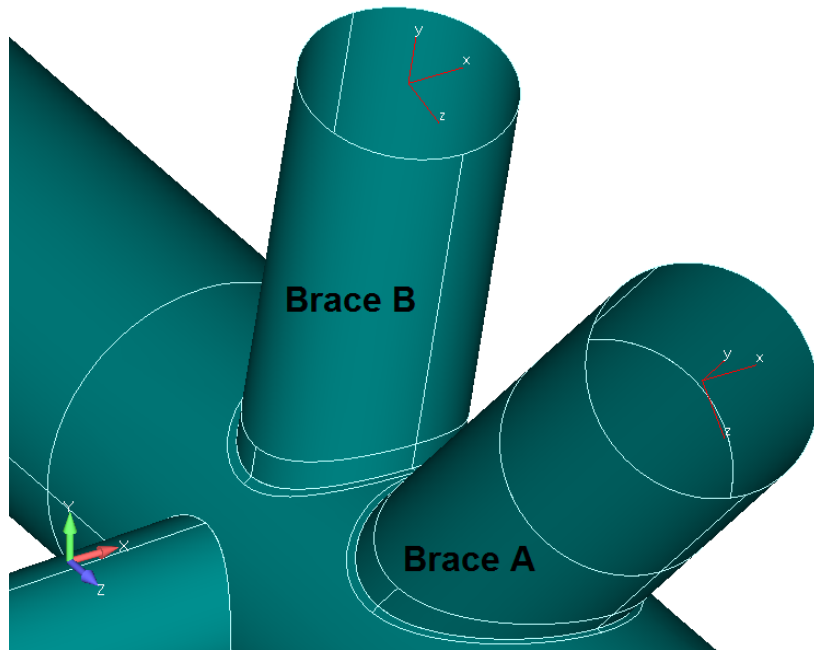


Figure 2.14: Member coordinate system

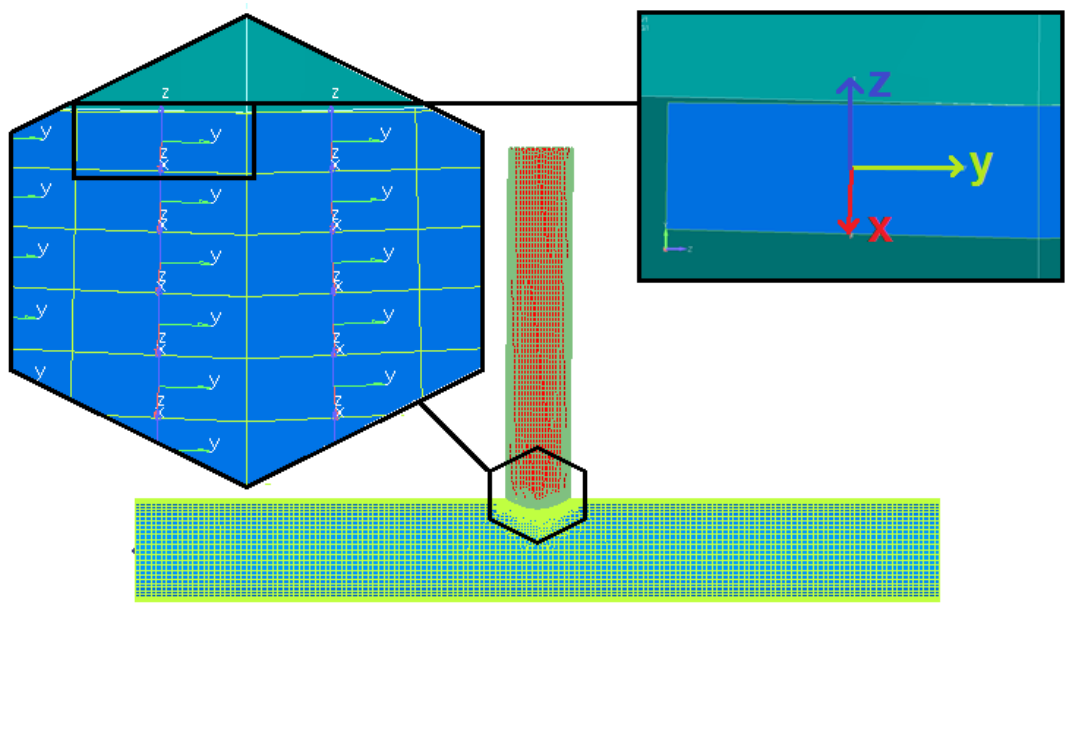


Figure 2.15: Element coordinate system

3

STRAIN GAUGE DATA ANALYSIS

This Chapter elaborates on the strain gauge measurements that were performed on one of the stinger joints. Firstly the locations and properties of the strain gauges are explained. Secondly the strain data is converted to stresses and decomposed into axial forces, in-plane and out-of-plane bending moments.

In understanding the structural behavior of the stinger structure, Allseas has performed strain measurements on a complex stinger joint. The results from these measurements have been used by previous Master students in order to research the fatigue assessment of the stinger [23] and in order to evaluate and analyse the stress and strain concentration factors in multiplanar joints [24] [25]. In this study the strain data will be used as load input for the finite element model of the stinger joint.

3.1. STRAIN GAUGE LOCATIONS

The stinger structure attached to the Solitaire vessel as depicted in Figure 1.1 is subject of investigation. The one stinger joint that has been equipped with strain gauges is shown in Figure 3.1 and highlighted by the green circle. The joint is positioned in 'section 2' on the starboard side and is a welded circular hollow section multiplanar joint. The members have complete joint penetration welds. The joint specifications are shown in Table 3.1 and Figure 3.2.

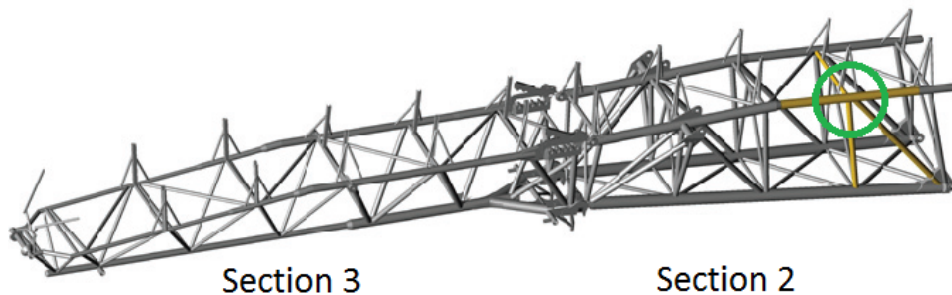


Figure 3.1: Stinger joint for strain gauge measurements

Table 3.1: Joint specifications

	d [mm]	t [mm]	L [mm]	α (= $2L/D$)	β (= d/D)	γ (= $D/2T$)	τ (= t/T)	Gap A-B [mm]	θ (in-plane)	ϕ (out-of-plane)
Chord	813	38	8223	20,23	-	10,7	-	-	-	-
Brace A	559	25,4	7760	20,23	0,69	10,7	0,67	50	134,46	0
Brace B	508	22,2	5550	20,23	0,62	10,7	0,58	50	103,93	0
Brace C	406	25,4	3935	20,23	0,5	10,7	0,67	-	90	85,45

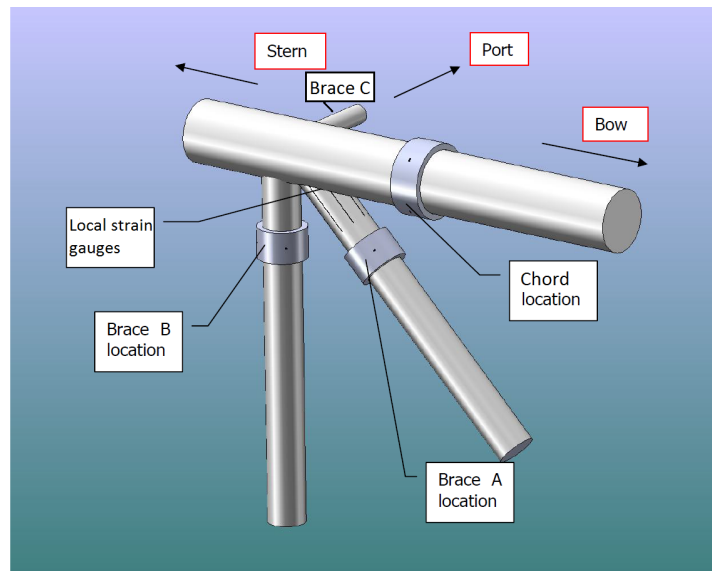


Figure 3.2: Stinger joint for strain gauge measurements

Of the 28 in total strain gauges installed, 12 are nominal strain gauges, four per member, and 16 are local strain gauges at the brace A connection. Figure 3.2 illustrates their respective locations. For this study only the data of the nominal strain gauges are used, so they are explained in more detail. The gauges are placed at one meter distance away from the weld toe for braces A and B. The nominal strain gauges on the chord are 1.48 meter away from the weld toe. It was not possible to install gauges on brace C due to the neighbouring rollerboxes.

At each location a set of four nominal strain gauges are installed and they are equally distributed around the circumference of the member, see Figure 3.3. The numbering of the 12 gauges relevant for this study are depicted in the same figure and by the following numbering:

- Brace A: nominal strain gauges A1-A4
- Brace B: nominal strain gauges B1-B4
- Chord C: nominal strain gauges C1-C4

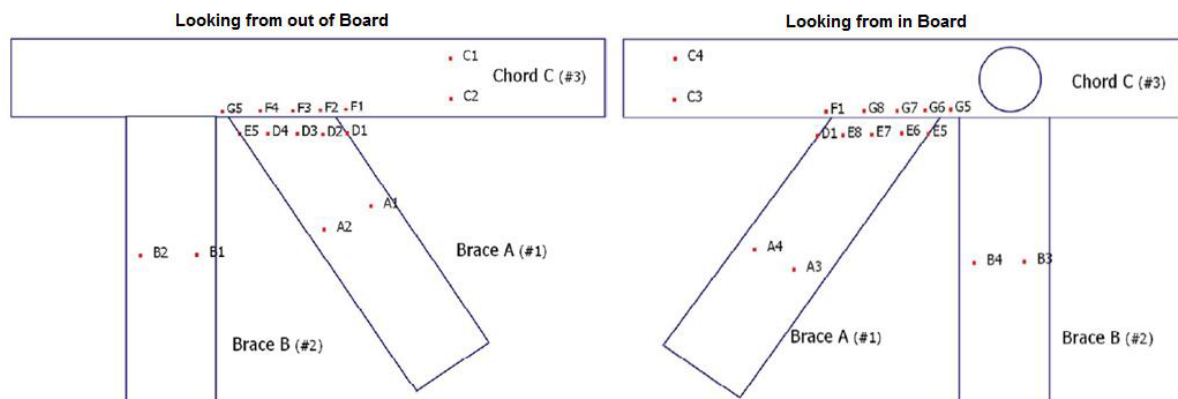


Figure 3.3: Numbering of the strain gauges

3.2. STRAIN GAUGE PROPERTIES

The properties of the nominal strain gauges are as follows [26]:

- The strains are measured along the longitudinal axis of the respective braces and chord,
- The system is only able to measure relative changes in strain, so not absolute strains,
- The maximum design strain measurement has a range of $\pm 10,000$ microstrains (1 %) and a resolution of 8 microstrain (0.008%),
- Each strain gauge bridge is temperature compensated over a temperature region from 0° C to 50° C,
- The strain of each bridge is set to zero after installation. However it is noted that the Stinger structure is already subject to strain during gauge installation,
- Each bridge is tested electronically, although it is not possible to perform a calibration test in the field,
- Each strain gauge system is connected to the corresponding data logger by a sub-sea cable.

Additionally, the more specific features of the strain gauge measurements are:

- A sampling frequency of 10 Hz,
- A data record that starts on 2009.11.20-09:00:00 and ends on 2009.12.03-24:00:00,
- A data record consisting of 29 minutes every half hour, starting from the third second of the term (e.g. from XX:00:02 or XX:30:02),
- 17430 measurements are recorded in each half hour file that is saved. This means that every file consists of 29.05 minutes of data (= 17430 : 60s : 10Hz),
- Unfortunately the data from strain gauges C1-C4 are not usable, for the gauges failed to work.

3.3. VOLTAGE TO STRAIN

As the measured data is in voltages, a conversion has to be performed in order to obtain strains. This is done by Equation 3.1

$$\epsilon = 2 * \frac{0.001 * V_0 - V_{off}}{Gaugefactor * V_e * Gain} \quad (3.1)$$

Where:

V_0 = bridge output voltage for the channel [mV]

V_{off} = offset voltage for the channel [V]

V_e = excitation voltage [V]

Gaugefactor = ratio of relative change of electrical resistance to mechanical strain

Gain = calibration factor

And the corresponding values of the just mentioned factors are given in Table 3.2 for the relevant strain gauges A1-A4 and B1-B4. C1-C4 are not mentioned, as the data is not usable.

Table 3.2: Strain gauge parameters

Location	V_{off}	V_e	Gain	Gaugefactor
A1	1.441	2.5078	48.1097	2.04
A2	1.445	2.5078	48.1779	2.04
A3	1.459	2.5044	47.9733	2.04
A4	1.399	2.5044	48.0415	2.04
B1	1.455	2.5094	47.9733	2.04
B2	1.235	2.5094	47.9733	2.04
B3	1.244	2.5139	47.9733	2.04
B4	1.178	2.5139	48.1097	2.04

3.4. DATA SELECTION

For this study not all data terms are considered. A first selection is made based on two factors:

1. Data terms when the vessel is laying pipe are of interest,
2. Data terms when the vessel is pulling are of interest.

For the fatigue assessment of the stinger structure the load variations are important. Hence, the data terms with the greatest load variations are desired for further investigation from a fatigue point of view. The greatest variations are achieved when the vessel is operational, thus laying pipe. From the Daily Progress Reports from the Solitaire vessel the information necessary is obtained, resulting in a selection of time slots when the Solitaire is laying-pipe.

For the second factor, the 'pull', the vessel its tensioners are doing hard work. The data of the tensioners speeds are a good indicator of the exact moments when the pipe-laying is taking place. The Daily Progress Reports and the tensioner records are combined in order to come up with the first time slot selection as shown in Table 3.3.

Table 3.3: Time slots of pipe-laying

Date	Time	Job
20-11-2009	12:30-24:00	Lay pipe
21-11-2009	00:00-13:00	Lay pipe
27-11-2009	22:30-23:30	Lay pipe
28-11-2009	00:00-24:00	Lay pipe
29-11-2009	00:00-24:00	Lay pipe

The final data series that will be used for this study are taken from the date 20-11-2009 from 12:30-13:00. For the investigation into the change of principal stress direction during loading the first 100 data points are used, which is equal to a period of 10 seconds. For the HSS determination at brace A 500 data points are used from data point 3200 to 3700.

3.5. STRAINS TO STRESSES

This section shows the method to obtain the axial force, in-plane bending moment and out-plane bending moment. These three force components are used as input for the finite element modelling.

3.5.1. STRAIN MEASUREMENTS

The starting point in the process of obtaining the force components are the strain measurements. As explained in Chapter 3.2, braces A and B each have four strain gauges that measure only unidirectional strain, see Figure 3.4 for the gauge locations and numbering. With these measurements it is possible to obtain the axial force and bending moments in the braces. Throughout this chapter, for example purposes, each time

only 1000 data points of just one data series are used. In this way the results are more clear. The basis of the following calculations are the original strains, as shown in Figure 3.5.

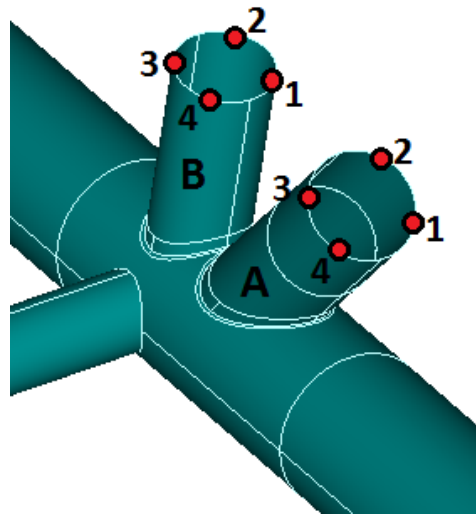


Figure 3.4: Joint under investigation with the strain gauge locations.

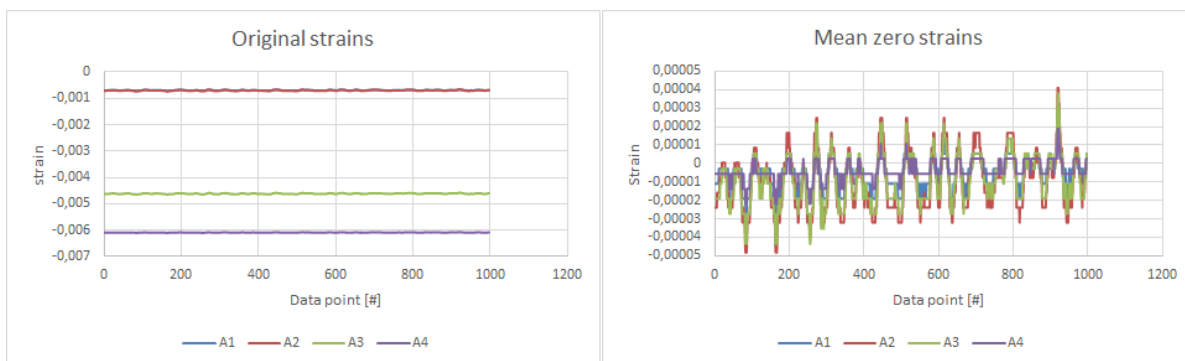


Figure 3.5: Original Strains

Figure 3.6: Mean Zero Strains

Firstly the data from the measurements is such that it is influenced by the initial forces in the structure. There is a difference in time between the placement of the strain gauges and the start of the measurements. This results in a situation where the data is biased in a way that it is difficult to draw any conclusions on the meaning of it. Therefore it is important to know the starting point of the measurements to be able to use the data correctly. The starting point is assumed to be the static load consisting of the self-weight of the stinger structure, the buoyancy and the rollerbox loads. From the original strains graph it can be seen that the means of the four strain gauges are different. Assuming the starting point to have a value of zero, the means of the measurements are subtracted to obtain the mean zero strains, see Figure 3.6. This gives the strain variation around the zero mean value. To obtain the starting point at the strain gauges, a statics check is performed using the software Staad.Pro. Figures 3.7 and 3.8 show the strain gauge locations of braces A and B, together with the plane location of the cross-section where the stresses were obtained. As can be seen, Staad.Pro has a member coordinate system for each member individually, where the x-axis is parallel to the longitudinal direction of the corresponding brace.

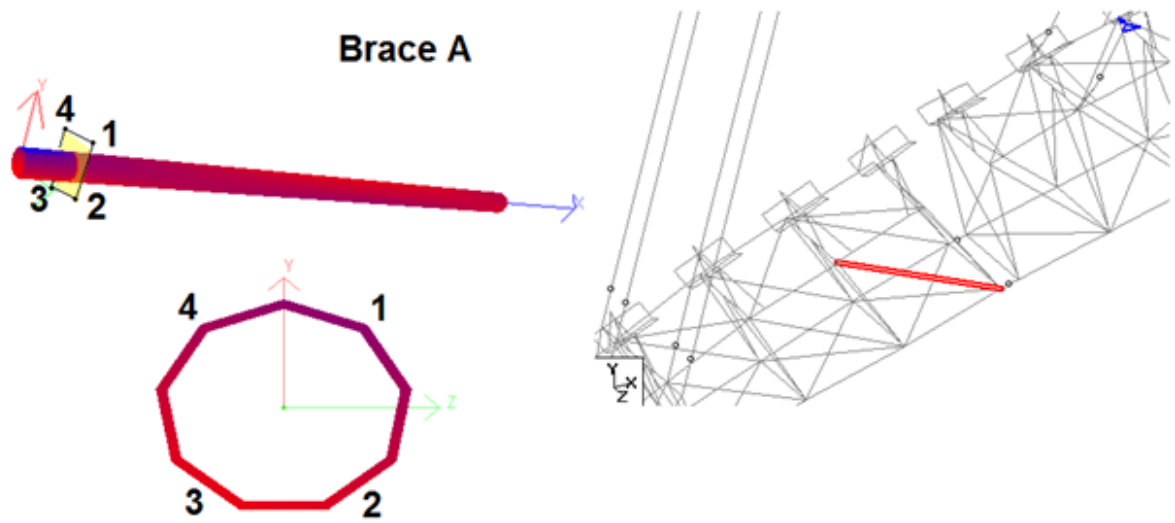


Figure 3.7: Brace A within the Staad.Pro model with the strain gauge locations depicted

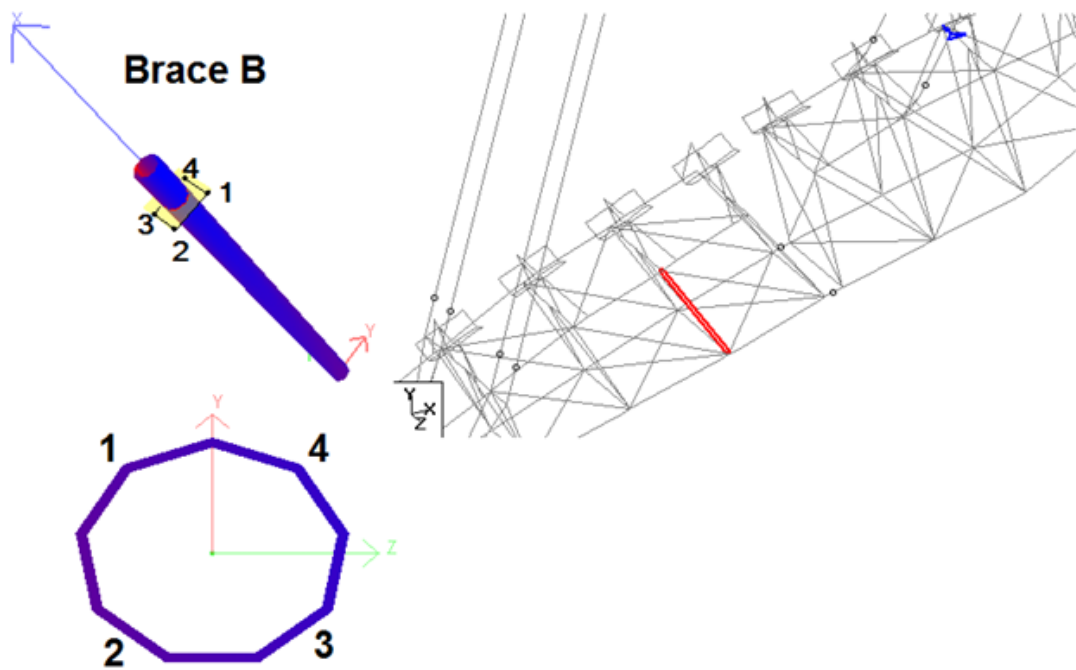


Figure 3.8: Brace B within the Staad.Pro model with the strain gauge locations depicted

3.5.2. STATICS CHECK

The software Staad.Pro is used by Allseas Engineering B.V. to perform structural analysis. In this thesis the software is used to do a statics check after applying self-weight, buoyancy and rollerbox loads to the structure. The configuration of the stinger is based on information acquired from the Daily Progress Reports, Allseas' Pipelay Procedure of the project and corresponds with the stinger drawing in Appendix A.

SELF-WEIGHT

The self-weight of the structure is calculated by Staad.Pro itself and applied on the complete structure. The software applies the load as uniformly distributed. As an example, See Figure 3.11 for the In-plane (M_z) and out-of-plane (M_y) bending moment, and Figure 3.12 for the axial force due to self-weight in Brace A.

BUOYANCY

The buoyancy is applied as a percentage of the body weight, but in the opposite direction. The buoyancy is calculated using the pipe properties of the structure, which are the nodal coordinates to determine the pipe lengths in combination with the corresponding outer diameters. Only the chords and braces under the waterline (-25m to 0m) are taken into account, see Figure 3.10. The buoyancy force is equal to 4.6 MN. The self-weight calculated by Staad.Pro is equal to 10.5 MN. This means that the buoyancy force equals 44 percent of the selfweight and this percentage will be applied on the model in positive y-direction. Figures 3.13 and 3.14 present the resulting forces due to buoyancy in Brace A.

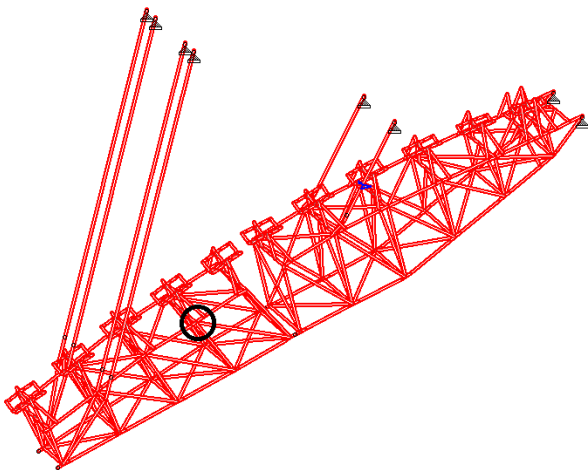


Figure 3.9: Selfweight applied on complete model with the relevant joint under investigation indicated by the black circle.

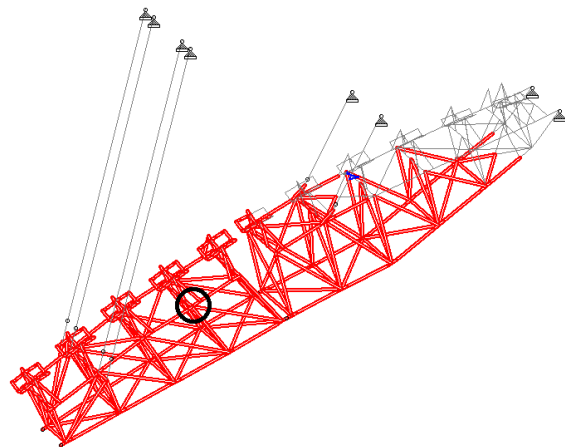


Figure 3.10: Buoyancy applied on part of structure under the waterline with the relevant joint indicated by the black circle.

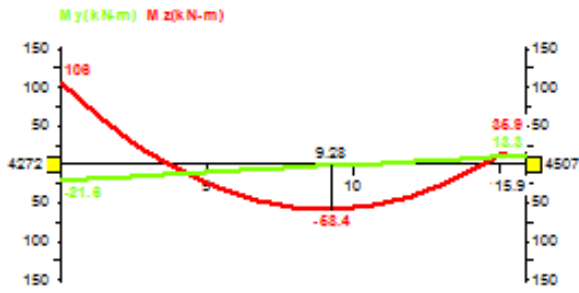


Figure 3.11: Brace A: Bending Moments due to SelfWeight

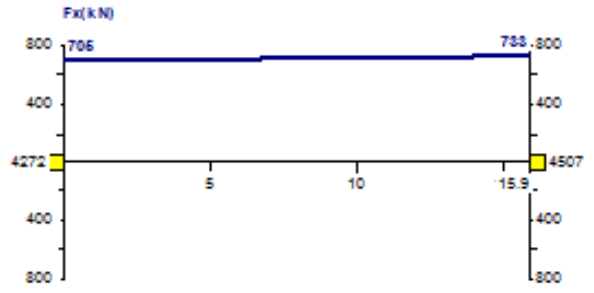


Figure 3.12: Brace A: Axial Force due to Selfweight



Figure 3.13: Brace A: Bending Moments due to Buoyancy

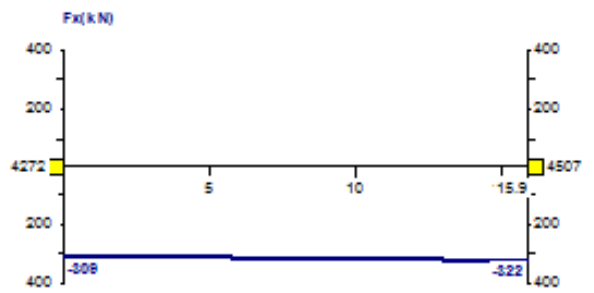


Figure 3.14: Brace A: Axial Force due to Buoyancy

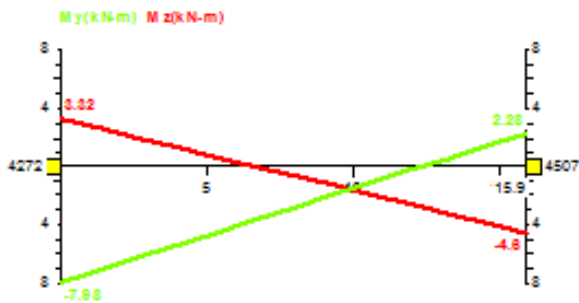


Figure 3.15: Brace A: Bending Moments due to Rollerbox Loads

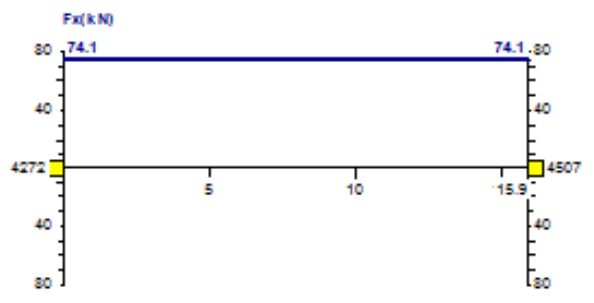


Figure 3.16: Brace A: Axial Force due to Rollerbox Loads

ROLLERBOX LOADS

The pipe that is laying on the structure is responsible for forces acting on the stinger. The pipe is guided towards the seabed with the help of rollerboxes. The locations where the pipe is in contact with the rollerboxes experience the load, and this load is applied on the centre node of the corresponding rollerbox in the model, as depicted in Figure 3.17. The values are obtained from an OFFPIPE analysis performed for this project for KP20.950-0.000 with a water depth of 71.8m and a pipe diameter of 24 inch. This corresponds with the KP at the time of measurements of around KP20.690. KP stands for Kilometer Point and explains the location with respect to the total pipeline length. The in-plane (M_z) and out-of-plane (M_y) bending moments are shown in Figure 3.15 and the axial force due to the rollerbox loads is shown in Figure 3.16.

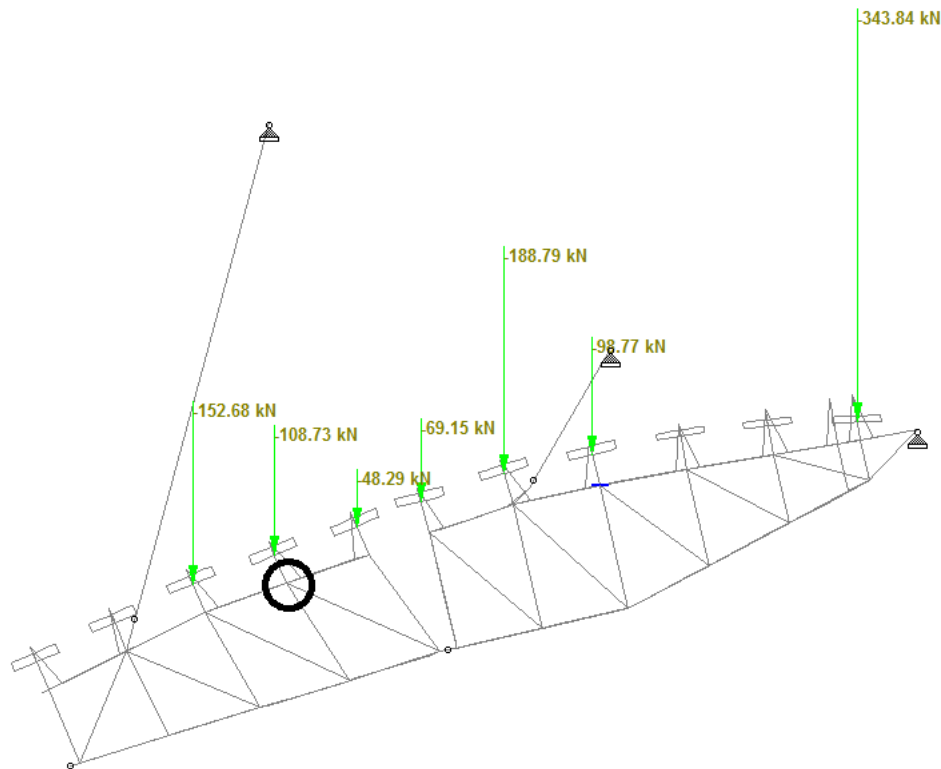


Figure 3.17: Rollerbox loads applied on the corresponding nodes in the model with the joint under investigation indicated by the black circle.

RESULTING STATIC STRESSES

The desired output of the Staad.Pro analysis is the stress level at the locations of the strain gauges. These values will be added to the stress ranges that will be calculated later. The stresses are within the elastic limit, so this is allowed. The stresses will be converted to forces and bending moments, but that will be explained in Section 3.6. In Figure 3.18 the stress at location 1 of Brace A is given. The point closest to the outside of the pipe and with an angle of 45 degrees with the y and z-axes is chosen, for that is by approximation the location of the strain gauge. This is done for all strain gauges and Table 3.4 shows the stresses for Braces A and B, and Chord C. From these results, it can be concluded that Brace A is in tension and Brace B is in compression.

Table 3.4: Static Stresses at strain gauge locations

Location	A1	A2	A3	A4	B1	B2	B3	B4	C1	C2	C3	C4
Stress [MPa]	3.55	14.23	18.68	8.14	-13.70	-9.57	-0.67	-4.52	3.44	3.72	-0.98	-1.41

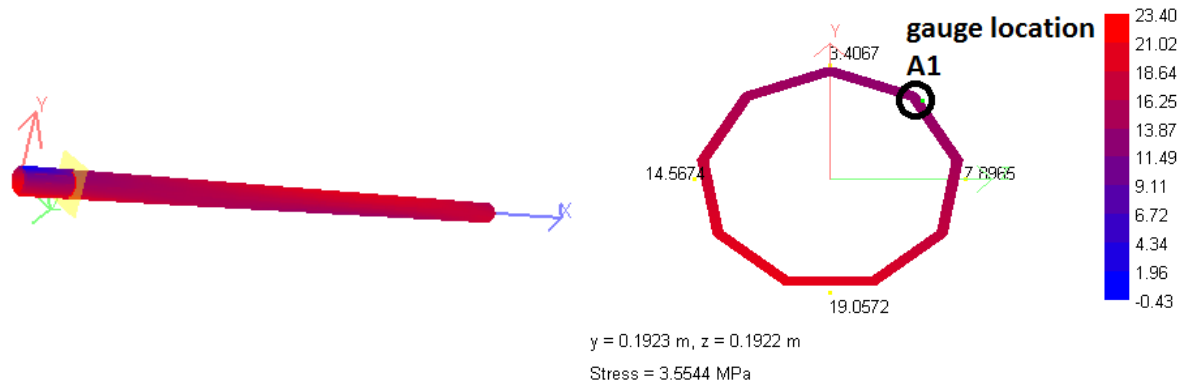


Figure 3.18: Resulting static stress in Brace A at strain gauge location 1

TIME TRACE OF TOTAL STRESSES

With the static stresses and strain ranges determined, the next step is to add them together to obtain the time trace of total stresses. In order to do this, firstly the strain variation has to be converted to stress variation. This is done using Hooke's law by assuming linear-elastic behaviour of the material:

$$\sigma = [constant] = E\epsilon \quad (3.2)$$

where

σ = stress [Pa]

E = Modulus of Elasticity[Pa]

ϵ = strain [-]

The time trace of total stresses, so after adding the stress variation to the static stresses, of the four gauges on Brace A is depicted in Figure 3.19.

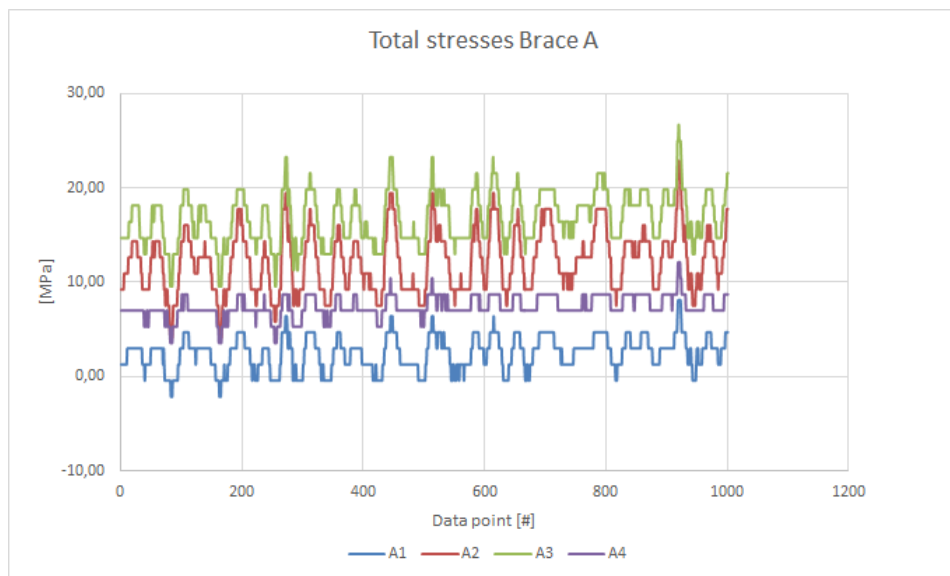


Figure 3.19: Total Stresses at the strain gauge locations of Brace A

3.6. STRESSES TO FORCES

For the finite element modelling it is important to have a usable input. Stresses are not suited and thus it is needed to decompose the stresses into corresponding forces, namely axial force, in-plane bending moment and out-of-plane bending moment. In addition, it is widely accepted to use member forces for tubular joint analyses.

3.6.1. AXIAL FORCE

Firstly the axial forces of the braces at the location of the strain gauges are determined. This can simply be done by averaging the value of the total stresses at any point in time:

$$\sigma_{average} = \frac{\sigma_1 + \sigma_2 + \sigma_3 + \sigma_4}{4} \quad (3.3)$$

The average stress $\sigma_{average}$ is multiplied with the cross-sectional area of the brace to end up with the axial force:

$$F_{axial} = \sigma_{average} * A \quad (3.4)$$

Figure 3.20 shows the axial force in both Brace A and B for the first thousand data points.

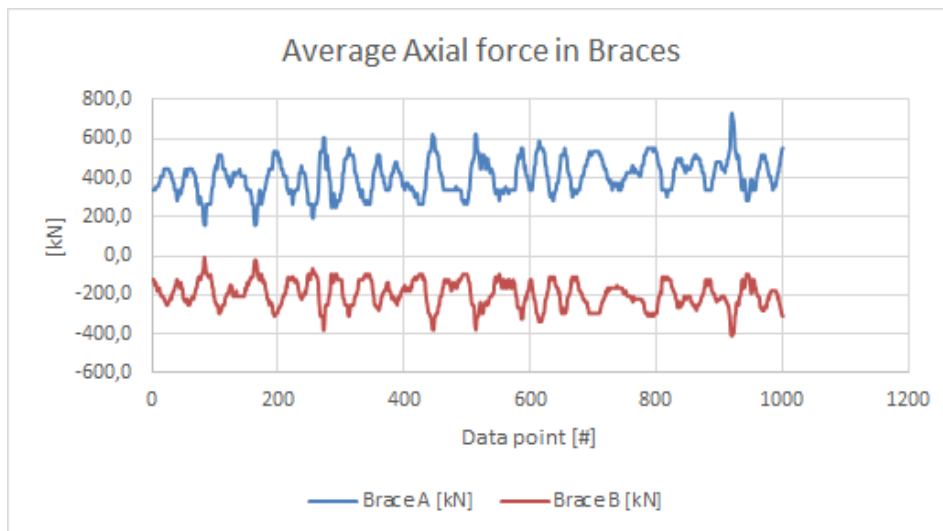


Figure 3.20: Axial force in Braces A and B

3.6.2. BENDING MOMENT

With the axial forces calculated, the bending moments can be calculated next. The stresses due to bending are the stresses that remain after the contribution due to axial forces is taken out of the equation:

$$\text{Stresses due to bending} = \text{total stresses} - \text{axial force stresses}$$

Then with the simple beam theory the in-plane and out-of-plane bending moments can be calculated.

$$\sigma = \frac{M * y}{I} \rightarrow M = \frac{\sigma * I}{y} \quad (3.5)$$

where:

σ = stress at location of interest [Pa]

M = Bending Moment [Nm]

I = second moment of inertia [m^4]

y = distance from neutral axis to location of interest [m]

$$I = \frac{\pi}{4}(r_{out}^4 - r_{in}^4) \quad (3.6)$$

Where r_{out} and r_{in} are the outer and inner radius of the pipe in meters. As the strain gauges are located at 45 degrees with respect to the y and z-axes, for convenience the locations A, B, C and D are chosen for the bending moment calculations. The stresses at these locations are calculated by using the two neighbouring gauge locations, see Formulae (3.7-3.10) and Figure 3.21:

$$\sigma_A = \frac{1}{2}\sqrt{2}(\sigma_1 + \sigma_4) \quad (3.7)$$

$$\sigma_B = \frac{1}{2}\sqrt{2}(\sigma_1 + \sigma_2) \quad (3.8)$$

$$\sigma_C = \frac{1}{2}\sqrt{2}(\sigma_2 + \sigma_3) \quad (3.9)$$

$$\sigma_D = \frac{1}{2}\sqrt{2}(\sigma_3 + \sigma_4) \quad (3.10)$$

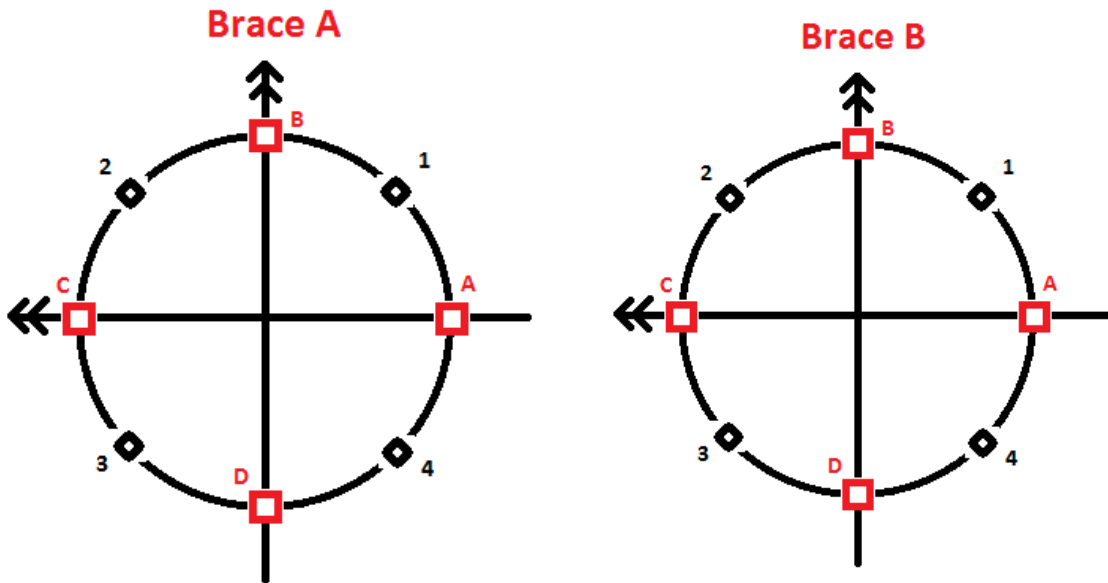


Figure 3.21: The strain gauge locations 1-4 and the locations used for bending moment calculations A-D

The stresses at locations A and C are used to calculate the in-plane bending moment, whereas σ_B and σ_D are used to calculate the out-of-plane bending moment:

$$M_{ipb} = \frac{\sigma * I}{y} = \frac{0.5(|\sigma_A| + |\sigma_C|) * I}{r_{out}} \quad (3.11)$$

$$M_{opb} = \frac{\sigma * I}{y} = \frac{0.5(|\sigma_B| + |\sigma_D|) * I}{r_{out}} \quad (3.12)$$

The average value of the two opposite strain gauges is used. However, the opposite values are identical except for the sign, as can be seen in Table 3.5. This is also an indication that the calculations have been performed correctly, for it would be logical that opposite locations have identical absolute values, assuming pure bending. The bending moment directions are according to the axes in Figure 3.21. The different bending moments for Braces A and B are depicted in Figure 3.22 .

Table 3.5: Average stresses during measurements at locations depicted in Figure 3.21

Location	1	2	3	4	A	B	C	D	
Brace A	-7.6	3.08	7.53	-3.01	-7.5	-3.19	7.5	3.19	[MPa]
Brace B	-6.59	-2.45	6.45	2.59	-2.83	-6.39	2.83	6.39	[MPa]

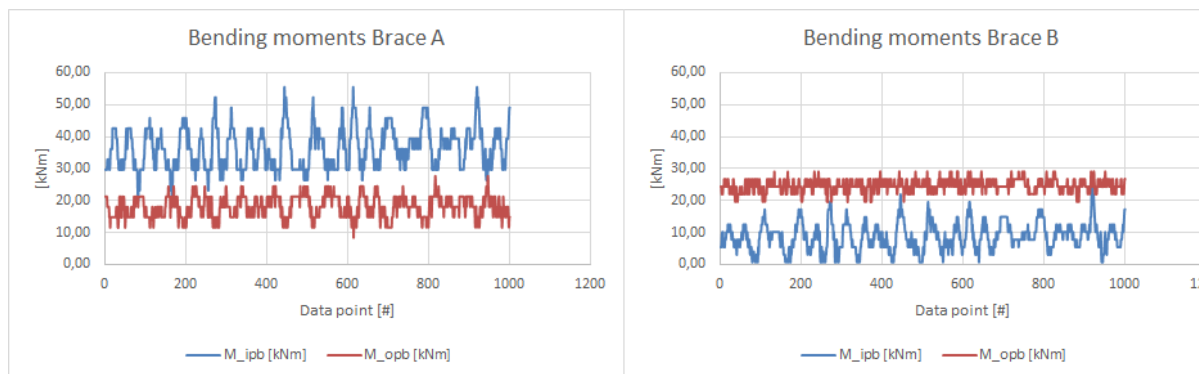


Figure 3.22: In-plane and out-of-plane bending moments in Brace A

As an extra check, the average bending moments of the complete data set are determined and compared with the static bending moments given by Staad.Pro, see Table 3.6. The negative value of Staad.Pro for the out-of-plane bending moment of Brace A is due to the direction of the axis chosen by the software. In the manual calculations the axis is chosen in the opposite direction compared to Staad.Pro. The percentage difference does not exceed 6.12 percent, which indicates that the calculations have been performed correctly.

Table 3.6: Comparison of Bending Moments

		Staad.Pro [kNm]	Calculations [kNm]	Difference [%]
Brace A	M_{ipb}	42.74	40.2	6.12
	M_{opb}	-17.99	17.12	4.96
Brace B	M_{ipb}	11.34	11.08	2.32
	M_{opb}	26.00	25.00	3.92

3.6.3. LOAD ANALYSIS

A first look at the three load components in Figure 3.23 gives a good indication of the stochastic Variable Amplitude loading the stinger is subjected to, see Figure 2.9. These data points are the first hundred from the top time slot in Table 3.3. Although the peaks seem to occur more or less at the same time, the high volatility implies that there is non-proportional loading, as explained in Section 2.3.1. However, the level of non-proportionality can not be concluded directly from these graphs. That is why the change in principal stress direction during loading is investigated using these time histories, for that is an indication of the level of non-proportionality.

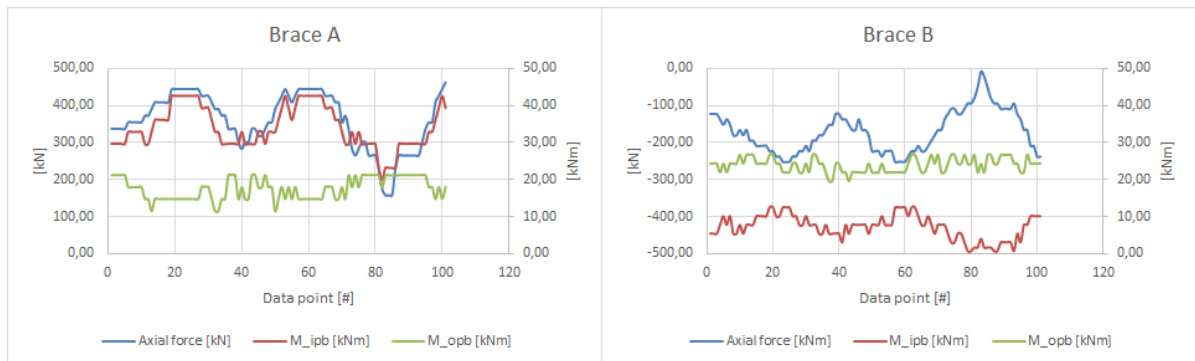


Figure 3.23: Load components acting on braces A and B

4

FINITE ELEMENT MODELS

The finite element method originated from a need to solve complex structural problems. With upcoming computation capabilities and improvements in the field of computer simulation nowadays there exists a wide variety of finite element software. From all available software only one program is chosen for this research. The decision is based on the company's expertise within their structural engineering department. Their mostly used finite element software is Femap, that uses NX Nastran code for analyses. Together with the advice of several experienced users within the company, it was concluded that Femap should be suitable for this investigation.

This study is mainly built around finite element models. Two main investigations can be distinguished:

- Stinger joint
- Simple T/Y-joints

The following chapter elaborates on the creation of the finite element models. Firstly the specifications of the Stinger joint model are given. Secondly the method of creating the T/Y-joints is presented in detail.

4.1. STINGER JOINT

4.1.1. ELEMENT TYPE

Roughly two types of finite element models can be distinguished for the analysis of welded tubular joints: solid models and shell models. Solid models normally require a longer computation time compared to shell models, because of a higher number of elements. In addition, creating a solid model is more complex than creating a shell model. An advantage is that solid models can provide more accurate stress and strain results. For welded tubular joints this is partly due to the reason that the weld can be better modelled.

However, a negligible stress perpendicular to the tubular surface, σ_z , results in a plane stress assumption. Assuming this leads to the acceptance of shell modelling.

The shell model is created by using the mid-surfaces of the joint member walls and the corresponding joint dimensions, as given in Table 3.1. Figure 4.1 shows the Femap shell model. No weld is modelled. At the locations where the braces connect to the chord the mesh is refined to accurately capture the desired output, as can be seen in Figure 4.2. The mesh refinement will be explained further in the next section.

4.1.2. MESH REFINEMENT

Mesh refinement is an important aspect of modelling, for it determines the accuracy of the results. According to DNV [2] in case of using shell elements, 8-noded elements are recommended with a mesh size from $t \times t$ to $2t \times 2t$. However, due to unsolved issues with the Femap program, 4 noded elements are used with a finer mesh size so the stress gradients are still captured properly. This increases the number of elements by a factor of 4, as illustrated in Figure 4.3, and increases the computational time of the model. However, the computational time still remained within one hour which is acceptable.

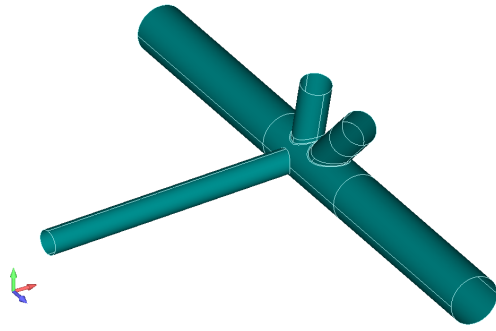


Figure 4.1: Shell model of the Stinger joint

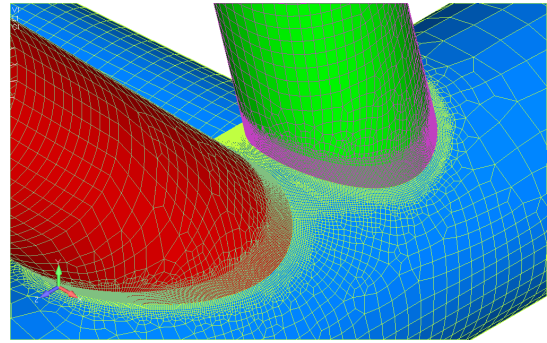


Figure 4.2: Finer mesh at the brace-chord connections

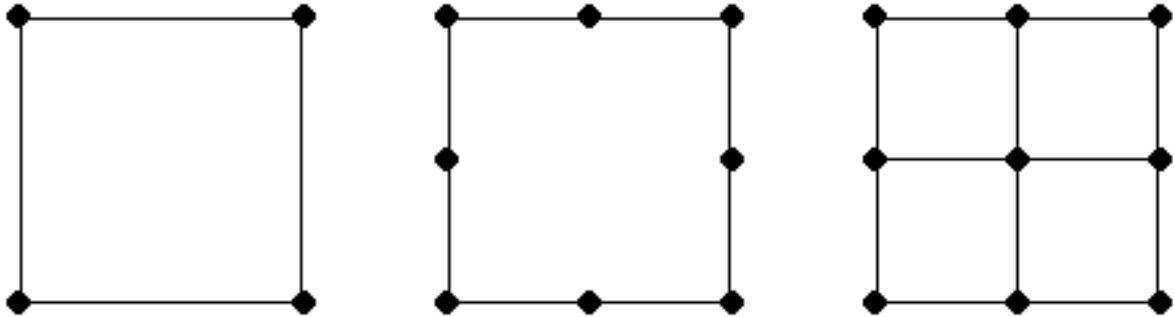


Figure 4.3: Shell element: (l) 4 noded, (c) 8 noded, (r) four times 4 noded

TWO MODELS WITH DIFFERENT MESH REFINEMENT

Two finite element models of the Stinger joint are created. One to check the variation of principal stress directions during loading at all brace to chord connections. A second model is created to check the difference in hot spot stresses between extrapolating primary stresses versus extrapolating principal stresses. The second model only focuses on the connection of the Chord with Brace A.

The difference between these two models is the mesh refinement around the connection areas. For the first investigation the mesh needs to be refined at all connections, see Figure 4.2. For the investigation into the hot spot stresses, only one connection needs to be refined. The reason for the second mesh refinement is the need for a sufficient extrapolation length. This is necessary in order to be able to extract the values at the extrapolation locations at a specified distance away from the welded connection, as explained in Section 2.2.6. The difference between the two models is shown in Figures 4.4 and 4.5, zoomed in on the gap area.

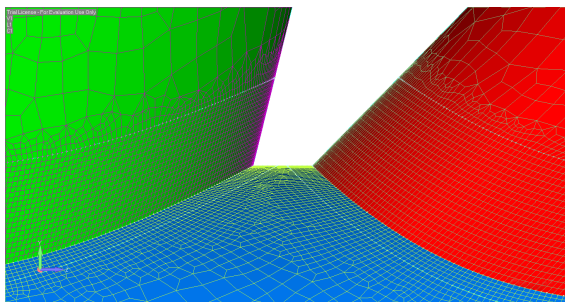


Figure 4.4: Mesh refinement model for principal stress direction determination

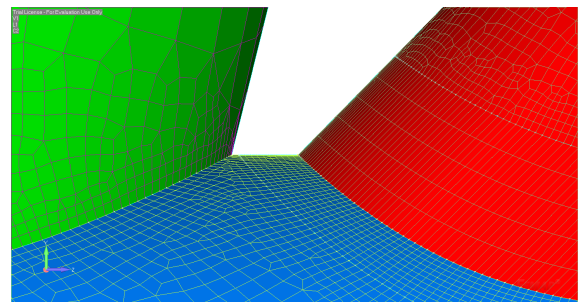


Figure 4.5: Mesh refinement model for Hot spot stress determination

4.1.3. SPIDER NODES

The constraints and loads are applied on spider nodes. These are superelements that create a rigid node at the ends of the tubular members exactly in the center connected to the nodes on the mid-surface. This is illustrated in Figure 4.6. These spider nodes make it easy to apply axial forces, in-plane bending moments and out-of-plane bending moments.

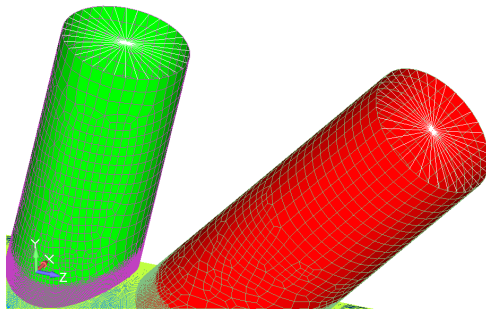


Figure 4.6: Spider nodes

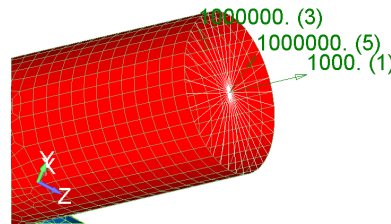


Figure 4.7: Loads on Brace A; Axial force (1), IPB moment (5), OPB moment (3)

4.1.4. BOUNDARY CONDITIONS

The finite element models need to be constrained in a correct way to capture reality as accurately as possible. In previous research [25] six different boundary condition combinations were tested by calculating the Von Mises maximum stress. Combinations 1 and 2 in Figure 4.8 led to the highest Von Mises stress. Combination 6, the fixed chords showed the lowest Von Mises stress.

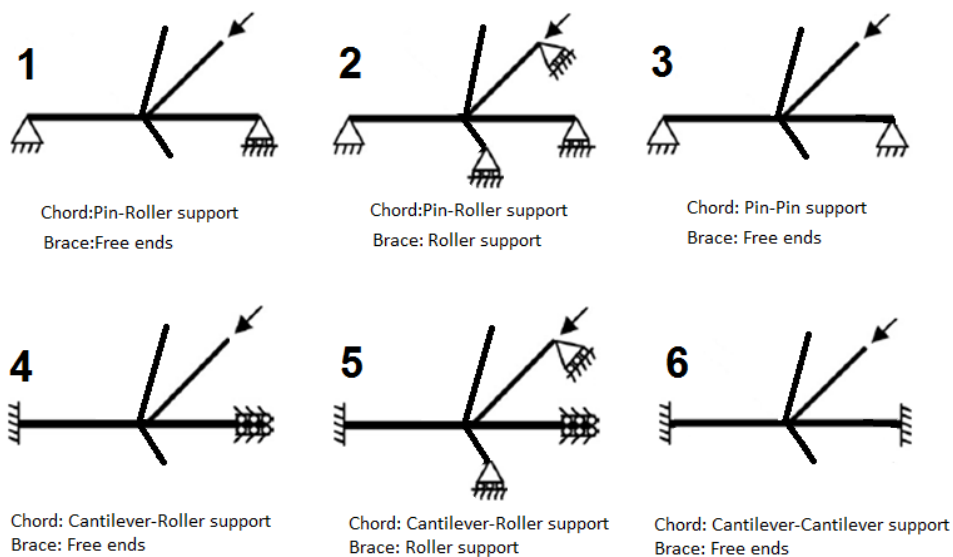


Figure 4.8: Boundary conditions tested on maximum Von Mises stress

The above results together with external advice of dr.A. Romeijn (personal communication) led to the decision to analyse two different boundary condition combinations, namely an all fixed case and a pinned-rollers case, illustrated in Figure 4.9. The rollers allow translation in the parallel brace/chord direction only.

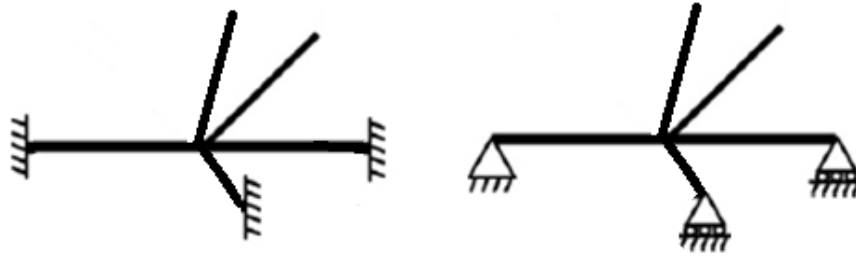


Figure 4.9: Boundary conditions used, left: all fixed, right: pinned-rollers

4.1.5. LOADS

In Chapter 3 the strain data of the nominal strain gauges on braces A and B is converted to axial forces, in-plane bending moments and out-of-plane bending moments. This resulted in individual time histories for each load component. In fact, the time histories consist of data points obtained by measuring at 10 Hz. Each data point is used to create a function in Femap. Figure 4.10 shows an example of the time history of the axial force in brace A. The figure shows the function type to be 'vs. Time'. The creation of functions is necessary to be able to perform the analysis within Femap, in combination with the analysis type 'transient dynamic/time history'.

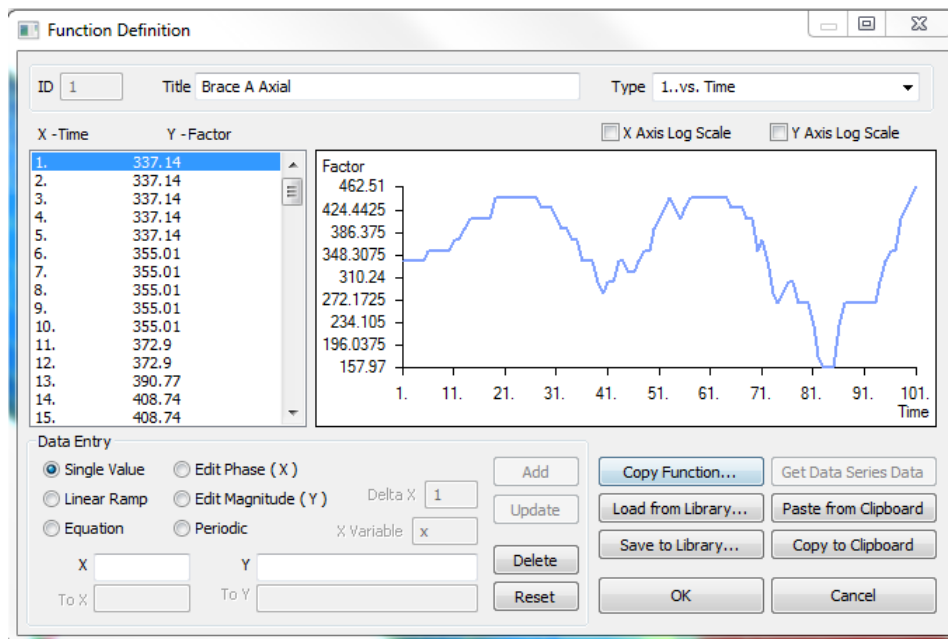


Figure 4.10: Femap function of the axial force in Brace A

Axial forces The axial forces are applied in the direction parallel to the corresponding brace. The axial forces are in kiloNewton. As in Femap the input is Newton, the standard value is 1000, as depicted in Figure 4.7 by (1).

Bending moments The in-plane and out-of-plane bending moments are depicted in Figure 4.7 by (5) and (3) respectively. The input of the bending moments is in kNm, which explains the 1,000,000, as Femap units for this model are in Newton and millimetres. The bending moments are applied within the coordinate systems of the braces.

The time histories that are used as load input are shown in Figure 3.23 for braces A and B respectively. As brace B is in constant compression, the axial forces are negative. The in-plane bending moment on brace A is bigger than the out-plane bending moment. For Brace B this is the opposite.

4.1.6. ANALYSIS TYPE

For the stinger joint research the analysis type is *linear quasi-static*. Still the stresses are below the elastic limit, which allows to assume linearity. The difference between the T/Y-joint research is the load input. There the load is just a single axial force applied at one time. In contrast, for the stinger joint the load input consists of six separate 'time histories', namely:

1. Brace A
 - (a) Axial force
 - (b) In-plane bending moment
 - (c) Out-of-plane bending moment
2. Brace B
 - (a) Axial force
 - (b) In-plane bending moment
 - (c) Out-of-plane bending moment

The term 'time history' is used for convenience. As mentioned above, the analysis will be quasi-static, which means that no dynamic effects are taken into account, e.g. inertia. So in fact the term 'time' is not correct, as that implies also dynamic effects.

Within Femap, the analysis type used is called 'transient dynamic/time history'. To avoid the dynamic effects, the time step is chosen such that it exactly matches the data points. This means that Femap only uses the data points for calculations, not the values between data points. This creates output data that shows the results at those exact moments only. This is in this case the meaning of quasi-static analysis: each time step is calculated individually and independently and results are a reflection of only the load input at that particular point. The 'transient dynamic/time history' type thus makes it easy to run multiple analyses at once by using functions, instead of running each data point one at a time by hand.

4.1.7. DESIRED OUTPUT

The output that is of interest for the stinger joint models is twofold:

Principal stress angles around the brace-to-chord connections. For the study into the change in principal stress directions during loading, the output required from Femap are the elemental principal stress angles. The variation of the angle around the zero mean is calculated. So any initial principal stress angle is not taken into account. So the results can be seen as taken from the center of that element. The locations of the elements are at a distance of half times the wall thickness of the respective chord or brace away from the connection. As only the change in angle is of importance, it is not necessary to align the material direction of the elements. This is important for the next study, as explained below.

Principal stresses and primary stresses perpendicular to the weld toe at the chord saddle location at the brace A connection. For the study into the difference between Hot Spot Stresses the nodal results of the stresses and angles are required at specified distances away from the welded connection: at extrapolation locations A and B, see Figure 4.13. Compared to the study into the change of principal stress angles during loading this time only the chord saddle location at the brace A connection is investigated. The process is explained further in section 4.2.8.

4.2. T/Y-JOINTS

4.2.1. ELEMENT TYPE

Just like the finite element model of the Stinger joint, the T/Y-joints are created with 4 noded shell elements.

4.2.2. MESH REFINEMENT

The mesh refinement for the T/Y-joints is similar to the stinger joint model. The mesh is refined such that the stress gradient is accurately captured along the brace-to-chord connection, as can be seen in Figure 4.11. The curve on the chord which runs parallel to the brace-to-chord intersection curve has a distance such that the extrapolation locations remain within the refined mesh area. At the chord saddle location, a perpendicular curve is projected on the chord that connects the two parallel curves. The extrapolation points A and B are located on this perpendicular curve.

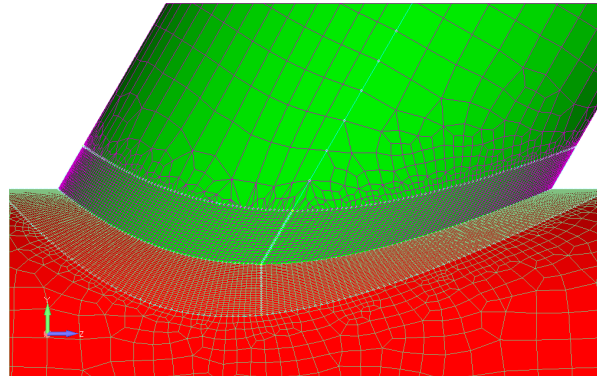


Figure 4.11: Mesh refinement at the brace-to chord connection

4.2.3. API-SCRIPT

Femap has the ability to communicate with languages like Visual Basic, VBA (Excel, Word, Access), C, or C++. This makes it possible to write a script in for example Microsoft Visual Studio Express 2013 and when one runs this script, a model will be created in Femap. The functions that are available in the User Interface of Femap can in that way be programmed as a routine.

This is exactly what has been done for this thesis. A script has been written and connected to the Femap environment. With this script it is possible to easily create a T/Y-joint with specified joint dimensions and to analyse it. The choice of joint dimensions has effect on the joint parameters γ , τ , β and θ . The length parameter α is dependent on chord diameter and length and is kept constant for all configurations, namely $\alpha = 15$. The exact script can be found in appendix B and the different joint configurations that have been created and analysed are given next.

4.2.4. JOINT CONFIGURATIONS

The dimensions for all 13 configurations are based on pipes that are fabricated following Trouvay & Cauvin standards, [27]. Additionally the pipe dimensions are chosen such that they are in close correspondence with the dimensions used by Allseas Engineering B.V. for their Stinger Structures, in order to increase the relevance of this research for the company. For convenience the dimensions in Table 4.1 are given in inches. Within Femap millimetres are used, obtained by multiplying inches by a factor of 25.4. All joint configurations can be found in Appendix C.

4.2.5. BOUNDARY CONDITIONS

Both chord ends are fixed, see Figure 4.12 for a graphical representation.

4.2.6. LOAD

The load applied on the model is an axial force in the direction parallel to the brace longitudinal axis, as indicated by the arrow in Figure 4.12. The size of the force is chosen such that it equals a nominal stress in

Table 4.1: Dimensions and joint parameters of the FEM configurations

Conf. #	Dimensions				Joint parameters			
	Diameter Chord [inch]	Diameter Brace [inch]	Wall Thickness Chord [inch]	Wall Thickness Brace [inch]	θ [Degrees]	τ	β	γ
1	32	20	1.25	0.25	45	0.2	0.63	12.8
2	32	20	1.25	0.75	45	0.6	0.63	12.8
3	32	20	1.25	1	45	0.8	0.63	12.8
4	32	20	1.25	1.25	45	1	0.63	12.8
5	32	6.625	1.25	0.75	45	0.6	0.21	12.8
6	32	12	1.25	0.75	45	0.6	0.38	12.8
7	32	26	1.25	0.75	45	0.6	0.81	12.8
8	40	24	1.25	0.75	45	0.6	0.60	16
9	32	20	0.625	0.375	45	0.6	0.63	25.6
10	40	24	0.625	0.375	45	0.6	0.60	32
11	32	20	1.25	0.75	30	0.6	0.63	12.8
12	32	20	1.25	0.75	60	0.6	0.63	12.8
13	32	20	1.25	0.75	90	0.6	0.63	12.8

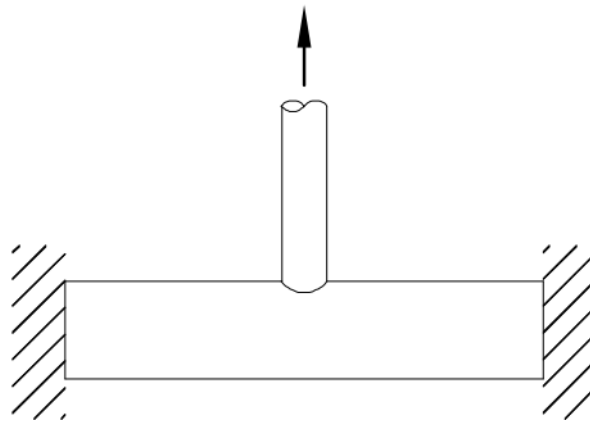


Figure 4.12: Configuration with fixed chord ends and axial force on brace

the brace of 1 MPa. This makes it easy to calculate the SCF, as the SCF is then the exact same value as the extrapolated hot spot stress. In order to achieve the 1 MPa nominal stress for all joint configurations, the script uses the input dimensions to calculate the corresponding axial force with the simple equation :

$$F = \frac{\sigma_N}{A} \quad (4.1)$$

Where F is the axial force in N, σ_N is the nominal stress of, in this case, 1 MPa and A is the area of the brace cross-section in mm^2 .

4.2.7. ANALYSIS TYPE

The study of the T/Y-joints involves a *linear-elastic static analysis*.

4.2.8. DESIRED OUTPUT

The output that is of interest is located at the extrapolation points A and B, as depicted in Figure 4.13. These points are located on a curve perpendicular to the weld at the saddle location of the joint. The results are obtained as follows:

1. Femap analyses the load case with specified constraints and loads

2. The following results are copied to Excel:
 - (a) Element corner results at extrapolation location A (see Figure 4.13)
 - (b) Element corner results at extrapolation location B (see Figure 4.13)
3. The results of the four element corners closest to the node of interest are averaged
4. The averaged result is considered the nodal result
5. Results considered are:
 - (a) Plate top major/minor Principal stress and strain
 - (b) Plate top Principal stress and strain *angle*
 - (c) Plate top X normal stress and strain
 - (d) Plate top Y normal stress and strain
 - (e) Plate top XY shear stress and strain

The strains are used for the research into the ratio between SCF and SNCF. Averaging of the corner results is accepted in case the difference between the elemental results is small. This is achieved by refining the mesh size.

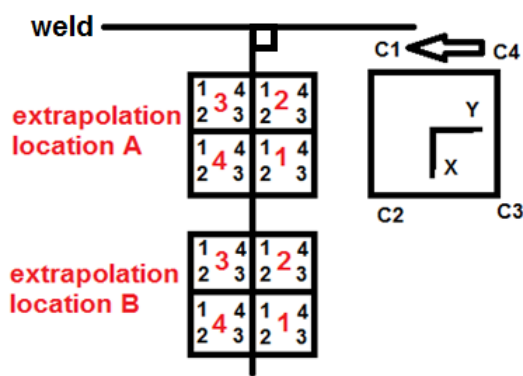


Figure 4.13: Extrapolation locations

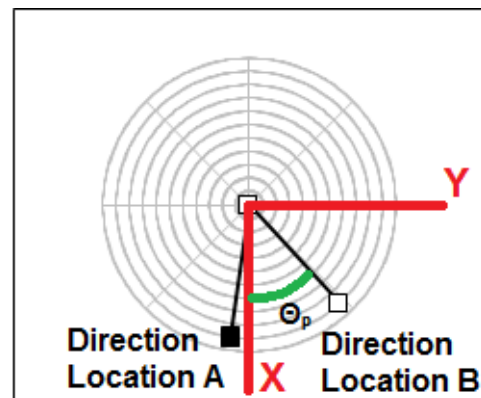


Figure 4.14: Principal Stress directions

For the 13 configurations that are analysed, the extrapolation locations are given in Table 4.2. The columns 2 and 3 show the theoretical locations according to DNV C203, as explained in Section 2.2.6. The last two columns show the actual locations that follow from Femap. The difference between the actual locations and the theoretical locations are in close correspondence. However they are not the identical. It is noted that for HSS determination according to the code [2] the values at the points of interest need to be interpolated first from the nodes closest to locations 'a' and 'b'. The interpolated values at locations 'a' and 'b' are then used for extrapolation. Although this has been noted, for convenience the pre-interpolated values are used for extrapolation. This should not lead to issues regarding the validity of this study, for there is only an interest in the difference in HSS value between the principal stress extrapolation versus primary stress perpendicular to the weld extrapolation. Extrapolation locations are in this regard less trivial.

The principal stress directions at the extrapolation locations A and B are shown in Figure 4.14. The x-axis is perpendicular to the intersection line so the principal stress angle θ_p is defined positive in counter-clockwise direction. Chapter 5 shows these polar plots to visualize the principal stress direction at the respective locations.

Table 4.2: Extrapolation points

Conf. #	Extrapolation points DNV [mm]		Actual points Femap [mm]	
	a	b	a	b
1	8.0	70.9	8.2	70.0
2	13.9	70.9	14.8	69.9
3	16.1	70.9	16.0	70.6
4	18.0	70.9	17.2	69.9
5	8.0	70.9	8.7	71.1
6	10.8	70.9	11.2	70.7
7	15.9	70.9	16.0	69.8
8	15.2	88.7	15.2	88.0
9	9.8	70.9	10.8	69.8
10	10.8	88.7	9.1	87.9
11	13.9	70.9	14.5	71.0
12	13.9	70.9	15.2	70.3
13	13.9	70.9	14.2	70.7

5

RESULTS

This chapter shows the results of the investigations that were performed. The results are given in a particular sequence, namely:

1. Stinger joint
 - (a) Principal stress direction change along the brace-to-chord connections during loading,
 - (b) Hot Spot Stresses obtained by extrapolating principal stresses versus extrapolating primary stresses perpendicular to the intersection line at the in-board chord saddle location of the brace A connection.
2. T/Y-joints
 - (a) Difference in Stress Concentration Factor between extrapolating principal stresses versus extrapolating primary stresses perpendicular to the intersection line due to a difference in principal stress directions between extrapolation locations,
 - (b) Influence of joint parameters on the snf-ratio.

5.1. STINGER JOINT

As explained in Chapter 3 measurements were done on a welded tubular joint of the Stinger structure of the Solitaire vessel. The data obtained from these measurements can be seen as the basis of this investigation. The data is used as input for numerical research. That numerical research is explained next. It starts with investigating the change in principal stress directions along the welded connections during loading .

5.1.1. PRINCIPAL STRESS DIRECTIONS

Due to the different loadings on the Stinger structure it is likely that that leads to multiaxiality. A sign, or property, of multiaxiality is a *change of principal stress direction during loading*. It is exactly this property that will be investigated using finite element modelling. The approach will be:

1. Create a Finite Element model of the joint under investigation,
2. Apply forces and bending moments obtained from strain measurements on the model and analyse for different boundary conditions,
3. Extract the principal stress angles at desired locations from the results,
4. Analyse the extracted output.

ANGLES

Steps 1 and 2 were described in Chapter 4. After successful completion of the Femap analyses, the data results need to be extracted at the desired locations of the Stinger joint. To get an impression of the multi-axial sensitive locations, the crown, saddle and in-between points as illustrated in Figure 5.1 are investigated further. Both chord and brace are checked at these locations for their change of principal stress angles. This is done at one element that is closest to the location of interest, at the center of the element. As only the change in direction is of interest, the angle results during loading are averaged and the variation around the zero mean angle is seen as the change in principal stress direction. The blue line in the graphs in Figure 5.4 show the 'MAPS angle', which is the principal stress angle of the maximum absolute principal stress. As can be seen, these blue lines have a zero mean.

Two deformed models are shown in Figures 5.2 and 5.3 to illustrate the difference between the boundary condition sets that were analysed.

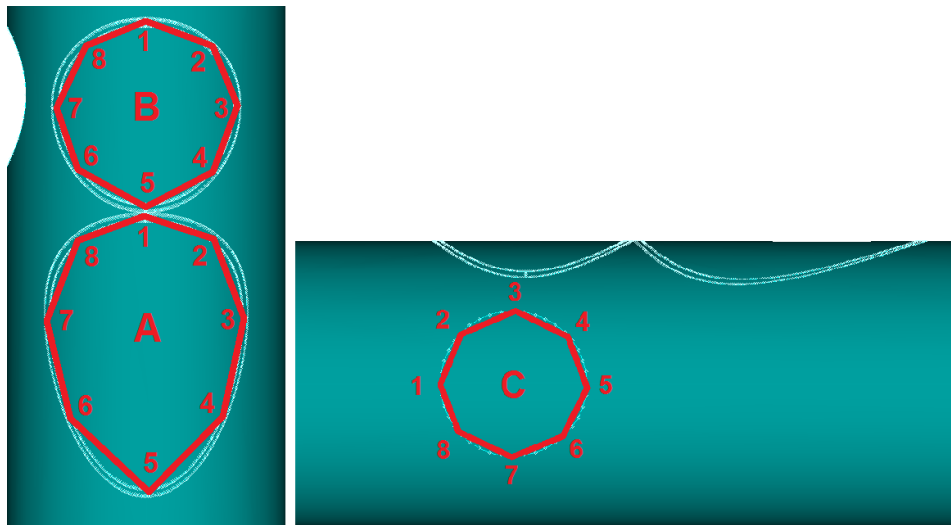


Figure 5.1: Investigated locations of braces A, B and C

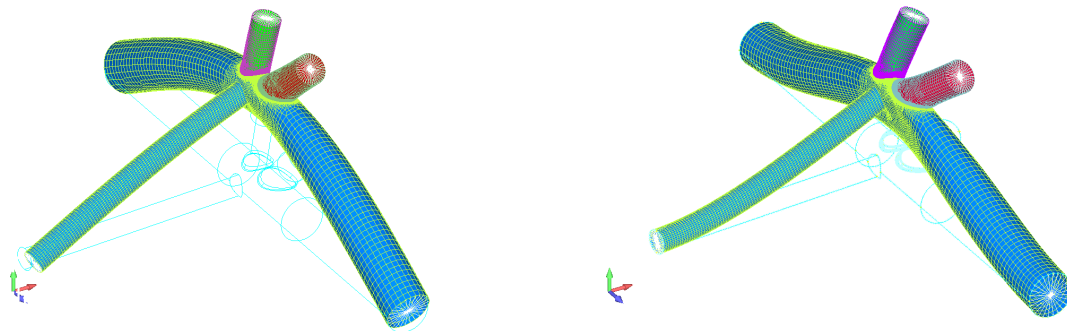


Figure 5.2: Typical deformation for the model with pinned-rollers boundary conditions Figure 5.3: Typical deformation for the model with fixed boundary conditions

CHANGE OF PRINCIPAL STRESS ANGLES

Next the results are shown for each brace separately for both boundary conditions. The results are presented in tables and by graphs.

BRACE A CONNECTION

Firstly the results of the Brace A connection are presented. Table 5.1 shows the maximum difference between the principal stress angles calculated by Femap for the 8 locations around the welded connection. The locations are as depicted in Figure 5.1. It can be seen that the choice of boundary conditions influences the

results. For example in the case of fixed constraints, location 4 on the chord side has a principal stress angle difference of 29.33. In contrast, for pinned-rollers constraints the value at the same location is just 8.67 degrees.

As the International Institute of Welding [28] proposes a change of 20 degrees or more as significant, angle differences above 20 degrees are assumed important for further investigating. For the case of the Brace A connection, this is for the locations with underlined values in Table 5.1. For these locations, the maximum absolute principal stresses (MAPS) are taken from Femap calculations and compared to the principal stress angles. This comparison is made in order to check if the stresses are high or low at possible peaks in angle variation. The comparison can be seen in Figures 5.4 and 5.5. The following is observed from the table and graphs:

The biggest change in principal stress angle seems to occur when the MAPS is lowest, between data points 80 and 100. Chord location 7 with pinned-rollers constraints appears to have the most volatile principal stress angles. The big differences at Brace location 3 for both constraint is explained by only a few spikes as depicted in their corresponding graphs. Location 6 shows a continuous change of principal stress angle, independent of the boundary conditions. It should be mentioned that these 100 data points only resemble a period of 10 seconds, for the measurement frequency is 10 Hz. So both a continuous change of principal stress angle like chord location 6 and a spike every 10 seconds like brace location 3 can be reason to assume high sensitivity to multiaxiality.

Chord location 7, which is the inboard chord saddle position, shows the highest volatility in principal stress angles when constraint with pinned-rollers. Therefore that location will be used for further investigation into the Hot Spot Stresses, see Chapter 5.1.2.

Table 5.1: Change of principal stress angles for chord and brace locations of the brace A connection for different boundary conditions

Location	Angle deviation Brace A connection [degrees]			
	Fixed		Pinned-rollers	
	Chord	Brace	Chord	Brace
1	5.19	7.55	3.34	5.17
2	5.61	11.29	3,21	18,95
3	10.33	<u>32.68</u>	2.85	<u>22.40</u>
4	<u>29.33</u>	15.24	8.67	4.73
5	15.82	12.57	4.13	10.60
6	<u>24.02</u>	7.84	<u>45.18</u>	4.82
7	3.44	3.77	<u>77.74</u>	3.00
8	<u>22,89</u>	2.17	8.34	4.04

BRACE B CONNECTION

The brace B connection is checked next. Table 5.2 shows that compared to brace A even more locations have a principal stress angle difference of 20 degrees or more, indicating that connection B is prone to more multiaxial fatigue than connection A. The following is observed:

1. Brace location 1 show high multiaxiality according to the graphs. Especially the pinned rollers constraints lead to a continuous change of angles.
2. Brace location 2 for both constraint sets look extreme. This could be due to the fact that graph shows a close to zero principal stress at data point 80. For example a small load acts in a direction different from the predominant loading, causing this sudden change in angle.
3. Chord AND Brace location 3 from table 3 seems highly multiaxial for both constraint sets. This is emphasized by graphs that show a highly variable principal stress angle. However, for the Brace locations only two to three spikes are seen after data point 80. Nevertheless, it is safe to say that location 3 is important from a multiaxial point of view.



Figure 5.4: Principal stress angle changes and MAPS of Brace A connection, fixed constraints

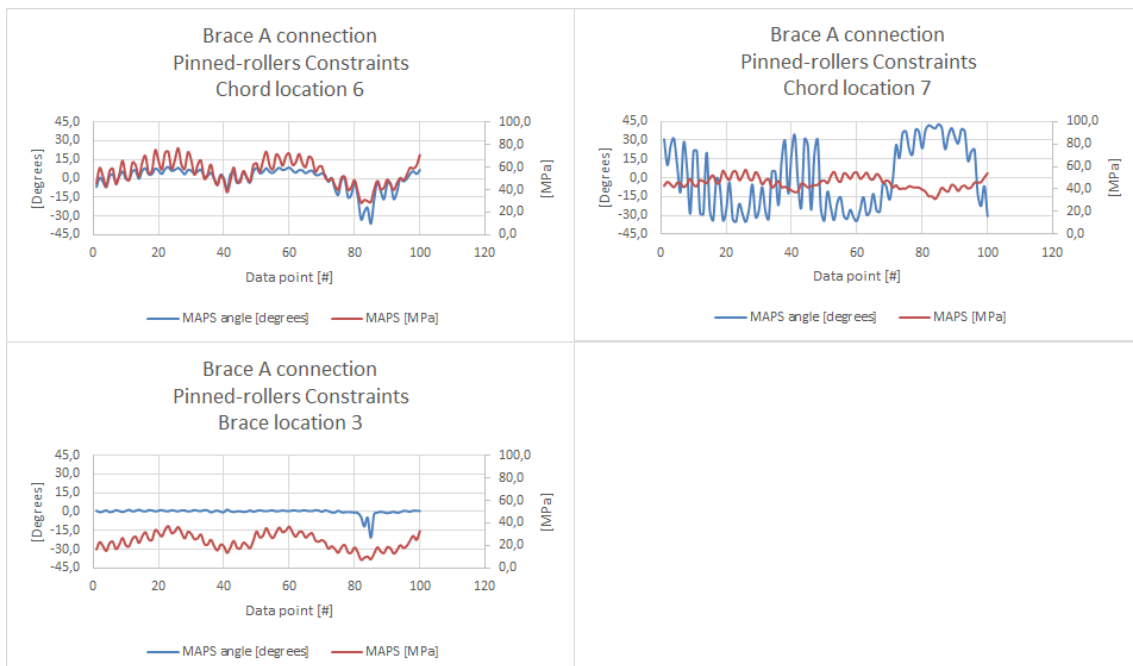


Figure 5.5: Principal stress angle changes and MAPS of Brace A connection, pinned-rollers constraints

4. Brace location 4 shows a big change of principal stress angle. However, this happens when the principal stresses are low.
5. Brace location 5 for the pinned-rollers constraint set shows a change at a moment when the principal stress is low. Therefore the effect of multiaxiality is less severe.
6. Chord locations 6 and 7 show high variability of principal stress angles. However, this is for only one constraint set. It is therefore difficult to state whether these locations are sensitive to multiaxial fatigue or not.

Table 5.2: Change of principal stress angles for chord and brace locations of the brace B connection for different boundary conditions

Location	Angle deviation Brace B connection [degrees]			
	Fixed		Pinned-rollers	
	Chord	Brace	Chord	Brace
1	3,35	31,04	9,28	43,24
2	26,30	82,91	13,05	81,60
3	33,83	74,06	58,54	63,07
4	19,86	24,15	9,71	24,94
5	6,42	19,83	4,03	29,96
6	38,60	4,95	13,82	1,27
7	4,73	0,88	52,97	2,59
8	20,95	4,07	12,35	1,83

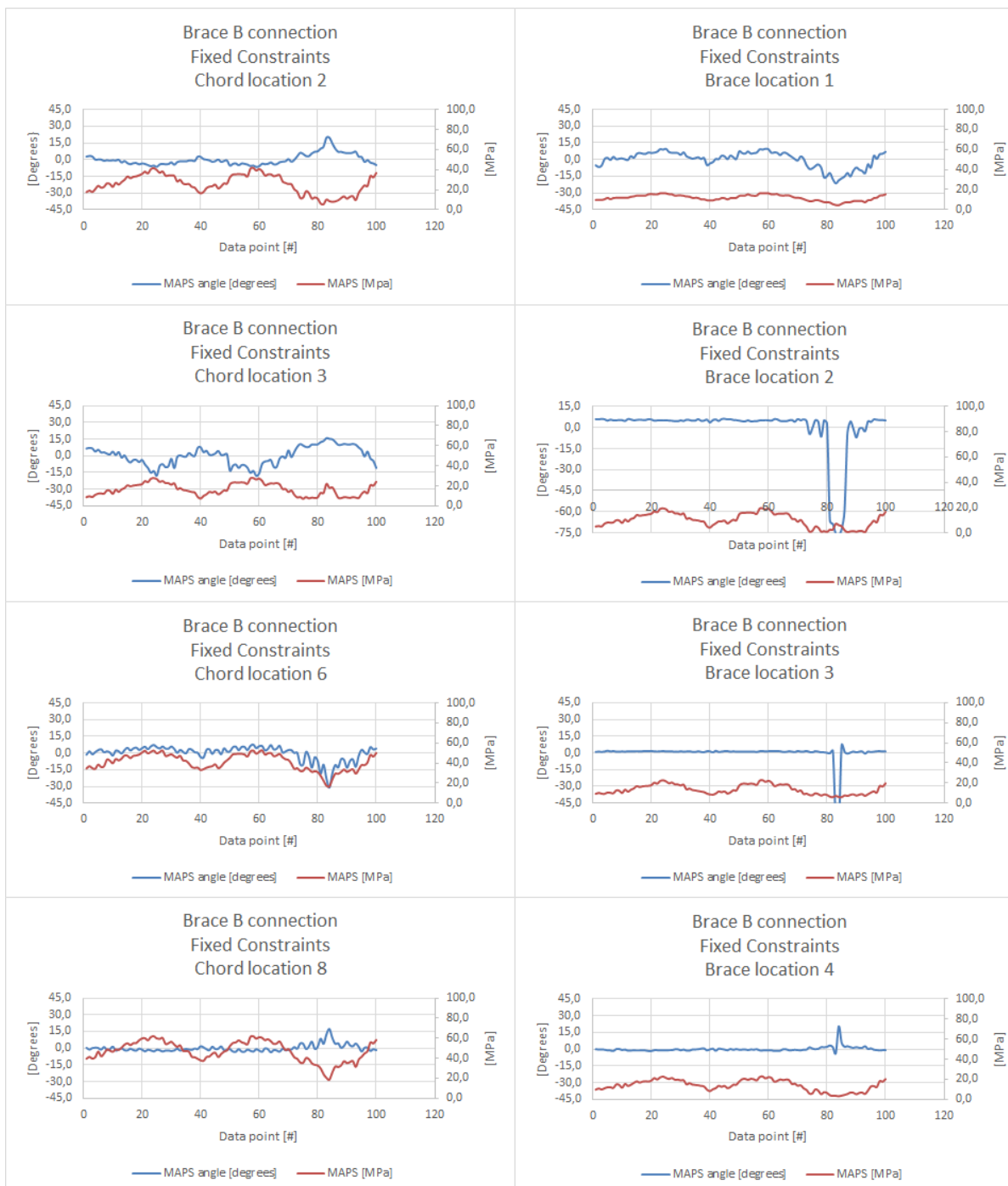


Figure 5.6: Principal stress angle changes and MAPS of Brace B connection, fixed constraints

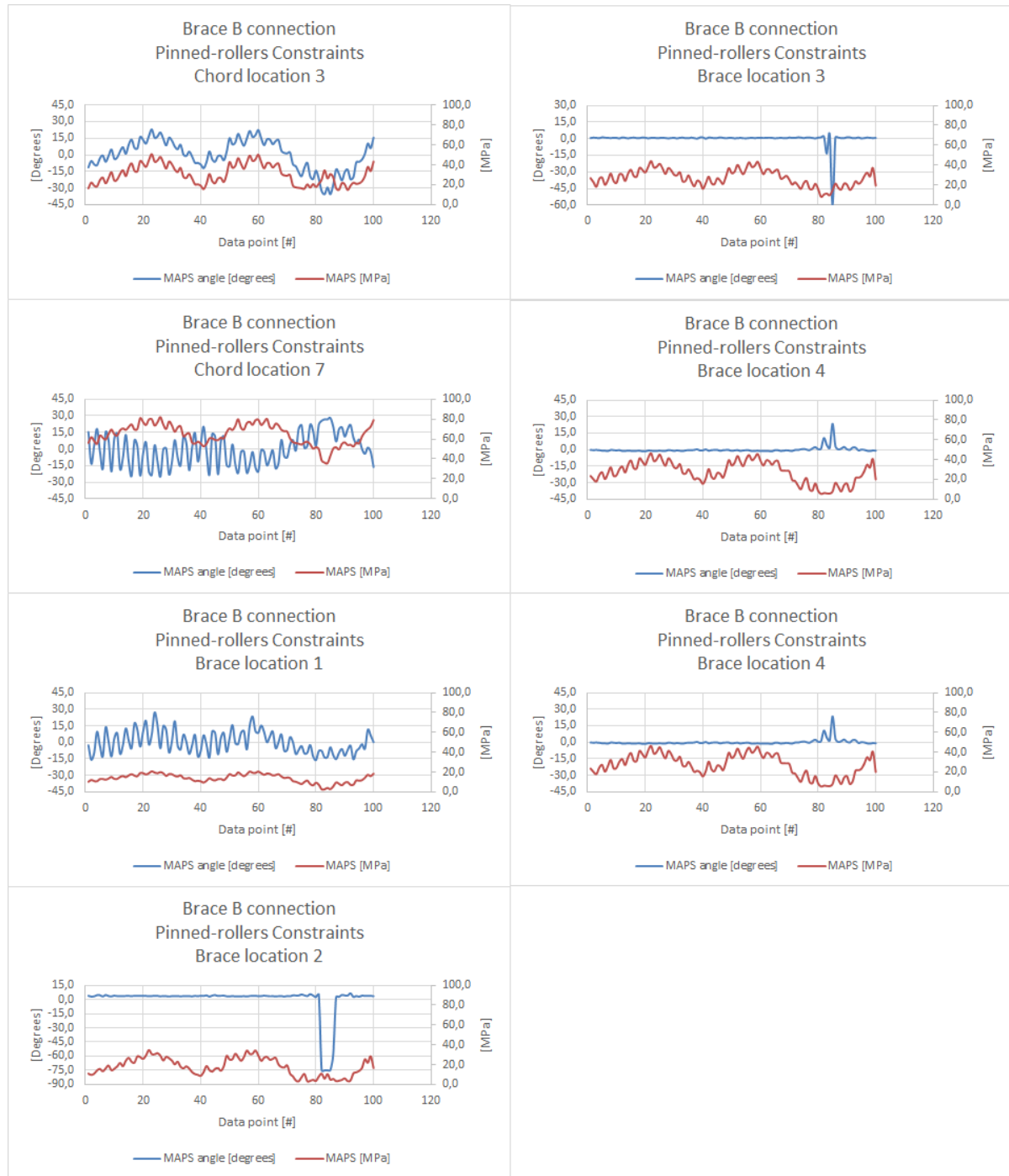


Figure 5.7: Principal stress angle changes and MAPS of Brace B connection, pinned-rollers constraints

BRACE C CONNECTION

Brace C is a good example for showing that the boundary conditions have a big effect on the results. For the fixed constraints only two locations have a principal stress angle difference exceeding 20 degrees. In contrast, the principal stress angle difference for the pinned-rollers constraint set exceed the 20 degree threshold at ten locations. The following is observed from Table 5.3 and the graphs of Figures 5.8 and 5.9:

1. Chord location 8 has highly varying principal stress angles for both constraint sets. In the situation of pinned-rollers constraints, the principal stress is twice as high as those stresses for the fixed constraint set. Again showing that the choice of boundary conditions is relevant.
2. Brace location 4 with fixed constraints does show a high change of principal stress angles. The low MAPS makes the effect less severe.
3. Chord locations 2,3 and 4 for the pinned-rollers constraint show peaks in principal stress deviations around data points 80 to 100. In combination with a high principal stress, these locations could be considered relevant from a multiaxial fatigue perspective.
4. Chord locations 6 and 8 show continuously varying principal stress angles compared to just the occasional peaks for locations 2,3 and 4.
5. The brace locations 2 and 3 with pinned-rollers constraints mainly change principal stress angles at certain moments, not constantly. Locations 1, 5 and 6 have a more constant up and down character of angle variation.

Table 5.3: Change of principal stress angles for chord and brace locations of the brace C connection for different boundary conditions

Location	Angle deviation Brace C connection [degrees]			
	Fixed		Pinned-rollers	
	Chord	Brace	Chord	Brace
1	2,02	16,90	11,40	22,68
2	6,48	7,01	52,59	58,26
3	1,94	2,07	86,46	78,53
4	10,74	25,41	39,82	13,65
5	11,80	6,42	10,30	25,98
6	14,78	10,65	34,97	23,37
7	7,51	6,03	12,26	3,07
8	89,17	7,27	27,68	11,59

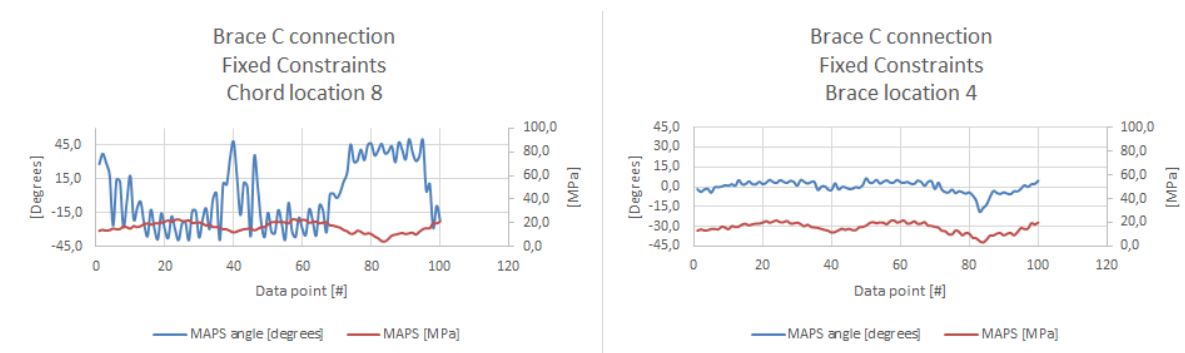


Figure 5.8: Principal stress angle changes and MAPS of Brace C connection, fixed constraints

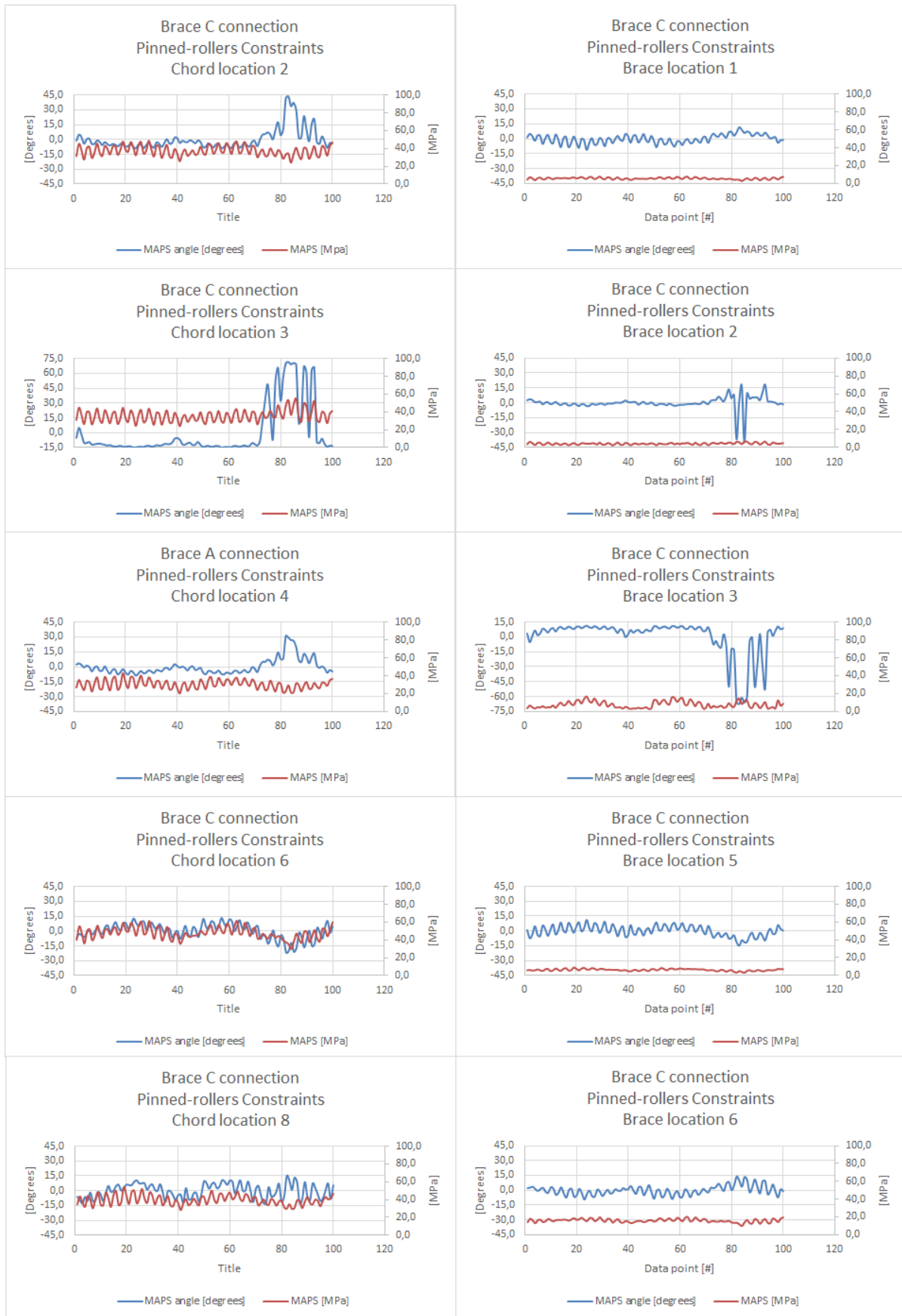


Figure 5.9: Principal stress angle changes and MAPS of Brace C connection, pinned-rollers constraints

5.1.2. HOT SPOT STRESSES

As mentioned in Chapter 5.1.1, chord location A7 shows high variation in principal stress direction during loading. That location is investigated further below. This time the principal stress direction is used in a different way, namely as the source of inequality between the Hot Spot Stresses determined by extrapolating the principal stresses versus extrapolating the primary stresses perpendicular to the weld toe. Romeijn [6] states that for the extrapolation of HSS primary stresses should be used, for *"the direction of principal stresses inside the extrapolation region changes, which causes problems when extrapolating stresses to the weld toe location."* As Allseas uses principal stresses for extrapolation, this could be a reason to change their method. Next the process is described that leads to the T/Y-joint study into this effect, as shown in Chapter 5.2.

TIME HISTORY

For this particular study a second stinger joint finite element model has been created that allows for extrapolating to the hot spot. Compared to the first model the circle radius around brace A that is projected on the chord has been increased, making it possible to extrapolate the stresses perpendicular to the weld toe, see Figure 5.10. The boundary conditions used for this investigation were again a combination of pinned-rollers.

Firstly the hot spot stresses are calculated for the original time history, as given in Figure 5.11. Next the bending moments are shifted out-of-phase, as depicted in the right graphs of Figure 5.11. Additionally two more analyses were performed. One where the bending moments were increased by a factor 10 to see the effect on the difference between the HSS. For the last analysis only the time histories of the axial forces were applied on the model. The results are given in Table 5.4. It appears that bending neutralises the difference and axial forces are responsible for an increase in difference.

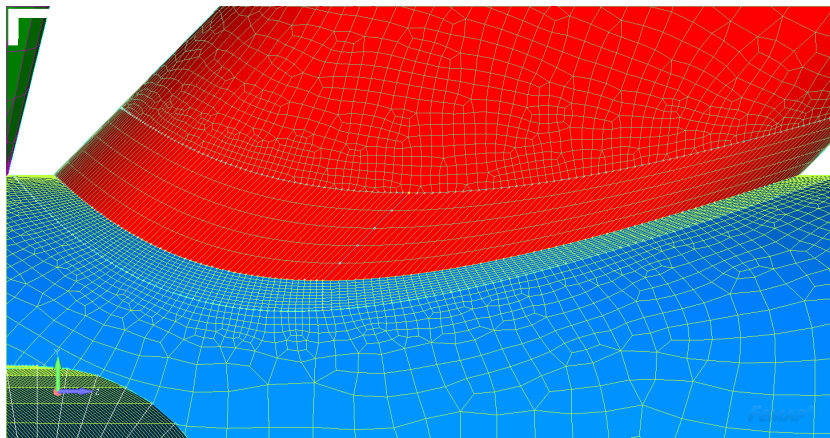


Figure 5.10: Refined mesh along extrapolation region at weld toe of brace A

PRINCIPAL STRESS DIRECTION DEVIATION

From Table 5.4 it can be seen that for axial forces only the difference can lead to 18 per cent higher hot spot stresses when extrapolating principal stresses. This is not in-line with the statement made by Romeijn [6]. Nevertheless, the difference between the two extrapolation methods could possibly be explained by the difference in principal stress direction at the two extrapolation locations. In order to check this theory, an investigation has been done on simple T/Y joints, as showed in the next section.

Table 5.4: Maximum difference in HSS between extrapolation methods

Load input	$\frac{\sigma_p}{\sigma_{\perp}}$
Original	1.04
Out-of-phase	1.05
Bending * 10	1.02
Axial force only	1.18

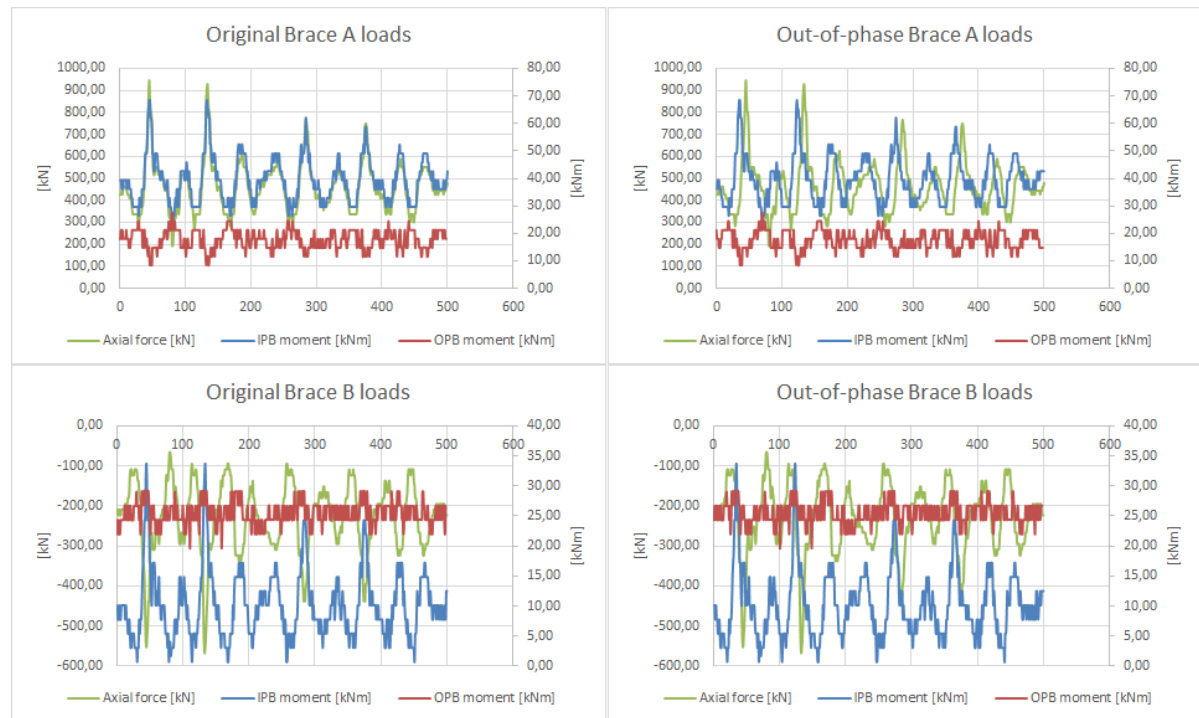


Figure 5.11: Load histories used for HSS calculation

5.2. T/Y-JOINTS

Next the investigation into the difference between extrapolation of principal stresses and perpendicular primary stresses will be explained. Secondly the results of the investigation into the ratio between SCF and SNCF will be explained.

5.2.1. SCF CALCULATION USING THREE METHODS

Using the developed API script 13 joint configurations were created in Femap. The dimensions and joint parameters are given in the Table 4.1. The variations of joint parameters are depicted by the bold and underlined values. The standard joint configuration is number 2, which has an in plane angle θ of 45 degrees, a τ of 0.6, β of 0.63 and a γ of 12.8. Only one joint parameter changes in comparison with any other configuration, so only the effect of the joint parameter of interest is analysed.

The basic configuration is shown in Figure 5.12. Thus the boundary conditions used are fixed for both chord ends and the axial force is applied in the direction parallel to the brace. Only the SCF equation of the Chord saddle is of importance for this investigation.

PRINCIPAL STRESS ANGLE

Figure 4.14 shows an example of the difference in principal stress directions for the two extrapolation locations A and B. The black square represents the principal stress direction at location A, the white square the principal stress direction at location B. The coordinate system is identical to the Femap models, where the X-axis is perpendicular to the weld. The principal stress directions are calculated as principal stress angles θ_p as shown below in equation 5.1:

$$\tan(2\theta_p) = \frac{2\tau_{xy}}{\sigma_x - \sigma_y} \quad (5.1)$$

Where τ_{xy} is the shear stress and σ_x and σ_y are the primary stresses in x and y direction, respectively. This has been illustrated in Figure 2.6.

Next the results are presented obtained with the analyses within the Femap environment. The SCF values calculated with the Efthymiou equations adopted by DNV are given in order to have a comparison with the

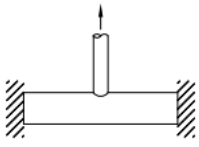
Load type and fixity conditions	SCF equations	Eqn. No.	Short chord correction
Axial load- Chord ends fixed 	Chord saddle: $\gamma \tau^{1.1} (1.11 - 3(\beta - 0.52)^2) (\sin \theta)^{1.6}$	(1)	F1
	Chord crown: $\gamma^{0.2} \tau (2.65 + 5(\beta - 0.65)^2) + \tau \beta (0.25\alpha - 3) \sin \theta$	(2)	None
	Brace saddle: $1.3 + \gamma \tau^{0.52} \alpha^{0.1} (0.187 - 1.25\beta^{1.1}(\beta - 0.96)) (\sin \theta)^{(2.7-0.01\alpha)}$	(3)	F1
	Brace crown: $3 + \gamma^{1.2} (0.12 \exp(-4\beta) + 0.011\beta^2 - 0.045) + \beta \tau (0.1\alpha - 1.2)$	(4)	None

Figure 5.12: Basic configuration with SCF equations of Efthymiou [2]

values obtained with Femap. The percentage difference column shows the difference between the SCF calculated by extrapolating the principal stresses and the Efthymiou equations. This comparison is most logical, for Efthymiou [8] uses the principal stresses as well. The principal stress column shows the SCFs obtained by extrapolating the principal stresses. SCFs of the extrapolated perpendicular primary stresses are shown as well in the next column.

CHANGE OF θ

The Table 5.5 below shows the principal stress angles and SCFs for different θ , the in-plane angle between chord and brace. The other joint parameters are kept constant. The SCFs are thus determined in three ways at the chord saddle position:

1. By the Efthymiou equations adopted by DNV
2. By extrapolating the principal stresses
3. By extrapolating the primary stresses perpendicular to the weld toe

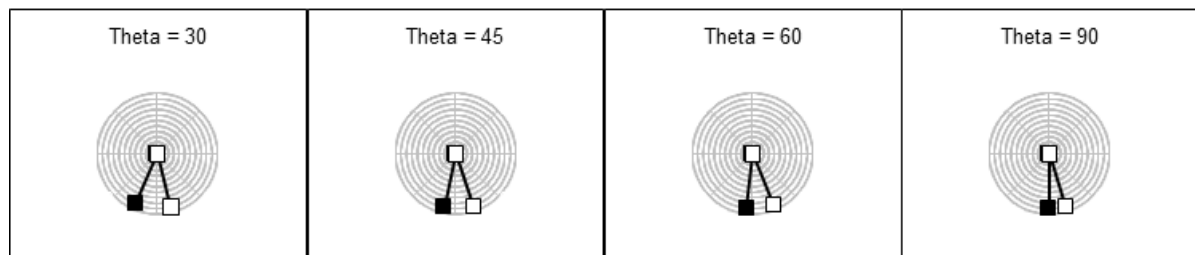
Table 5.5: Change of θ

θ	Principal stress angle location A [degrees]	Principal stress angle location B [degrees]	DNV's Efthymiou [SCF]	Difference DNV-Femap [%]	Principal stress [SCF]	Primary stress [SCF]
30	-23.82	14.19	2.59	38.07	1.76	1.76
45	-12.53	18.00	4.51	19.27	3.72	3.75
60	-7.50	22.01	6.24	7.63	5.78	5.81
90	-0.66	16.96	7.86	0.24	7.88	7.91

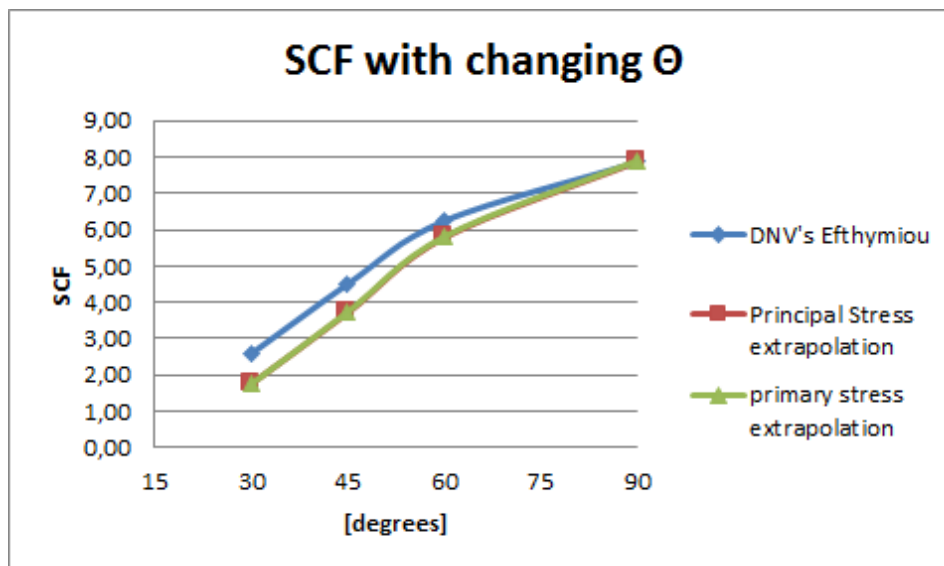
The graph 5.14 below shows the SCF as a function of Theta for the different extrapolation methods. The shape is similar to Efthymiou, despite the lower values. Looking at Table 5.5 above the difference between the principal stress and primary stress methods is small. A maximum of 0.03 higher SCF obtained with primary stress than with principal stress.

What can be noticed is that as the in-plane angle decreases, the deviation between the Femap and Efthymiou results increases. The T-joint results ($\theta = 90$) are a close match. However, the results of the joint with a 30 degrees angle differ 38%. This raises questions regarding:

1. The reliability of the Femap software

Figure 5.13: Principal Stresses directions for different θ

2. The reliability of the Efthymiou equations
3. The legitimacy of the way of modelling, namely by shell elements without a weld.

Figure 5.14: SCF for different θ

CHANGE OF τ

Joint parameter τ represents the brace over chord wall thickness ratio. The chord wall thickness is kept at 1.25 inch, where the brace wall thickness varies from 0.25 to 1.25 inch, resulting in τ values of 0.2, 0.6, 0.8 and 1.0. Table 5.6 gives the SCFs. The difference between DNV and Femap results increases as τ decreases. For a τ of 1.0 the SCF of Femap matches perfectly with Efthymiou. However, for a τ of 0.2, there is a 48% difference. Just as for the joint parameter θ , the differences are small between the two extrapolation methods.

Figure 5.15 shows the principal stress directions for the different τ values. The principal stress angle of -39.14 degrees for $\tau = 1.0$ at location B is not in line with the other angles. This is due to the fact that for this case the Y normal stress is smaller than the X normal stress, resulting in a negative value according to Formula 5.1. Besides this outlier, the difference in principal stress angle between the locations A and B tends to increase as τ increases. This does not lead to a noticeable difference in SCFs obtained with principal stresses or primary stresses, as can be seen in Table 5.6.

Table 5.6: Change of τ

τ	Principal stress angle location A [degrees]	Principal stress angle location B [degrees]	DNV's Efthymiou [SCF]	Difference DNV-Femap [%]	Principal stress [SCF]	Primary stress [SCF]
0.2	-24.00	3.14	1.35	48.38	0.82	0.82
0.6	-12.53	18.00	4.51	19.27	3.72	3.75
0.8	-10.37	33.46	6.19	8.23	5.70	5.70
1	-9.33	-39.14	7.92	0.01	7.92	7.88

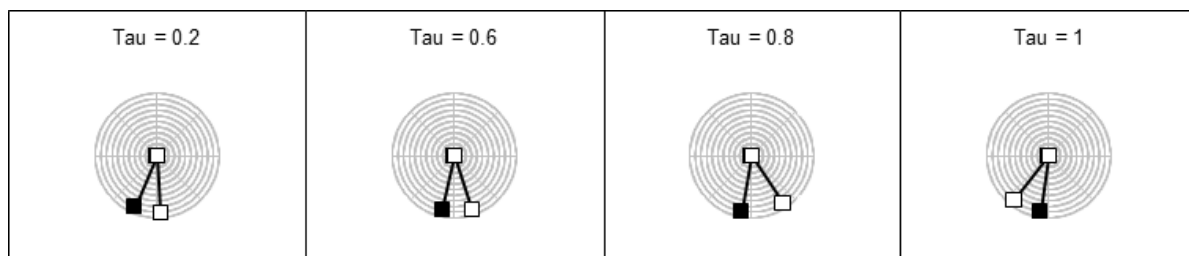


Figure 5.15: Principal Stresses directions for different τ

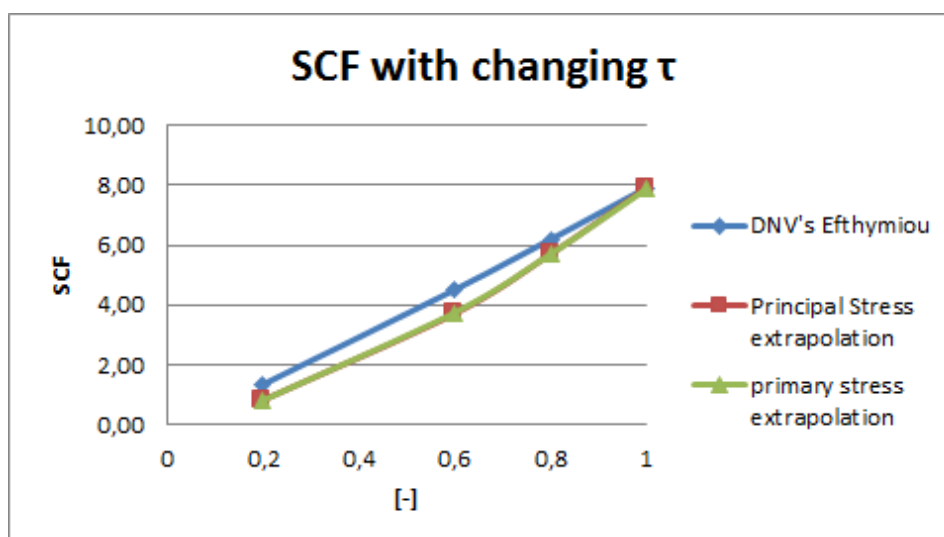


Figure 5.16: SCF for different τ

CHANGE OF β

Joint parameter β represents the brace over chord diameter ratio. The chord diameter is kept constant at 32 inch, where the brace diameter varies from 6.625 to 26 inch, resulting in β values of 0.21, 0.38, 0.63 and 0.81. Again there is one big outlier in comparison to the DNV Efthymiou equations. This is for a β of 0.81, where the difference is 49%. Furthermore when looking at Figure 5.18 the SCFs do not follow the Efthymiou equations, except for $\beta = 0.38$.

The deviation of principal stress directions between locations A and B increases for decreasing β , as Figure 5.17 illustrates.

Table 5.7: Change of β

β	Principal stress angle location A [degrees]	Principal stress angle location B [degrees]	DNV's Efthymiou [SCF]	Difference DNV-Femap [%]	Principal stress [SCF]	Primary stress [SCF]
0.21	-9.07	41.83	3.42	16.39	4.03	4.00
0.38	-9.45	34.80	4.39	1.69	4.46	4.45
0.63	-12.53	18.00	4.51	19.27	3.72	3.75
0.81	-22.44	3.03	3.58	48.91	2.17	2.23

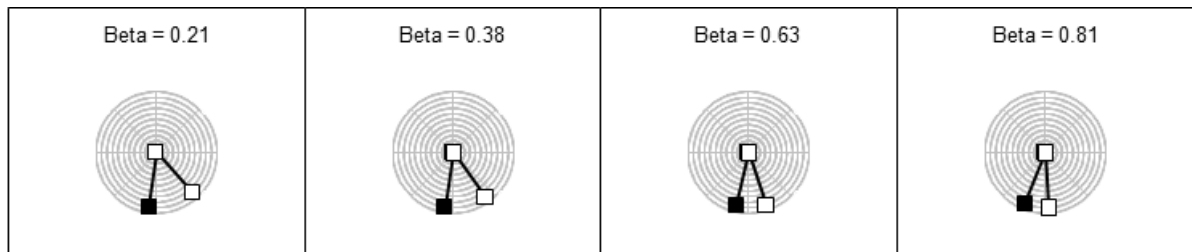


Figure 5.17: Principal Stresses directions for different β

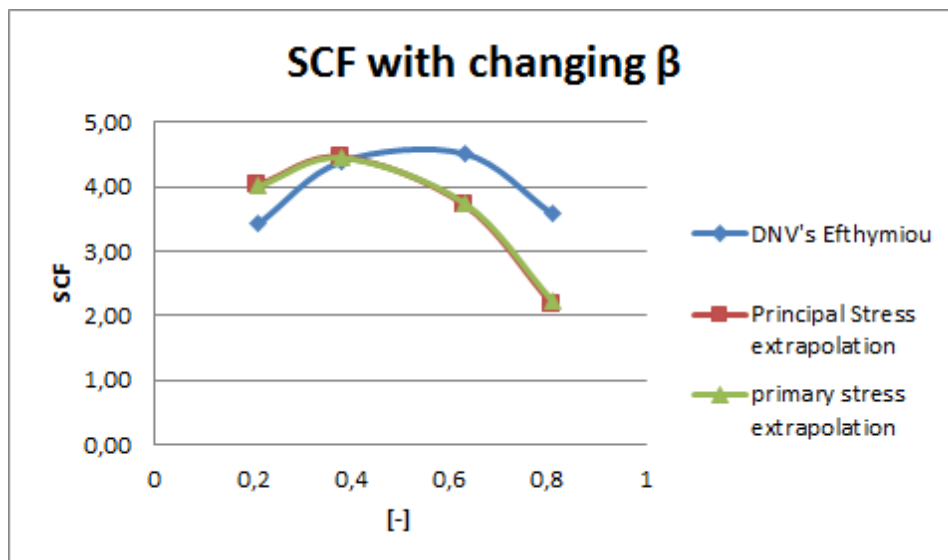


Figure 5.18: SCF for different β

CHANGE OF γ

Joint parameter γ represents the chord radial stiffness. It is an important parameter in many SCF formulae. To achieve the desired gammas, the dimensions of chord diameter, brace diameter and their respective thickness were altered. Gammas of 12.8, 16, 25.6 and 32 were analysed while keeping the other joint parameters constant. The biggest outlier in comparison with the Efthymiou SCF is 19.27 and it can be seen in Table 5.8 that for increasing γ the percentage difference in SCF between Efthymiou and Femap decreases.

Table 5.8 and Figure 5.19 both show that γ has no noticeable effect on the deviation of principal stress directions for the two extrapolation locations A and B. Nevertheless the difference in direction is 30 degrees for all four configurations.

The SCFs from the primary stresses are slightly higher than the SCFs from the principal stresses. Despite the consistently lower values compared to Efthymiou, the extrapolation values do show a similar path for increasing γ , as can be seen in Figure 5.20.

Table 5.8: Change of γ

γ	Principal stress angle location A [degrees]	Principal stress angle location B [degrees]	DNV's Efthymiou [SCF]	Difference DNV-Femap [%]	Principal stress [SCF]	Primary stress [SCF]
12.8	-12.53	18.00	4.51	19.27	3.72	3.75
16	-8.64	24.78	5.71	11.99	5.07	5.08
25.6	-5.59	28.43	9.03	9.76	8.19	8.20
32	-4.12	28.01	11.43	8.68	10.48	10.48

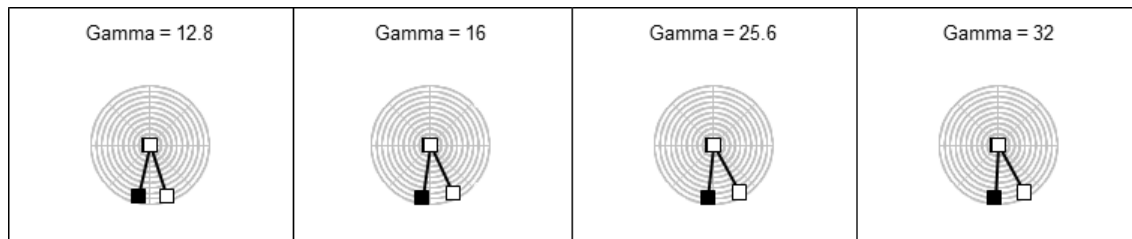


Figure 5.19: Principal Stresses directions for different γ

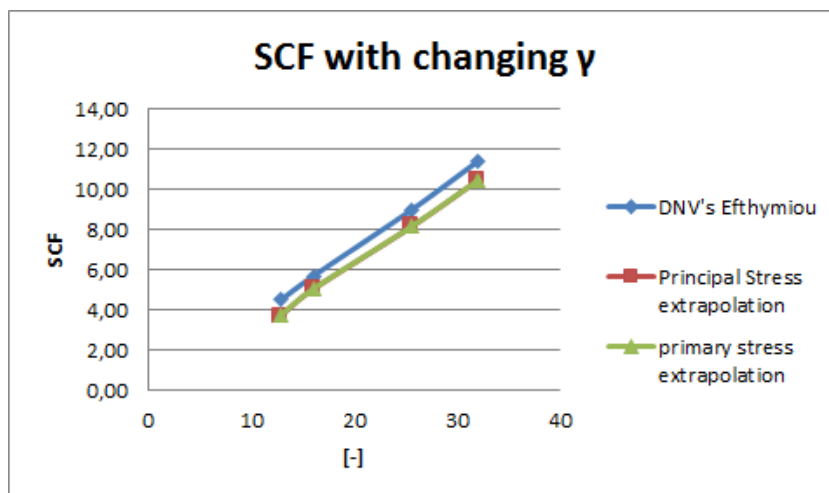


Figure 5.20: SCF for different γ

5.2.2. PARAMETRIC STUDY SCF TO SNCF RATIO

In order to maximize the output results of the investigated joint configurations described above, not only the difference in SCFs will be researched. Also the relationship between the SCF and SNCF will be investigated for all the configurations. Again this is done for the Chord saddle position under axial loading on the brace.

Experimental research of welded tubular joints commonly involves the use of strain gauges to measure an extrapolated strain at the position of the weld toe. This is the hot spot strain ϵ_{hs} . As fatigue calculations usually make use of a stress concentration factor and not a strain concentration factor, the measured strain is converted to stress by $\sigma = E * \epsilon$.

CALCULATION OF SNF

According to [6] the perpendicular stress component σ_{\perp} should be used as input for the fatigue analysis, for the initial fatigue crack propagation is usually oriented along the weld toe. Additionally, the SCF and SNCF that should be used are:

$$SCF = \frac{\sigma_{x;hs}}{\sigma_{nom}} \quad (5.2)$$

$$SNCF = \frac{\sigma_{x;hs} - \nu\sigma_{y;hs}}{\sigma_{nom}} \quad (5.3)$$

As mentioned in Chapter XX, besides the stresses also the strains were extracted from Femap. Just like there is a Stress Concentration Factor at the hot spot, there is a Strain Concentration Factor. This SNCF is calculated in the same manner as the SCF, but with strains instead of stresses. The ratio between SCF and SNCF is important in order to get from experimental obtained strains to desired stresses. This so called snf-ratio (=SCF/SNCF) is used for the conversion of the experimentally measured SNCF into SCF and comes down to the following:

$$snf = \frac{SCF}{SNCF} \quad (5.4)$$

$$= \frac{\frac{\sigma_{x;hs}}{\sigma_{nom}}}{\frac{\sigma_{x;hs} - \nu\sigma_{y;hs}}{\sigma_{nom}}} \quad (5.5)$$

$$= \frac{1}{1 - \nu \frac{\sigma_{y;hs}}{\sigma_{x;hs}}} \quad (5.6)$$

As this leads to a range of snf values between 0.8 and 1.4 for $|\frac{\sigma_{y;hs}}{\sigma_{x;hs}}| \leq 1$, the question is what factors influence the snf-ratio. These factors are the joint parameters, type of loading joint geometry and the member under consideration, [6]. This investigation is aimed to check the effect of the joint parameters on the snf-ratio for axial loading. Again this is done for the 13 configurations used in the previous investigation into the different extrapolation methods for the SCF.

Despite that literature states that $\sigma_{x;hs}$ and $\sigma_{y;hs}$ should be used for snf determination, it is interesting to see what happens with the snf when principal stresses/strains are used. Thirdly the component extrapolation method is used to determine the snf. The way all three snfs are calculated is by dividing the SCF by the SNCF from the extrapolated stresses and strains at the hot spot location. So the SCFs from the previous investigation are used and divided by the SNCFs for that location.

OUTCOME

The results in Table 5.9 show the snf-ratios for the investigated configurations. The variable joint parameters are the in-plane angle θ , the wall thickness ratio τ , the diameter ratio β and the half chord diameter to thickness ratio γ . The graphs in Figure 5.21 illustrate the relationship between the individual joint parameters and the snf. A second order polynomial trendline has been fitted through the points.

τ From the results in Table 5.9 and corresponding graph in Figure 5.21 it can be seen that the snf increases for a decreasing τ with a maximum of 1.30 and a minimum of 1.18. Compared to the other joint parameters, this difference is biggest, concluding that τ has the greatest influence on the snf.

γ Joint parameter γ has a slight increase in snf for decreasing values. A maximum for $\gamma = 12.8$ of 1.22 and a minimum of 1.16 for $\gamma = 32$.

θ In-plane brace to chord angle θ has effect on the snf, such that it varies between 1.19 and 1.27 for angles between 90 and 30 degrees. A smaller angle results in a lower snf.

β β appears to have little effect on the snf, with values varying between 1.21 and 1.25. However, as the validity range of β has a maximum of 1.0, the difference in snf could be bigger. This is not tested, because it was difficult to analyse a model with a beta of 1.0. If an imaginary parabolic trendline is extended through the points in the corresponding β -snf graph, this might results in a higher snf.

Table 5.9: snf-ratios at chord saddle for 13 T/Y-joint configurations with axial loading

Conf. #	snf principal stress/strain	snf $\sigma_{x;hs}$ and $\sigma_{y;hs}$	θ [Degrees]	τ	β	γ
1	1,29	1,30	45	0,2	0,6	12,8
2	1,22	1,22	45	0,6	0,6	12,8
3	1,19	1,19	45	0,8	0,6	12,8
4	1,17	1,18	45	1	0,6	12,8
5	1,21	1,22	45	0,6	0,2	12,8
6	1,21	1,21	45	0,6	0,4	12,8
7	1,27	1,25	45	0,6	0,8	12,8
8	1,20	1,20	45	0,6	0,6	16,0
9	1,18	1,18	45	0,6	0,6	25,6
10	1,17	1,17	45	0,6	0,6	32,0
11	1,27	1,27	30	0,6	0,6	12,8
12	1,21	1,20	60	0,6	0,6	12,8
13	1,20	1,19	90	0,6	0,6	12,8

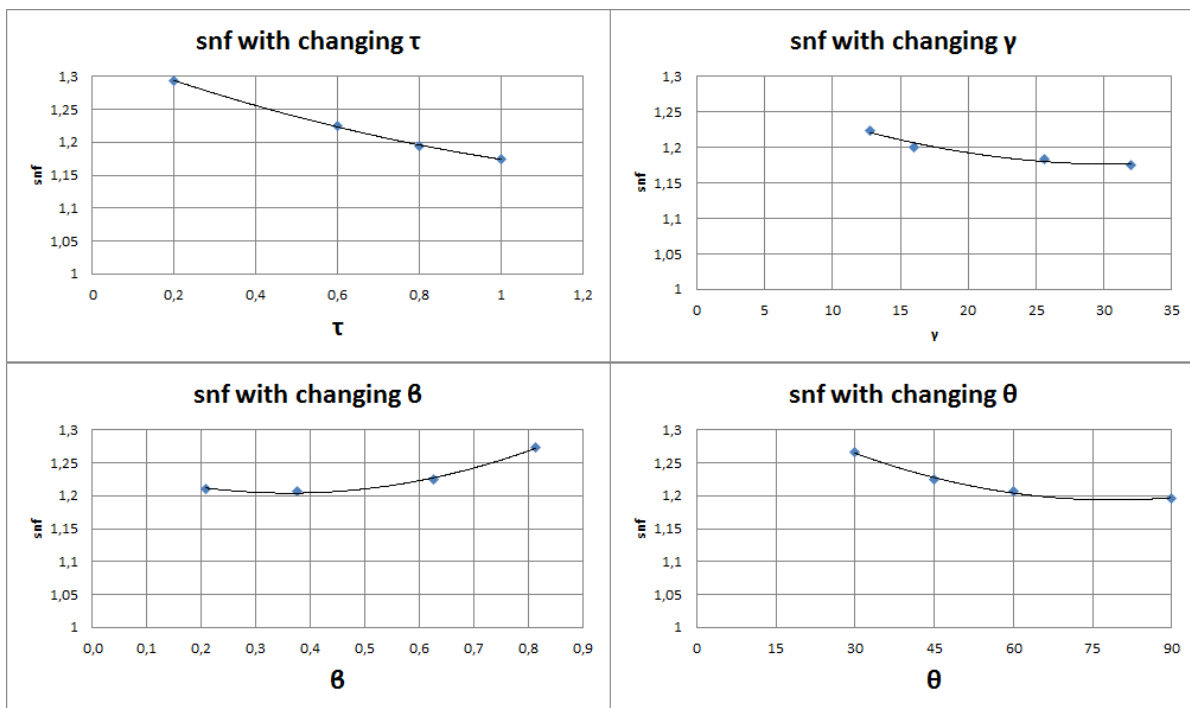


Figure 5.21: relationship between snf-ratio and individual joint parameters

6

SUMMARY AND CONCLUSIONS

This chapter gives a summary of the research done together with the conclusions drawn based on the results obtained. Finally a couple of recommendations are given.

6.1. STINGER JOINT

PRINCIPAL STRESS DIRECTION VARIATION

Firstly an analysis of the change in principal stress directions during loading along the connections of a tubular joint on the stinger structure from the Solitaire vessel has been performed. Strain data obtained from strain measurements on the Solitaire stinger resulted in a load input for a created finite element model. The data from the nominal strain gauges on braces A and B are used for this research. The strain data is decomposed into axial forces, in-plane bending moments and out-plane bending moments to be able to use it as input for the model. Two boundary condition sets are used for analysis, namely an all fixed ends set and a pinned-roller combination set. Elemental results at 8 locations around each brace to chord connection are extracted from Femap containing the principal stress angles at each data point. Based on the change in the principal stress angle during loading multiaxial response locations of the joint have been found.

Extracting the principal stress angles along the brace to chord connections has led to the following conclusions on which locations are sensitive to multiaxial fatigue. See Table 6.1, Figure 6.1 and the bullet points below:

- The most sensitive locations are indicated by '++' in Table 6.1. These locations show variations of more than 20 degrees in principal stress angles for both constraint sets.
- The locations indicated by '+' are shown for the two constraint sets separately. The choice of boundary conditions has a clear effect on the results, which is why they are presented in such a way.
- As there are clear signs of non-proportional multiaxial fatigue loading, namely the change in principal stress direction during loading, the stinger joints could experience additional strain hardening due to the interaction of slip planes. This will result in a decrease of fatigue life and leads to the statement that an appropriate multiaxial fatigue assessment method should be chosen for fatigue calculations.

Table 6.1: multiaxial fatigue sensitive locations of investigated stinger joint

	sensitivity	Brace A		Brace B		Brace C	
		chord	brace	chord	brace	chord	brace
Both sets	++	6	3	3	1,2,3,4	8	
Fixed	+	4,8		2,6,8			4
Pinned-rollers	+	7		7	5	2,3,4,5	1,2,3,5,6

HOT SPOT STRESS

One of the locations that showed a high change of principal stress direction during loading is the chord saddle position of the brace A connection, as depicted by location A7 in Figure 6.1. For there exists a debate about which stresses to use for Hot Spot Stress extrapolation, principal stresses or primary stresses perpendicular to the weld toe, location 'A7' on the chord was subjected to further research. This is the chord saddle. A finite element model with a new mesh was created to be able to extract the stresses at the correct extrapolation locations according to DNV [2]. The analyses were performed with in-phase loading and out-of-phase loading with the original time histories of the load components. Additionally two analyses were performed with 1) the bending moments multiplied by a factor of 10 and 2) only axial forces. The HSS differed most when only axial forces were applied on the braces. For this case the principal stress extrapolation resulted in a 18 percent higher HSS compared to extrapolating the primary stresses. As previous studies suggest that this is due to a difference between principal stress directions at the extrapolation locations a and b, this hypothesis was investigated further for simple CHS T/Y-joints.

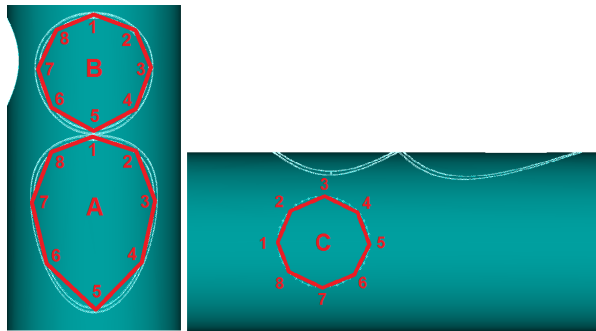


Figure 6.1: Investigated locations of braces A, B and C

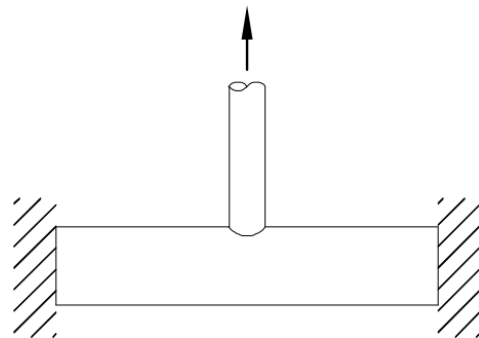


Figure 6.2: Investigated T/Y-joint configuration

6.2. T/Y-JOINTS

A more fundamental research has been done on T/Y-joints. SCFs of simple tubular T/Y-joints have been determined for different extrapolation methods. SCFs and SNCFs are used to determine the snf-ratio. This section elaborates on the investigation of T/Y-joints by using the finite element method.

SCF

SCFs are often calculated by extrapolating the principal stresses and so does Allseas. Det Norske Veritas recommends this in their code DNV-RP-C203. However, others recommend using the primary stresses σ_{\perp} perpendicular to the weld toe, e.g. Romeijn [6]. Stated is that primary stresses need to be used, for it is possible that the principal stresses have different directions at the extrapolation locations A and B. This could lead to an underestimation of the SCF if principal stresses are used. An analysis was done on the difference in SCF between extrapolation methods to find a relation with the principal stress direction deviation from the normal to the intersection line at the extrapolation locations. A script has been written that creates and analyses T/Y-joints based on specified dimensions. The dimensions are chosen such that the joint parameters τ , γ , β and θ are changed one at a time. An interaction between joint parameters was not part of this study. By doing this the influence of each joint parameter on the principal stress angle difference between extrapolation locations A and B can be checked. In the end the difference in SCF between the extrapolation methods is calculated and compared. This comparison leads to a conclusion involving principal stress directions, joint parameter influence and SCFs. The chord ends are fixed and only an axial force is applied on the brace, see Figure 6.2. Parametric formulae by Efthymiou are used to compare the results obtained from finite element modelling.

Joint parameter influence on principal stress directions The joint parameters that are changed by changing the joint dimensions are τ , γ , β and θ . Their individual influence on the principal stress directions are checked and shown in Table 6.2. As can be seen, the principal stress angle differences decrease for increasing θ and β . As τ increases, so does the angle difference. γ is found to have no noticeable effect on the principal stress angles. After these relations are found, the SCFs are determined to see what the effect of the principal stress direction deviation is.

Table 6.2: joint parameter influence on principal stress angle difference between extrapolation locations A and B

	value	angle difference
τ	↑	↑
θ	↑	↓
β	↑	↓
γ	↑	≈

Extrapolation principal stresses vs. primary stresses perpendicular to the weld toe With the previous results showing that the principal stress directions do differ between extrapolation locations, the SCFs are calculated and compared. For all 13 configurations that have been analysed, concluding that either principal or primary stresses result in higher SCFs is not reasonable. For certain configurations extrapolating the principal stresses result in higher SCFs. For other configurations extrapolating the primary stresses result in higher SCFs. The difference does not reach 1 percent. So based on these results it can be concluded that the difference in principal stress direction between locations A and B does not have an effect on the value of the Stress Concentration Factor for T/Y-joints under axial loading. This conclusion is extended to the stinger joint in the sense that the difference in principal stress direction at the extrapolation locations is not the reason for the difference in Hot Spot Stress. This leads to the statement that other factors must be responsible for the difference in HSS. One factor could be that the difference is due to the presence of the other brace members, which changes the stiffness distribution around the welded intersection area.

SNF-RATIOS

Commonly the stress concentration factors of welded tubular joints are obtained by experimental research, by measuring an extrapolated strain at the hot spot ϵ_{hs} and converting it to stress by $\sigma_{hs} = E * \epsilon_{hs}$. Due to a triaxial stress state at the weld toe with a negligible stress perpendicular to the surface, σ_z , only the x and y components of the assumed plane stress are considered, with $\epsilon_x = \frac{1}{E}(\sigma_x - \nu\sigma_y)$ and $\epsilon_y = \frac{1}{E}(\sigma_y - \nu\sigma_x)$. In order to arrive at the SCF, the SNCF needs to be multiplied by a snf-ratio, which is in fact the coupling between the SCF and SNCF. As this snf-ratio depends among other things (i.e. type of loading and joint geometry) on joint parameters, this influence is researched. Again the 13 Femap configurations of the T/Y-joints are used to calculate the snf-ratio. Therefore the already calculated SCFs from the previous research are divided by the matching SNCFs calculated at the chord saddle hot spot. Extrapolation was done with principal stresses.

Table 6.3 shows the snf-ratios with respect to the different joint parameters. It gives the maximum and minimum values that were calculated and the behaviour when the value of the individual joint parameters is increased. From these results it can be concluded that τ has the greatest effect on the snf-ratio, then the in-plane brace to chord angle θ . It should be noted that the difference caused by β could be bigger, for the entire validity range has not been used. However, γ and β have the smallest effect on the snf-ratio.

So, when converting strains to stresses by using a standard value, e.g. 1.20 [6], this can lead to a too conservative fatigue life estimation in case the real ratio is lower and vice versa.

Table 6.3: snf-ratios with respect to joint parameters

	min snf	max snf	value joint parameter	snf
τ	1.18	1.30	↑	↓
γ	1.17	1.22	↑	↓
β	1.21	1.25	↑	↑
θ	1.19	1.27	↑	↓

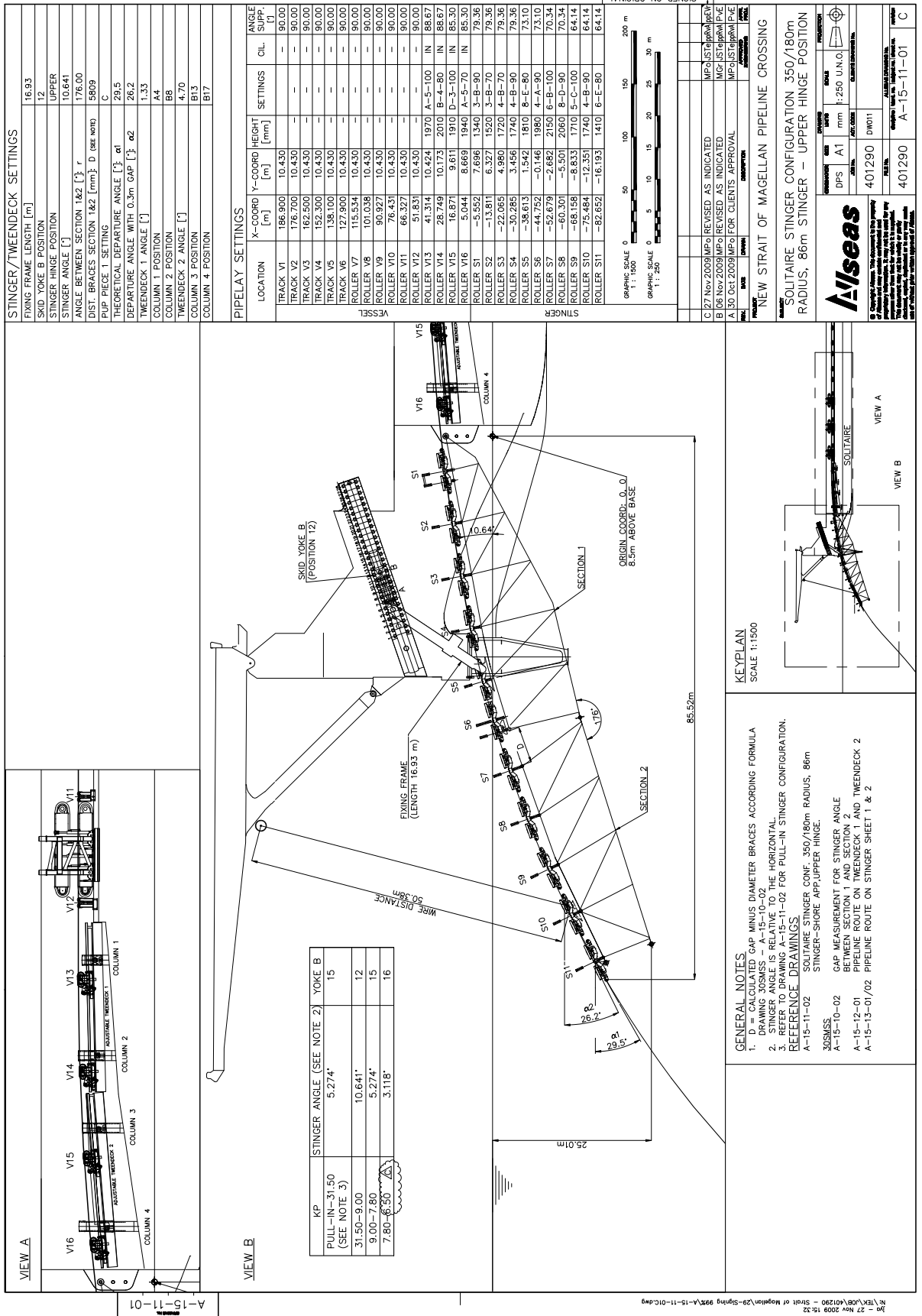
6.3. RECOMMENDATIONS

This section points out possible directions for further research.

- In order to improve the conclusion on the difference in HSS between the two extrapolation methods, with σ_p and σ_{\perp} , a larger variety of multiplanar joints needs to be numerically researched. Attention should be paid to the boundary conditions, for these effect the outcome substantially based on the results from this study.
- This study only qualitatively investigated the locations prone to multiaxial fatigue. As the results indicate that the stinger is subjected to non-proportional multiaxial fatigue loading, a correct multiaxial fatigue calculation method should be incorporated in the in-house developed fatigue assessment of Allseas. The question of which multiaxial fatigue method needs to be used is subject to debate due to the complexity of the phenomenon. So this supports the ongoing research on multiaxial fatigue that is done by the 4D-fatigue project, of which Allseas is a sponsor. This research project can help Allseas in choosing the correct multiaxial fatigue calculation method.
- The snf-ratios have been determined only with respect to a variation of individual joint parameters. The influence of the interaction of joint parameters on the snf-ratio was not part of this study and could be done numerically in order to have a more complete overview of the factors influencing the snf-ratio.

A

STINGER DRAWING



30 - 27 Nov 2009 15:32
N:\EN\08\401290 - Strait of Magellan\28-Stinger\995\A-15-11-01.dwg

B

API-SCRIPT FOR FEMAP CONFIGURATIONS OF T/Y-JOINT

```

1  Module Module1
2
3  '-----This is the Y joint ....
4  part-----
5  Dim vWeight As Object ()
6  Dim vfaceArray As Object ()
7  Dim DOFArray As Object
8  Dim Weight As Object
9  Dim faceArray As Object
10 Dim nodeArray As Object
11
12 Sub Main ()
13 Dim App As femap.model
14 App = GetObject(, "femap.model")
15 App.feAppMessage(1, "To calculate principal stress ...
16 App.feAppMessage(1, "directions/angles - by Mtvdl")
17 '-----"
18 'App.feAppMessage(1, "Please select curves for spider nodes")
19
20 Dim execute As Object
21 Dim kracht As Double
22 '-----GEOMETRY-----
23 '-----
24 '1. creating geometry
25 '1.0 delete all and rebuild
26 execute = App.feDeleteAll(True, True, True, True)
27 execute = App.feFileRebuild(False, True)
28
29 '1.1 Basic Surface
30 Dim angle As Double
31 Dim brace1 As Double
32 Dim brace2 As Double
33 Dim chord1 As Double
34 Dim chord2 As Double
35 Dim DiameterBrace As Double
36 Dim DiameterChord As Double
37 Dim wallthicknessbrace As Double
38 Dim wallthicknesschord As Double
39 Dim chordlength As Double
40 Dim loadednode As Double
41
42 'Choose the joint parameters and loading (kracht) will be ...
43 calculated as IMPa nominal stress
44 'based on the parameters of the brace. This makes it easier ...
45 to determine the SCF.
46 '-----
47 loadednode = 83904 'Change node to spider node of brace
48
49 DiameterChord = 32 * 25.4 'use inches as input, times the ...
50 25.4 conversion it becomes millimeters
51 DiameterBrace = 6.625 * 25.4 'use inches as input, times the ...
52 25.4 conversion it becomes millimeters
53
54 wallthicknesschord = 0.5 * 25.4 'use inches as input, times ...
55 the 25.4 conversion it becomes millimeters
56 wallthicknessbrace = 0.5 * 25.4 'use inches as input, times ...
57 the 25.4 conversion it becomes millimeters
58
59 angle = 1 '1 to 60, NOT 0 and thus a T-joint. Take angle = 1 ...
60 for I joint as approximation
61 'When angle is changed, also change the Y and Z component at ...
62 loading part!
63
64 chord1 = 0.5 * DiameterChord - 0.5 * wallthicknesschord ...
65 'radius inner chord
66 chord2 = chord1 + 60 'radius outer chord
67 brace1 = 0.5 * DiameterBrace - 0.5 * wallthicknessbrace ...
68 'radius inner brace
69 brace2 = brace1 + 60 'radius outer brace
70 chordlength = 15 * (chord1 + 0.5 * wallthicknesschord) ...
71 'chordlength that corresponds to joint parameter alpha = 15
72
73 kracht = 3.1415926535897931 * ((brace1 + 0.5 * ...
74 wallthicknessbrace) ^ 2 - (brace1 - 0.5 * ...
75 wallthicknessbrace) ^ 2) 'S = F/A --> F= S*A is equal to ...
76 IMPa nominal stress, to easily determine the SCF at the ...
77 joint connection
78 '-----
79
80 '1.1.1. Define the chord circle's 1 and 2
81 Dim circenter(3) As Double
82 Dim cirstart(3) As Double
83 circenter = {0, 0, 0}
84 cirstart = {chord1, 0, 0}
85 execute = App.feCircleRadius(circenter, cirstart, True)
86
87
88
89
90
91
92
93
94
95
96
97
98
99
100

```



```

71 Dim circenter2(3) As Double
72 Dim cirstart2(3) As Double
73 circenter2 = {0, 0, 0}
74 cirstart2 = {chord2, 0, 0}
75 execute = App.feCircleRadius(circenter2, cirstart2, True)
76
77 '1.1.2.extrude the chord circles
78 Dim chords As femap.Set
79
80 Dim chordvector(3) As Double
81
82 chords = App.feSet
83 chords.Reset()
84 chords.Add(1)
85 chords.Add(2)
86
87 chordvector = {0, 0, 100}
88 execute = App.feSurfaceExtrude(chords.ID, chordlength, ...
      chordvector)
89
90 '1.1.3.Define brace circles 1 and 2
91
92 Dim pt1brace1(3) As Double
93 Dim pt2brace1(3) As Double
94 Dim pt3brace1(3) As Double
95 pt1brace1 = {brace1, chordlength / 2, chordlength / 2}
96 pt2brace1 = {-brace1, chordlength / 2, chordlength / 2}
97 pt3brace1 = {0, chordlength / 2, (chordlength / 2) + brace1}
98 execute = App.feCircle3Point(pt1brace1, pt2brace1, pt3brace1, ...
      True)
99
100 Dim pt1brace2(3) As Double
101 Dim pt2brace2(3) As Double
102 Dim pt3brace2(3) As Double
103 pt1brace2 = {brace2, chordlength / 2, chordlength / 2}
104 pt2brace2 = {-brace2, chordlength / 2, chordlength / 2}
105 pt3brace2 = {0, chordlength / 2, (chordlength / 2) + brace2}
106 execute = App.feCircle3Point(pt1brace2, pt2brace2, pt3brace2, ...
      True)
107
108 '1.1.4.extrude the bracecircles 1 and 2
109
110 Dim braces As femap.Set
111 Dim braceLength As Double
112 Dim bracevector(3) As Double
113
114 braces = App.feSet
115
116 braces.Reset()
117 braces.Add(15)
118 braces.Add(16)
119
120 braceLength = chordlength / 2 + 100
121 bracevector = {0, -1, 0}
122 execute = App.feSurfaceExtrude(braces.ID, braceLength, ...
      bracevector)
123
124 '1.1.5.rotate brace to desired angle
125 Dim SurfacesRotate As femap.Set
126 Dim axisLoc(3) As Double
127 Dim axisVec(3) As Double
128 Dim rotAngle As Double
129 Dim rotThrust As Double
130
131 axisLoc = {chord1 - ((chord1 - brace1) / 2), (chord1 ^ 2 - ...
      (chord1 - (chord1 - brace1) / 2) ^ 2) ^ 0.5, ...
      chordlength / 2}
132 'axisLoc = {0, chord1, 2500}
133 axisVec = {1, 0, 0}
134 rotAngle = angle
135 rotThrust = 0
136 SurfacesRotate = App.feSet
137 SurfacesRotate.Reset()
138 SurfacesRotate.Add(5)
139 SurfacesRotate.Add(6)
140 SurfacesRotate.Add(7)
141 SurfacesRotate.Add(8)
142
143 execute = App.feRotateBy(femap.zDataType.FT_SURFACE, ...
      SurfacesRotate.ID, axisLoc, axisVec, rotAngle, rotThrust)
144
145 '1.1.6.intersect surfaces
146 Dim surfaces As femap.Set
147 surfaces = App.feSet
148 surfaces.Reset()
149 surfaces.AddAll(femap.zDataType.FT_SURFACE)
150
151 execute = App.feSolidIntersect(surfaces.ID, True)
152
153
154 '1.1.7.delete surfaces
155 Dim SurfaceDelete As femap.Set
156
157 SurfaceDelete = App.feSet

```

```

158 SurfaceDelete.Reset()
159 SurfaceDelete.Add(3)
160 SurfaceDelete.Add(4)
161 SurfaceDelete.Add(7)
162 SurfaceDelete.Add(8)
163 SurfaceDelete.Add(10)
164 SurfaceDelete.Add(11)
165 SurfaceDelete.Add(13)
166 SurfaceDelete.Add(14)
167 SurfaceDelete.Add(15)
168 SurfaceDelete.Add(18)
169 SurfaceDelete.Add(19)
170 SurfaceDelete.Add(20)
171
172 execute = App.feDelete(femap.zDataType.FT_SURFACE, ...
    SurfaceDelete.ID)
173
174
175 '1.1.8 Create saddle lines used for meshing
176 Dim projectsurfaces As femap.Set
177 Dim projectcurves As femap.Set
178 Dim axisVect(3) As Double
179
180 axisVect = {0, 1, 0}
181
182 projectsurfaces = App.feSet
183 projectsurfaces.Reset()
184 projectsurfaces.Add(12)
185
186 projectcurves = App.feSet
187 projectcurves.Reset()
188 projectcurves.Add(53)
189
190 Dim pt39 As femap.Point
191 Dim pt40 As femap.Point
192
193 Dim pointcoor39(3) As Double
194 Dim pointcoor40(3) As Double
195
196 pt39 = App.fePoint
197 pt39.Get(39)
198 pointcoor39 = {pt39.x, pt39.y, pt39.z}
199 pt40 = App.fePoint
200 pt40.Get(40)
201 pointcoor40 = {pt40.x, pt40.y, pt40.z}
202
203
204 execute = App.feCircle3Point(pointcoor39, pointcoor40, ...
    {chord1, 0, pt39.z}, True)
205
206 execute = App.feCurveProjectOntoSurfaces(False, axisVect, ...
    projectsurfaces.ID, projectcurves.ID, False)
207
208
209 Dim LP1(3) As Double
210 Dim LP2(3) As Double
211
212 LP1 = {0, 0, 0}
213 LP2 = {0, 0, chordlength}
214
215 projectsurfaces = App.feSet
216 projectsurfaces.Reset()
217 projectsurfaces.Add(12)
218 projectsurfaces.Add(21)
219
220 projectcurves = App.feSet
221 projectcurves.Reset()
222 projectcurves.Add(58)
223
224
225 execute = App.feLinePoints(False, LP1, LP2, True)
226 execute = App.feCurveProjectOntoSurfaces(False, axisVect, ...
    projectsurfaces.ID, projectcurves.ID, False)
227
228 'delete the extra points by deleting their curves,
229 ''Can only be done one curve at a time...
230 Dim extracurves As femap.Set
231 extracurves = App.feSet
232 extracurves.Reset()
233 extracurves.Add(35)
234 execute = App.feDelete(4, extracurves.ID)
235
236 extracurves = App.feSet
237 extracurves.Reset()
238 extracurves.Add(57)
239 execute = App.feDelete(4, extracurves.ID)
240
241 'crown curves on brace
242 Dim pt1(3) As Object
243 Dim pt2(3) As Object
244 Dim axisvector(3) As Double
245 axisvector = {0, 0, 1}
246 pt1 = {0, 0, 0}
247 pt2 = {0, 2500, 0}

```

```

248 execute = App.feLinePoints(False, pt1, pt2, True)
249 projectsurfaces = App.feSet
250 projectsurfaces.Reset()
251 projectsurfaces.Add(16)
252 projectsurfaces.Add(17)
253
254 projectcurves = App.feSet
255 projectcurves.Reset()
256 projectcurves.Add(66)
257
258 execute = App.feCurveProjectOntoSurfaces(False, axisvector, ...
    projectsurfaces.ID, projectcurves.ID, False)
259
260
261 '-----MESHING-----'
262 '-----'
263
264
265 '2. Meshing
266 '2.1. Material
267 Dim Steel As femap.Mat1
268 Dim MatID As Integer
269 Steel = App.feMat1
270 MatID = Steel.NextEmptyID
271
272 Steel.ID = MatID
273 Steel.title = "Steel S450"
274 Steel.Ex = 210000
275 Steel.Ey = 210000
276 Steel.Ez = 210000
277 Steel.Nuxy = 0.3
278 Steel.Nuxz = 0.3
279 Steel.Nuyz = 0.3
280 Steel.Density = 0.000007885
281
282 Steel.Put(MatID)
283
284
285 '2.2 properties
286 '2.2.1. Chord
287 Dim prop As femap.Prop
288 Dim pflag(4) As Integer
289 Dim pval(188) As Double
290 prop = App.feProp

```

```

292 prop.ID = 1
293 prop.title = "Chord"
294 prop.type = femap.zElementType.FET_L_PLATE
295 prop.matID = MatID
296 prop.vflag = pflag
297 prop.vflagi = pflag
298 prop.vpval = pval
299 prop.pval(0) = wallthicknesschord
300 prop.Put(prop.ID)
301
302 '2.2.2. Brace
303 prop.ID = 2
304 prop.title = "brace"
305 prop.type = femap.zElementType.FET_L_PLATE
306 prop.matID = MatID
307 prop.vflag = pflag
308 prop.vflagi = pflag
309 prop.vpval = pval
310 prop.pval(0) = wallthicknessbrace
311 prop.Put(prop.ID)
312
313 'mesh size curves
314 Dim curset As femap.Set
315
316 curset = App.feSet 'the quarter curves
317 curset.Reset()
318 curset.Add(29)
319 curset.Add(30)
320 curset.Add(31)
321 curset.Add(32)
322 curset.Add(36)
323 curset.Add(43)
324 curset.Add(44)
325 curset.Add(56)
326 curset.Add(61)
327 curset.Add(63)
328 curset.Add(64)
329 curset.Add(65)
330 curset.Add(69)
331 curset.Add(70)
332 curset.Add(71)
333 curset.Add(72)
334 execute = App.feMeshSizeCurve(curset.ID, 160, 0, 0, 0, 0, 0, ...
    0, 1.0, 2, True)
335
336 curset = App.feSet 'the saddle and crown curves
337

```

```

338 curset.Reset ()
339 curset.Add(54) 'on chord
340 curset.Add(55)
341 curset.Add(60)
342 curset.Add(59)
343
344 execute = App.feMeshSizeCurve(curset.ID, 60, 0, 0, 0, 0, 0, 0, ...
0, 1.0, 2, True)
345
346 curset = App.feSet 'the saddle and crown curves
347 curset.Reset ()
348 curset.Add(34) 'on brace
349 curset.Add(45)
350 curset.Add(67)
351 curset.Add(68)
352
353 execute = App.feMeshSizeCurve(curset.ID, 40, 0, 0, 0, 0, 0, 0, ...
0, 1.0, 2, True)
354
355
356
357 'mesh size surface
358 Dim surset As femap.Set
359 surset = App.feSet
360 surset.Reset ()
361 surset.AddAll(femap.zDataType.FT_SURFACE)
362
363 execute = App.feMeshSizeSurface(surset.ID, False, 40, 0, 0.0, ...
0, 0.0, 0.0, True, 0.0, 0.0, True)
364
365 'Quad mesh
366 'chord
367 surset = App.feSet
368 surset.Reset ()
369 surset.Add(1)
370 surset.Add(2)
371 surset.Add(9)
372 surset.Add(12)
373 surset.Add(21)
374 surset.Add(22)
375 surset.Add(23)
376
377 execute = App.feMeshSurface2(surset.ID, 1, 4, True, False)
378
379 'brace
380 surset = App.feSet
381 surset.Reset ()
382 surset.Add(5)
383 surset.Add(6)
384 surset.Add(16)
385 surset.Add(17)
386 surset.Add(24)
387 surset.Add(25)
388
389 execute = App.feMeshSurface2(surset.ID, 2, 4, True, False)
390
391 'check for coincident nodes and merge them
392 Dim merge As femap.Set
393 merge = App.feSet
394 merge.Reset ()
395 merge.AddAll(femap.zDataType.FT_NODE)
396
397 execute = App.feCheckCoincidentNode2(merge.ID, 1, True, 0, 0, ...
True, 0, False)
398
399 '-----SPIDER NODES-----
400
401
402 '3 Spider nodes
403 '1. Initialize variables.
404 Dim feNode As Object
405 Dim fN As Object
406 Dim nodeSet As Object
407 Dim feElem As Object
408 Dim nodeCount As Long
409 Dim nodeX As Double
410 Dim nodeY As Double
411 Dim nodeZ As Double
412 Dim nodeID As Long
413 Dim elemID As Long
414
415 Dim vDOF As Object
416 Dim vNodeArray As Object
417 Dim vDum As Object
418 Dim vWeight As Object
419 Dim vfaceArray As Object
420 vDOF = DOF
421
422 nodeSet = App.feSet ()
423
424 DO_IT_AGAIN:
425

```

```

426 nodeCount = 0
427
428 execute = nodeSet.Clear()
429
430 nodeX = 0.0#
431 nodeY = 0.0#
432 nodeZ = 0.0#
433
434 '2. Attach to FEMAP.
435
436 App = GetObject(, "femap.model")
437
438 '3. Ask the user to select nodes for the rigid element.
439 nodeSet.debug()
440
441 nodeSet = App.feSet
442 nodeSet.Reset()
443 curset = App.feSet 'assign curves of brace to use for spider node
444 curset.Reset()
445 curset.Add(17)
446 curset.Add(19)
447
448 execute = nodeSet.AddSetRule(curset.ID, ...
449 femap.zGroupDefinitionType.FGD_NODE_ATCURVE)
450
451 'execute = nodeSet.Select(7, True, "Select Nodes for Rigid ...
452 Spider")
453 nodeSet.debug()
454
455 'If nodeSet.Count = 0 Then
456 ' GoTo Jumping_Out
457 'End If
458
459 If execute = -1 Then
460
461 '4. Identify how many nodes were selected.
462 nodeCount = nodeSet.Count()
463
464 'If nodeCount > 0 Then
465
466 '5. Make some local arrays to hold the data that was ...
467 collected.
468
469 Redim nodeArray (nodeCount)

```

```

470 Redim faceArray (nodeCount)
471 Redim Weight (nodeCount)
472 Redim DOFArray (nodeCount * 6)
473
474 vDOF = DOFArray
475 vWeight = Weight
476 vfaceArray = faceArray
477
478 Dim passCount As Long
479
480 passCount = 0
481
482 '6. Walk the nodes.
483
484 FN = App.feNode()
485 execute = nodeSet.Reset()
486 nodeID = nodeSet.Next()
487
488 '7. Store the IDs.
489
490 Do While nodeID <> 0
491
492 nodeArray (passCount) = nodeID
493 passCount = passCount + 1
494 execute = FN.Get (nodeID)
495
496 nodeX = nodeX + FN.x
497 nodeY = nodeY + FN.y
498 nodeZ = nodeZ + FN.z
499
500 nodeID = nodeSet.Next()
501
502 Loop
503
504 '8. Compute the centroid and create the Node at the centroid.
505
506 feNode = App.feNode()
507 vNodeArray = nodeArray
508
509 nodeID = feNode.NextEmptyID
510
511 feNode.x = nodeX / nodeCount
512 feNode.y = nodeY / nodeCount
513 feNode.z = nodeZ / nodeCount
514
515 '9. Store the node.
516

```

```

517 execute = feNode.Put (nodeID)
518
519
520
521 If execute = -1 Then 'return code FE_OK
522
523 '10. Create the element.
524
525 feElem = App.feElem()
526
527 elemID = feElem.NextEmptyID
528
529 feElem.Type = 29 'Rigid
530 feElem.topology = 13 'Rigid
531 feElem.node(0) = nodeID 'Independent Node
532 feElem.Release(0, 0) = 1
533 feElem.Release(0, 1) = 1
534 feElem.Release(0, 2) = 1
535
536 vDum = nodeArray
537
538 execute = feElem.PutNodeList(0, nodeCount, vNodeArray, _
539 vfaceArray, vWeight, vDOF)
540
541 '11. Store the element.
542 execute = feElem.Put (elemID)
543
544
545 End If
546
547 End If
548
549 End If
550
551 Call App.feViewRegenerate(0)
552
553 'GoTo DO_IT_AGAIN
554
555 Jumping_Out:
556
557 Call App.feViewRegenerate(0)
558
559 '-----CONSTRAINTS-----
560 '-----
561
562
563
564
565
566
567
568
569
570
571
572
573
574
575
576
577
578
579
580
581
582
583
584
585
586
587
588
589
590
591
592
593
594
595
596
597
598
599
600
601
602
603
604
605
606

```

```

562 '3.0 constraints
563 Dim nodset As femap.Set
564 Dim conset As femap.BCSet
565 Dim connod As femap.BCNode
566
567 'select nodes by selecting curves
568 '3.1.0 constraint nodes set
569 nodset = App.feSet
570 nodset.Reset()
571 curset = App.feSet 'curset is used when spider nodes are not used
572 curset.Reset()
573 curset.Add(3)
574 curset.Add(4)
575 curset.Add(5)
576 curset.Add(7)
577 execute = nodset.AddSetRule(curset.ID, ...
578 femap.zGroupDefinitionType.FGD_NODE_ARCOURSE)
579 'execute = nodset.Select(femap.zDataType.FT_NODE, True, ...
580 "Select the nodes to be constrained")
581
582 '3.1.1 constraint set FIXED
583 conset = App.feBCSet
584 conset.Reset()
585 conset.ID = 1 'conset.NextEmptyID
586 conset.title = "fixed"
587 conset.Put (conset.ID)
588
589 '3.1.2
590 connod = App.feBCNode
591 connod.Reset()
592 connod.SetID = conset.ID
593 connod.ID = connod.NextEmptyID
594 connod.Add(nodset.ID, True, True, True, True, True, True)
595 connod.Put (connod.ID)
596
597 '3.1.1 constraint set PINNED
598 'conset = App.feBCSet
599 'conset.Reset()
600 'conset.ID = 2 'conset.NextEmptyID
601 'conset.title = "pinned"
602 'conset.Put (conset.ID)
603
604 '3.1.3
605 'connod = App.feBCNode
606 'connod.Reset()
607 'connod.SetID = conset.ID
608 'connod.ID = connod.NextEmptyID

```

```

607 'connod.Add(nodset.ID, True, True, True, False, False, False)
608 'connod.Put(connod.ID)
609
610 ''3.1.1 constraint set PINNED at left side of chord
611 'curset = App.feSet 'curset is used when spider nodes are not ...
    used
612 'curset.Reset()
613 'curset.Add(3)
614 'curset.Add(5)
615 'execute = nodset.AddSetRule(curset.ID, ...
    femap.zGroupDefinitionType.FGD_NODE_ATCURVE)
616 'conset = App.feBCSet
617 'conset.Reset()
618 'conset.ID = 3 'conset.NextEmptyID
619 'conset.title = "pinned leftside chord"
620 'conset.Put(conset.ID)
621
622 ''3.1.3
623 'connod = App.feBCNode
624 'connod.Reset()
625 'connod.SetID = conset.ID
626 'connod.ID = connod.NextEmptyID
627 'connod.Add(nodset.ID, True, True, True, False, False, False)
628 'connod.Put(connod.ID)
629
630 ''3.1.1 constraint set PINNED at left side of chord
631 'curset = App.feSet 'curset is used when spider nodes are not ...
    used
632 'curset.Reset()
633 'curset.Add(4)
634 'curset.Add(7)
635 'execute = nodset.AddSetRule(curset.ID, ...
    femap.zGroupDefinitionType.FGD_NODE_ATCURVE)
636 'conset = App.feBCSet
637 'conset.Reset()
638 'conset.ID = 4 'conset.NextEmptyID
639 'conset.title = "roller rightside chord"
640 'conset.Put(conset.ID)
641
642 ''3.1.3
643 'connod = App.feBCNode
644 'connod.Reset()
645 'connod.SetID = conset.ID
646 'connod.ID = connod.NextEmptyID
647 'connod.Add(nodset.ID, True, True, True, False, False, False)
648 'connod.Put(connod.ID)
649
650 Call App.feViewRegenerate(0)
651
652 '-----LOADS-----
653 '-----'
654
655 ''3.2 loads
656
657 'Dim lset As femap.LoadSet
658 'Dim loadt As femap.LoadGeom
659 'Dim surlo As femap.Set
660
661 ''3.2.0 load on surface 10
662 'surlo = App.feSet
663 'surlo.Reset()
664 'surlo.Add(17)
665 'surlo.Add(19)
666
667 ''3.2.1 load set
668 'lset = App.feLoadSet
669 'lset.Reset()
670 'lset.ID = lset.NextEmptyID
671 'lset.title = Str$(1) + "MPa"
672 'lset.Put(lset.ID)
673
674 ''3.2.2 load on surface, force on curve nodes #1
675 'loadt = App.feLoadGeom
676 'loadt.Reset()
677 'loadt.SetID = lset.ID
678 'loadt.ID = loadt.NextEmptyID
679 'loadt.geomID = 17
680 'loadt.CSys = 0
681 'loadt.vflag = {0, 1, 0}
682 'loadt.type = 123
683 'loadt.subtype = 0
684 'loadt.geomTYPE = femap.zDataType.FT_CURVE
685 'loadt.vload = {-(kracht / 22), 0, 0.0, 180, 0} 'should be ...
    0.5 * kracht divided by number of nodes on curve
686 'loadt.dirmode = 2
687 'loadt.dirID = 20
688 'loadt.midside = True
689 'loadt.FaceNumber = 1
690 'loadt.XOn = True
691 'loadt.YOn = True
692 'loadt.ZOn = True
693 'loadt.Put(loadt.ID)

```

```

694 ''3.2.2 load on surface, force on curve nodes #2
695 'loadt = App.feLoadGeom
696 'loadt.Reset()
697 'loadt.SetID = lset.ID
698 'loadt.ID = loadt.NextEmptyID
699 'loadt.geomID = 19
700 'loadt.CSys = 0
701 'loadt.vflag = {0, 1, 0}
702 'loadt.type = 123
703 'loadt.subtype = 0
704 'loadt.geomTYPE = femap.zDataType.FT_CURVE
705 'loadt.vload = {-(kracht / 22), 0, 0.0, 180, 0} 'should be ...
706 0.5 * kracht divided by number of nodes on curve
707 'loadt.dirmode = 2
708 'loadt.dirID = 20
709 'loadt.midside = True
710 'loadt.FaceNumber = 1
711 'loadt.XOn = True
712 'loadt.YOn = True
713 'loadt.ZOn = True
714 'loadt.Put(loadt.ID)
715
716 ''3.2 loads
717 'Dim kracht As Integer
718 Dim lset As femap.LoadSet
719 Dim loadt As femap.LoadMesh
720 Dim nodeload As femap.Set
721 ''3.2.0 pick the node where load will be applied
722 nodeload = App.feSet
723 nodeload.Reset()
724 'execute = nodeload.Select(femap.zDataType.FT_NODE, True, ...
725 'nodeload.Add(nodeload.ID)
726
727 ''3.2.1 load set
728 lset = App.feLoadSet
729 lset.Reset()
730 lset.ID = lset.NextEmptyID
731 lset.title = "loading " && Str$(Ften / 1000) + "kN"
732 lset.Put(lset.ID)
733
734 ''3.2.2 load on surface, bearing force
735 loadt = App.feLoadMesh
736 loadt.Reset()
737 loadt.SetID = lset.ID
738 loadt.ID = loadt.NextEmptyID
739
740
741 loadt.meshID = loadednode 'is specified above
742
743 loadt.CSys = 0
744 loadt.vflag = {0, 1, 0}
745 loadt.type = 1
746
747
748 'loadt.subtype =
749 'loadt.geomTYPE = 7
750 loadt.vload = {0.0, kracht, 0.0, 180, 0.0}
751 'loadt.dirmode = 1
752 'loadt.vdirection = {0.0, 0.0, 1.0}
753 'loadt.midside = True
754 loadt.FaceNumber = 1
755 loadt.XOn = True
756 loadt.YOn = True
757 loadt.ZOn = True
758 loadt.y = kracht '30deg: 0.5 * kracht, 45deg: 0.5*(2 ^
759 0.5)*kracht, 60deg: 0.5*(3^0.5)*kracht
760 0.5)*kracht, 60deg: 0.5*(3^0.5)*kracht, 45deg: 0.5*(2 ^
761 0.5)*kracht, 60deg: 0.5 *kracht
762 loadt.Put(loadt.ID)
763
764 Call App.feViewRegenerate(0)
765
766 '-----Analyze with FIXED ...
767 constraints
768 Dim Ana As femap.AnalysisMgr
769 Ana = App.feAnalysisMgr
770 Ana.title = Str$(1) + "MPa on brace, FIXED"
771 Ana.Solver = femap.zAnalysisMgrProgram.FAM_NX_NASTRAN
772 Ana.AnalysisType = femap.zAnalysisType.FAT_STATIC
773
774 Ana.BCSet(0) = 1 'select constraint set
775 Ana.BCSet(2) = lset.ID 'select load set
776
777 'Nodal Applied Load
778 Ana.Output(0) = -1
779
780 'Nodal Reaction Force
781 Ana.Output(1) = -1
782
783 'Nodal Displacement
784 Ana.Output(2) = -1
785

```



```

783 'Nodal Force Balance
784 Ana.Output(8) = -1
785
786 'Element Force
787 Ana.Output(15) = -1
788
789 'Element Stress
790 Ana.Output(16) = -1
791
792 'Element Strain
793 Ana.Output(17) = -1
794
795 Ana.LaunchWithVisQ = False
796
797 Ana.CornorOutput = True
798
799 Ana.Put (Ana.NextEmptyID)
800
801 Ana.Analyze (Ana.ID)
802
803 '-----Analyze with PINNED ....
804
805 'Dim Ana2 As femap.AnalysisMgr
806 'Ana2 = App.feAnalysisMgr
807 'Ana2.title = Str$(1) + "Mpa on brace, PINNED-Roller"
808 'Ana2.Solver = femap.zAnalysisMgrProgram.FAM_NX_NASTRAN
809 'Ana2.AnalysisType = femap.zAnalysisType.FAT_STATIC
810
811 'Ana2.BCSet(0) = 3 'select constraint set
812 'Ana2.BCSet(0) = 4
813 'Ana2.BCSet(2) = 1set.ID 'select load set
814
815 'Nodal Applied Load
816 Ana.Output(0) = -1
817
818 'Nodal Reaction Force
819
820 'Ana2.Output(1) = -1
821
822 'Nodal Displacement
823 Ana2.Output(2) = -1
824
825 'Nodal Force Balance
826 Ana.Output(8) = -1
827
828 'Element Force
829 Ana2.Output(15) = -1
830
831 'Element Stress
832 Ana2.Output(16) = -1
833
834 'Element Strain
835 Ana2.Output(17) = -1
836
837 'Ana2.LaunchWithVisQ = False
838
839 Ana2.CornorOutput = True
840
841 'Ana2.Put (Ana2.NextEmptyID)
842
843 'Ana2.Analyze (Ana2.ID)
844
845 '5.0 Enveloping
846
847 '100 Regenerate
848 'execute = App.feViewRegenerate(0)
849 End Sub
850
851
852
853
854 End Module

```


C

T/Y-JOINT CONFIGURATIONS

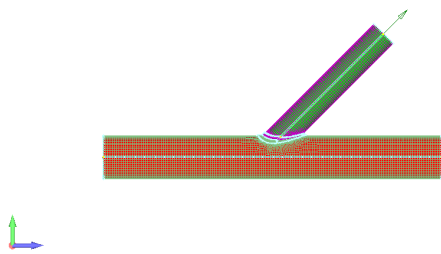


Figure C.1: Configuration 1

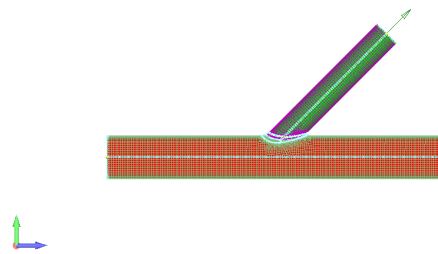


Figure C.2: Configuration 2

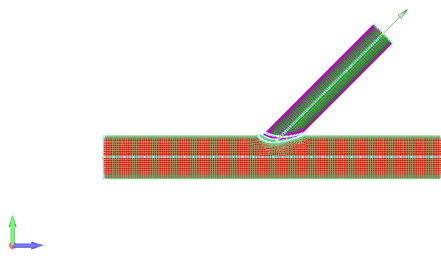


Figure C.3: Configuration 3

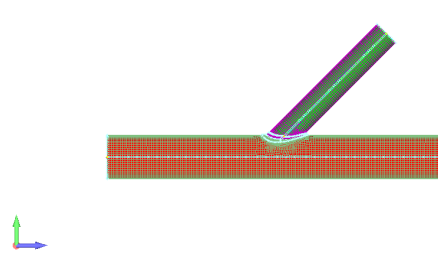


Figure C.4: Configuration 4

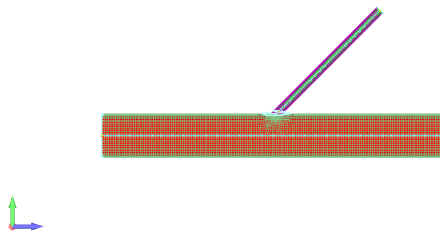


Figure C.5: Configuration 5

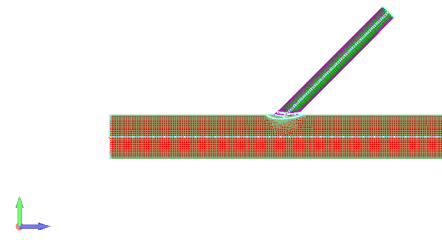


Figure C.6: Configuration 6

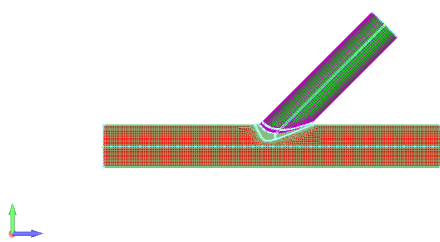


Figure C.7: Configuration 7

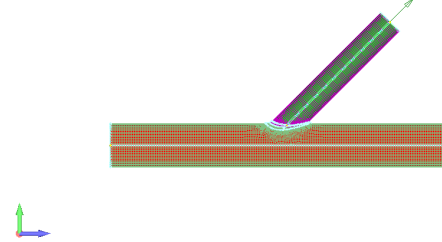


Figure C.8: Configuration 8

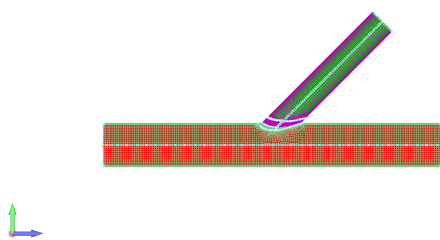


Figure C.9: Configuration 9

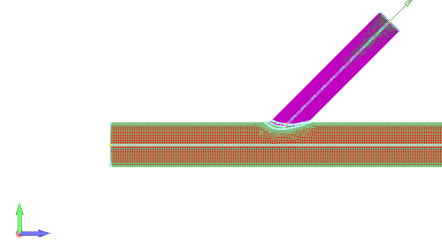


Figure C.10: Configuration 10

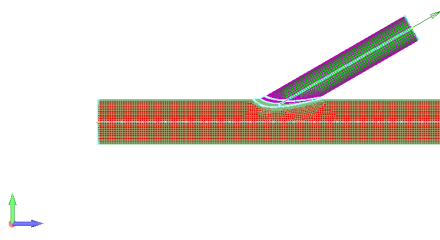


Figure C.11: Configuration 11

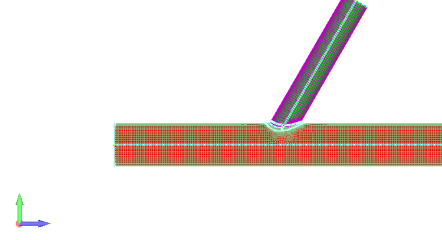


Figure C.12: Configuration 12

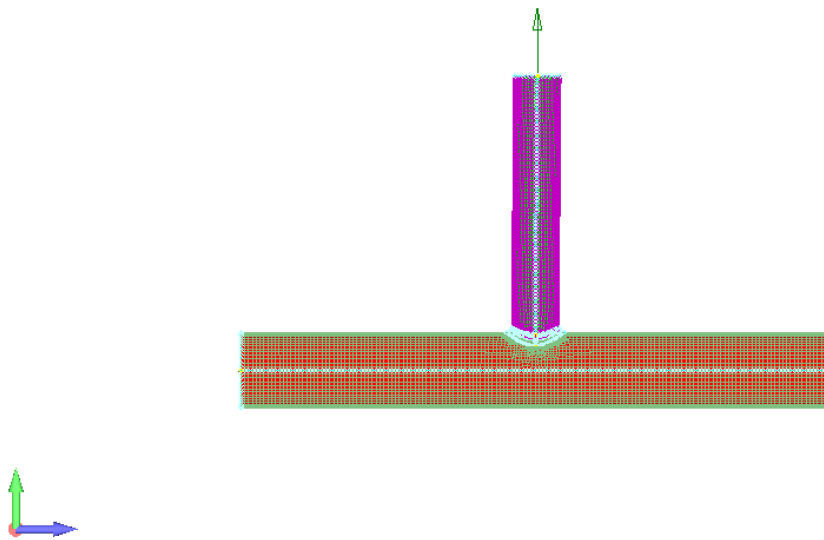


Figure C.13: Configuration 13

BIBLIOGRAPHY

- [1] S. Pel, *Solitaire: Stinger fatigue calculations*, Tech. Rep. (Allseas Engineering, Innovations department, 2010).
- [2] DNV, *DNV-RP-C203 - Fatigue design of offshore steel structures* (Det Norske Veritas, June 2014).
- [3] J. Wardenier, *Design guide for circular hollow section joints under predominantly static loading* (Cidect, 2008).
- [4] Zhao, *Design guide for circular and rectangular hollow section welded joints under fatigue loading* (Cidect, 2001).
- [5] R. Hibbeler, *Mechanics of Materials*, 7th ed. (Pearson, 2008).
- [6] A. Romeijn, *Stress and Strain Concentration Factors of welded Multiplanar Tubular Joint*, Ph.D. thesis, TU Delft (1994).
- [7] L. Tang, *Stress Concentration Factors for Partial Joint Penetration Plus welds for tubular joints*, Master's thesis, TU Eindhoven (2010).
- [8] M. Efthymiou, *Development of SCF Formulae and generalised influence functions for use in fatigue analysis* (1988).
- [9] S. A. Karamanos, A. Romeijn, and J. Wardenier, *Stress concentrations in tubular gap k-joints: mechanics and fatigue design*, *Engineering Structures* **22**, 4 (2000).
- [10] J. van Wingerde et al, *Criteria for the fatigue assessment of hollow structural section connections*, *J. Construct. Steel Research* **35**, 71 (1995).
- [11] AWS, *D1.1/D1.1M-Structural Welding Code-Steel* (American Welding Society, 2006).
- [12] API, *American Petroleum Institute RP2-WSD, Recommended practice for planning, designing and constructing fixed offshore platforms-working stress design* (American Petroleum Institute, 2000).
- [13] X.-L. Zhao and J. Packer, *Fatigue Design Procedure for Welded Hollow Section Joints: Recommendations of IIW Subcommittee XV-E* (International Institute of Welding, 2000).
- [14] C. M. Sonsino and K. Dieterich, *Fatigue design with cast magnesium alloys under constant and variable amplitude loading*, *International Journal of Fatigue* **28**, 183 (2006).
- [15] C. Sonsino, H. Zenner, and A. Carpinteri, *Selected papers from the 7th international conference on bi-axial/multi-axial fatigue and fracture, held in Berlin, on 28 June to 1 July 2004*, *International Journal of Fatigue* **28** (2006).
- [16] D. Socie, *Multiaxial fatigue damage models*, *J Eng Mater Technology Trans Asme* **109**(4), 293 (1987).
- [17] F. Ellyin, *In-phase and out-of-of-phase multiaxial fatigue*, *J Eng Mater Technology Trans Asme* **113**(1), 112 (1991).
- [18] T. Itoh and T. Miyazaki, *A damage model for estimating low cycle fatigue lives under nonproportional multiaxial loading*, *European Structural Integrity Society* **31**, 423 (2003).
- [19] D. Skibicki, *Phenomena and Computational Models of Non-Proportional Fatigue of Materials* (Springer, 2014).
- [20] Y.-Y. Wang and W.-X. Yao, *Evaluation and comparison of several multiaxial fatigue criteria*, *International Journal of Fatigue* **26**, 17 (2003).

-
- [21] E. Niemi and P. Tanskanen, *Hot spot stress determination for welded edge gussets*, International Institute of Welding **44(5)**, 31 (1999).
- [22] C. A. Felippa, *Introduction to finite element methods* (Department of Aerospace Engineering Sciences, University of Colorado, June 2014).
- [23] O. Korikadou, *Research into the fatigue assessment methodology of tubular joints in application to stinger structure*, Master's thesis, TU Delft (2013).
- [24] L. Zhao, *Evaluation of Stress Concentration Factors (SCF) in Multiplanar Tubular Joints*, Master's thesis, TU Delft (2010).
- [25] C. Fernando, *Analysis of Stress and Strain concentration factors of multiplanar tubular joints of a stinger structure*, Master's thesis, TU Delft (2014).
- [26] 2HOffshore, *Allseas stinger monitoring system supply*, Tech. Rep. (Allseas Engineering, Innovations department, 2010).
- [27] Trouvay and Cauvin, *Piping equipment*, (2001).
- [28] A. Hobbacher, *Recommendations for Fatigue Design Welded Joints and Components* (Springer, 2016).